JOURNAL OF TELECOMMUNICATIONS AND INFORMATION TECHNOLOGY

Preface

The tremendous growth of the Internet, the large increase in traffic demands, and the relentless demand for network capacity have produced a need for new flexible types of services. Optical networks are expected to support the diverse requirements of a broad range of applications as they are evolving dramatically in terms of technology and architecture. In particular, optical component technology is rapidly maturing, offering cost effective solutions to a point where optical networks are currently being deployed in core backbone networks, and are gaining increased interest for deployment in metro and access environments. Wavelength division multiplexing systems are widely deployed, thanks to low-cost and high reliability of optical components. Core, metropolitan, and access networks are increasingly based on optical technologies to overcome the electronic bottleneck at network edge. Even, traditional multi-layer architectures, such as the widely deployed IP/ATM/SDH protocol stacks, are already based on WDM transport systems increasing efforts to move some of functionalities available in higher layers to the optical layer. New components and subsystems for very high speed optical networks offer new design options to network operators and designers.

This issue of the *Journal of Telecommunications and Information Technology* addresses the most significant optical technologies for optical switching and networking and it contains twelve carefully selected papers which reflect the progress with all-optical devices and technologies for communications and computing applications.

The first, invited paper, by Armand Toguyéni and Ouajdi Korbaa from Ecole Centrale de Lille, France, and the University of Sousse, Tunisia, *DiffServ Aware MPLS Traffic Engineering for ISP Networks: State of the Art and New Trends*, addresses the issues of quality of service in multimedia applications or networked control application of novel Internet services. It reviews main MPLS approaches such as MATE, LDM or LBWDP as novel models for traffic engineering. The Authors introduce a PEMS model that adapts the offered QoS depending on the class of the routed traffic.

The second, invited paper, by Marian Marciniak from the Department of Transmission and Optical Technologies, National Institute of Telecommunications, Warsaw, Poland, *100/1000 Gbit/s Ethernet and beyond*, discusses the challenges, advantages and constraints of hyper-speed Ethernet optical networking and switching.

The third, invited paper, by Nicola Calabretta, Hyun-Do Jung, Javier Herrera Llorente, Eduward Tangdiongga, Ton Koonen, and Harm Dorren from the COBRA Research Institute, Eindhoven University of Technology, The Netherlands, *All-Optical Techniques Enabling Packet Switching with Label Processing and Label Rewriting*, introduces a 1×4 all-optical packet switch based on label swapping technique that utilizes a scalable and asynchronous label processor and label rewriter, and demonstrates an error-free operation indicating a potential utilization of the swapping technique in a multi-hop packet-switched network.

The fourth, invited paper, by Andrey Ananenkov, Anton Konovaltsev, Alexey Kukhorev, Vladimir Nujdin, Vladimir Rastorguev, and Pavel Sokolov from the Moscow Aviation Institute, State Technical University, Russia, *Features of Formation of Radar-Tracking and Optical Images in a Mobile Test Stand of Radio-Vision Systems of a Car*, reports on the features of formation of radar images and optical images in the mobile test stand of radio-vision systems of a car. The radio-vision system of a car of the millimeter-wavelength with frequency modulation is proposed and its performance analyzed in detail.

The fifth, invited paper, by Luca Tartara, Vittorio Degiorgio, Rim Cherif, and Mourad Zghal from the Department of Electronics, University of Pavia, Italy, and the Cirta'Com Laboratory, Engineering School of Communication of Tunis (Sup'Com), Ariana, Tunisia, *Setting an Upper-Wavelength Limit to the Supercontinuum Generated in a Photonic Crystal Fibre*, reports on a novel kind of supercontinuum generation in a photonic crystal fibre in which the spectral broadening occurs only on the blue side of the pump wavelength. A theoretical analysis along with experimental data which are supported by the results of a set of numerical simulations are presented in this paper.

The sixth, invited paper, by Maria C. R. Medeiros, Ricardo Avó, Paula Laurêncio, Noélia S. Correia, Alvaro Barradas, Henrique J. A. da Silva, Izzat Darwazeh, John E. Mitchell, and Paulo M. N. Monteiro from the Center for Electronics, Optoelectronics and Telecommunications (CEOT), University of Algarve, Faro, Portugal, and the Department of Electrical and Computer Engineering, University of Coimbra, Portugal, and the Telecommunications Research Group, Department of Electronic and Electrical Engineering, University College London (UCL), UK, and the Nokia Siemens Networks Portugal S.A., Amadora, Portugal, and the Institute of Telecommunications, University of Aveiro, Portugal, *RoFnet – Reconfigurable Radio over Fiber Network Architecture Overview*, introduces the basic operational concepts of the RoFnet – reconfigurable radio over fiber network, which is a project supported by the Portuguese Foundation for Science and Technology. The Authors propose an innovative radio over fiber optical access network architecture, which combines a low cost base station design, incorporating reflective semiconductor optical amplifiers, with fiber dispersion mitigation provided by optical single sideband modulation techniques. Optical wavelength division multiplexing techniques are used to simplify the access network architecture allowing for different base stations to be fed by a common fiber. Different wavelength channels can be allocated to different base stations depending on user requirements. Additionally, in order to improve radio coverage within a cell, it is considered a sectorized antenna interface. The combination of subcarrier multiplexing with WDM, further simplifies the network architecture, by using a specific wavelength channel to feed an individual base station and different subcarriers to drive the individual antenna sectors within the base station.

The seventh, invited paper, by Marek Jaworski from the Department of Transmission and Optical Technologies, National Institute of Telecommunications, Warsaw, Poland, *Methods of Step-Size Distribution Optimization Used in S-SSFM Simulations of WDM Systems*, introduces two novel methods of step-size distribution optimization used to improve symmetrized split step Fourier method (S-SSFM) numerical efficiency: pre-simulated local error S-SSFM and modified logarithmic S-SSFM. The pre-simulated local error S-SSFM contains two stages: in the initial stage step-size distribution optimization is carried out by combining local error method and pre-simulation with signal spectrum averaging; in the second stage conventional SSFM is used by applying optimal step-size distribution obtained in the initial stage. The modified logarithmic S-SSFM is generalization of logarithmic method proposed to suppress spurious FWM tones, in which a slope of logarithmic step-size distribution is optimized. Overall time savings exceed 50%, depending of a simulated system scenario.

The eighth, invited paper, by Nebiha Ben Sedrine, Jaouher Rihani, Jean-Christophe Harmand, and Radhouane Chtourou from the Laboratory of Photovoltaïc, Semiconductors and Nanostructures (LPVSN), Research and Technology Energy Center (CRTEn), Hammam-Lif, Tunisia, and the Laboratory for Photonics and Nanostructures (LPN), Marcoussis, France, *Spectroscopic Ellipsometry Analysis of Rapid Thermal Annealing Effect on MBE Grown* $GaAs_{1-x}N_x$, reports on the effect of rapid thermal annealing (RTA) on $GaAs_{1-x}N_x$ layers, grown by molecular beam epitaxy, using room temperature spectroscopic ellipsometry. A comparative study was carried out on a set of $GaAs_{1-x}N_x$ as-grown and the RTA samples with small nitrogen content ($x = 0.1\%$, 0.5% and 1.5%). Thanks to the standard critical point model parameterization of the $GaAs_{1-x}N_x$ extracted dielectric functions, the Authors determined the RTA effect, and its nitrogen dependence. They have found that RTA affects more samples with high nitrogen content. In addition, RTA is found to decrease the E_1 energy nitrogen blue-shift and increase the broadening parameters of E_1, $E_1+\Delta_1$, E_0' and E_2 critical points.

The ninth, invited paper, by Ridha Rejeb and Mark S. Leeson from the Institute for Advanced Engineering and Research, Germany, and the School of Engineering, University of Warwick, UK, *Control Mechanism for All-Optical Components*, provides a brief overview of security and management issues that arise in all-optical networks (AONs). Then the Authors introduce the idea of the multiple attack localization and identification (MALI) algorithm that can participate in some of the tasks for fault management in AONs. A hardware-based control unit that can be embedded in AON nodes to accelerate the performance of the MALI algorithm is discussed in detail, and an applicability and implementation of this device in AON management systems is demostrated.

The tenth, invited paper, by Yousef S. Kavian, Wei Ren, Majid Naderi, Mark S. Leeson, and Evor L. Hines, from the Faculty of Engineering, Shahid Chamran University, Ahvaz, Iran, and the School of Engineering, University of Warwick, UK, and the Electrical Engineering Department, Iran University of Science and Technology (IUST), Tehran, Iran, *Fault Tolerant Dense Wavelength Division Multiplexing Optical Transport Networks*, presents a genetic algorithm based approach for designing fault tolerant dense wavelength division multiplexing optical networks in the presence of a single link failure. The working and spare lightpaths are encoded into variable length chromosomes. Then the best lightpaths are found by use of a fitness function and these are assigned the minimum number of wavelengths according to the problem constraints using first-fit algorithm. The results, obtained from the ARPA2 test bench network, show that the method is well suited to tackling this complex and multi-constraint problem.

The eleventh, invited paper, by Yousef S. Kavian, Habib F. Rashvand, Mark S. Leeson, Wei Ren, Evor L. Hines, and Majid Naderi from the Faculty of Engineering, Shahid Chamran University, Ahvaz, Iran, and the School of Engineering, University of Warwick, UK, and the Electrical Engineering Department, Iran University of Science and Technology (IUST), Tehran, Iran, *Network Topology Effect on QoS Delivering in Survivable DWDM Optical Networks*, investigates the effect of network topology on QoS delivering in survivable dense wavelength division multiplexing optical transport networks using bandwidth/load ratio and design flexibility metrics. The dedicated path protection architecture is employed to establish diverse working and spare lightpaths between each node pair in demand matrix for covering a single link failure model. The simulation results, obtained for the Pan-European and the ARPA2 test bench networks, demonstrate that the network topology has a great influence on QoS delivering by network at optical layer for different applications.

Finally, the twelfth paper, by Krzysztof Borzycki from the Department of Transmission and Optical Technologies, National Institute of Telecommunications, Warsaw, Poland, *Fusion Splicing and Testing of Photonic Crystal Fibers*, is devoted to characterization of optical, thermal and opto-mechanical properties of new class of optical fibers finding applications in optical components, sensors and signal processing. Tests on two fibers developed by IPHT Jena, Germany, allowed for comparisons; in particular, temperature and twist dependence of polarization mode dispersion are very different. The paper also presents in detail fusion splicing techniques for splicing of photonic crystal fibers samples to conventional single mode fibers. This research was performed within COST Action 299.

We have to emphasize the excellent progress and valuable results in photonic technologies for optical switching and networking responds to growing demands of next generation networking and services in view of bandwidth offered to the customer, quality of service, and security, reported in this issue. We thank the Authors for their wide response to the call for contributions which was intended to reflect the scope of the International Conference on Transparent Optical Networking ICTON and ICTON – Mediterranean Winter to which a majority of the Authors have contributed.

Marian Marciniak (National Institute of Telecommunications, Poland)
Ridha Rejeb (Institute for Advanced Engineering and Research, Germany)
Bouchta Sahraoui (Université d'Angers, France)
Guest Editors

Invited paper

DiffServ Aware MPLS Traffic Engineering for ISP Networks: State of the Art and New Trends

Armand Toguyéni and Ouajdi Korbaa

Abstract—In the recent ten years, with the development of new applications through Internet such as multimedia or networked control applications, users need more and more quality of service (QoS). However, the requested QoS is not the same depending on the application. Most of the new models to manage internet traffic are based on specific QoS criteria which should be optimized. This paper presents main multiprotocol label switching (MPLS) approaches such as MPLS adaptive traffic engineering (MATE), load distribution in MPLS (LDM) and load balancing over widest disjoints paths (LBWDP) that are new models for traffic engineering. It also introduces periodic multi-step (PEMS) algorithm that adapts the offered quality depending on the class of the routed traffic.

Keywords*— *differentiated service, multipath routing, QoS routing, quality of service, traffic engineering.

1. Introduction

The growth of multimedia applications over wide area networks has increased research interest in quality of service (QoS). The communication delay and synchronization needed for voice, data and images are major concerns. Internet telephony (voice over IP) and other multimedia applications such as video conferencing, video on demand and media streaming require service guarantees and have strict timing requirements. The size and quality of display devices, and resources such as central processing unit, battery power and bandwidth (BW) are always limited.

Quality of service can be parameterized as throughput, delay, delay variation (jitter), loss and error rates, security guarantees and so on, that are acceptable in an application. As such, QoS depends on characteristics of applications. For instance, the variation in delay, the difference between the largest and the smallest delay, is called delay jitter and jitter is an important quality for Internet protocol (IP) telephony, which can tolerate a certain percentage of packet loss without any degradation of quality. For data transfer, loss is a crucial QoS parameter.

Internet is also more frequently used to control real time industrial system such as power plants or car production chains. All these applications should guarantee some features of the network with regard to the quality of transmission flows but with different criteria.

Quality of service control requires an understanding of the quantitative parameters at the application, system and network layers. This paper concerns the way we can achieve QoS at network layer and more precisely in an Internet service provider (ISP) network. The ISP networks are essential for QoS because they assume the transit of flows at the network core. The problem is that very often the ISP must increase the capacity of its network resources because of the increase of users' flows. The ISP also notices that some parts of their networks are often congested while other parts are less. The idea developed here is to propose load balancing approaches to allow better performances of ISP networks.

The rest of the paper is organized as follows. Section 2 presents a state of the art of QoS in Internet. Section 3 concerns more particularly traffic engineering (TE) and illustrates this technique to improve QoS by examples of the models based on multiprotocol label switching (MPLS). Section 4 shows periodic multi-step algorithm (PEMS) – a new model to ingrate differentiated service (DiffServ) and traffic engineering. Finally, Section 5 presents conclusions.

2. Quality of Service in Internet: State of the Art

The convergence of networks and telecommunications networks has resulted in new requirements in terms of quality of service for networks. In this new framework, services based on networks are diverse and therefore have different requirements. One can easily understand that the requirements are different between a telerobotics application and an application on video on demand. As an example, let us consider the case where a cardiologist needs to control a remote robot to perform a heart surgery. We understand that in this context, the network must guarantee a continuous control flow which meets the requirements of real time.

In recent years, a network such as asynchronous transfer mode (ATM) has been designed for this purpose [1] but it was not imposed as architecture to replace transmission control protocol/Internet protocol (TCP/IP) model. ATM is often limited to function as a lower layer of the Internet. As ATM is not used as an end-to-end protocol, the Internet still works in best effort manner. This model does not meet the requirements of service quality for all applications. Indeed, the main difficulty in achieving this objective is the bottleneck limiting the services provided by Internet routers. A main reason lies in the functioning of interior gateway protocols of Internet. These protocols tend to route packets according to one privileged path regardless the load. As a consequence, it is the unbalanced distribution of the load on the networks of Internet service providers. They try to solve problems of congestion through the regular adding of new resources to increase the bandwidth offered by the most congested roads. But this is a short-term solution that is quickly inadequate and costly.

In recent years several studies were interested in providing more robust answers to this problem. We can classify them into two main categories. The first category is the work aiming to accommodate the phenomena of congestion. The second category concerns efforts to develop models to better distribute the flow in a network. This is called traffic engineering.

The general idea of work to accommodate the phenomenon of congestion is to define classes of traffic, so that each router handles a flow of each class according to their respective priority rules. So it breaks with the usual first in first out technique, and a flow of a priority class may be sent before the other, even if received last. The implementation of this approach also relies on the use of appropriate scheduling techniques implementing the priority rules of each class. Among the principal techniques for scheduling, we can cite the generalized processor sharing (GPS), which is a theoretical ideal technique but impossible to implement in a network based on packet switching, because the emission of packets is not preemptive. Other sequencing techniques have been proposed to achieve results similar to those of GPS: weighted fair queue (WFQ) or W2FQ [2]. In this context, two main models have been tested by the Internet Engineering Task Force (IETF): the Intserv [3] and Diffserv model [4].

The Intserv is based on the definition of micro flow that crosses routers in a domain. The maintenance of a path requires the regular exchange of messages between pairs of routers to indicate that the path is still in service. Maintaining a soft state by micro flow in each crossed router, as well as the scheduling of these flows, creates a complexity that makes Intserv not scalable.

Diffserv (DS) is based on the aggregation of flows into a reduced number of classes divided into three categories of services: expedited forwarding (EF), assured forwarding (AF) and best effort (BE) service. The EF service meets the requirements of reliable and real-time traffics (low delay and low jitter). The AF service provides the bandwidth required for applications such as video over IP. The limited number of flow, the simplicity of scheduling algorithms and the limitation of the most complex mechanisms at ingress routers make Diffserv a scalable model.

In terms of traffic engineering, there are two scopes: one corresponding to pure IP networks [5] and another based on the use of multiprotocol label switching. The MPLS is suitable in the networks of Internet service providers because it allows establishing paths in architecture that basically operate in disconnected mode. In this context, the works that are generally developed propose models to select a set of candidate paths (CPs) that meet specific criteria of QoS. The combination of criteria is generally a NP-complete problem. This leads to propose heuristics such as MPLS adaptive traffic engineering (MATE) or load distribution in MPLS (LDM) that will we describe in Section 3.

To reconcile the advantages of Diffserv and TE, one looks now to their integration: it is the DS-TE model. The objective of DS-TE is to ensure an end-to-end QoS meeting the requirements of a given flow. The approach does not consist to define paths with the same quality as in the case of conventional traffic engineering. It has also different QoS routing that proceeds hop by hop. The idea of DS-TE is to define traffic classes of which are allocated priorities to be assigned to a layered service providers (LSPs). These traffic classes can share same links in a network using different modes of bandwidth management such as max allocation with reservation bandwidth constraints [6], [7] or "Russian doll" management [8]. This requires the development of techniques allowing a preemption flows belonging to a higher-priority class to assure LSP meets their requirements instead of a stream belonging to a lower-priority class [9].

The reader will find in [10] a more complete survey of the state of the art, in the integration of traffic engineering and Diffserv for DS-TE.

3. Illustration of Traffic Engineering in a MPLS Network

Several models are proposed in the literature to perform traffic engineering based on MPLS. In this section, we consider particularly three models: MATE, LDM and LBWDP (load balancing over widest disjoints paths). Theses models will be compared with traffic bifurcation (TB) that is a mathematical formulation of route optimization problem [10], [11]. It is a theoretical model that cannot be implemented online because it requires knowing a priori all flows that must be routed. So it gives a reference to compare the different propositions.

3.1. MPLS Adaptive Traffic Engineering

The main goal of MATE [12] is to avoid network congestion by adaptively balancing the load among multiple paths based on measurement and analysis of path congestion. This approach uses a constant monitoring of the links using probe packets to evaluate link properties such as packet delay and packet loss. Using these statistics the MATE algorithm is able to optimize packets repartition among multiple paths to avoid link congestion.

Formally a MATE network is modeled by a set L of unidirectional links. It is shared by a set S of ingress-egress (IE) node pairs, indexed $1, 2, 3, \ldots, S$. Each of these IE pairs s has a set $P_s \subseteq 2^L$ of LSPs available to it. The P_s are disjoint sets. An IE pair s has a total input traffic of rate r_s and routes x_{sp} amount of it on LSP $p \in P_s$ such that

$$\sum_{p \in P_s} x_{sp} = r_s \,, \quad \text{for all} \;\; s \,. \tag{1}$$

Let $x_s = (x_{sp},\ p \in P_s)$ be the rate vector of s, and $x = (x_{sp},\ p \in P_s,\ s \in S)$ the vector of all rates. The flow on a link $l \in L$ has a rate that is the sum of source rates on all LSPs that traverse link l:

$$x^l = \sum_{s \in S} \sum_{l \in P,\, p \in P_s} x_{sp} \,. \tag{2}$$

Associated with each link l is a cost $C_l(x^l)$ as a function of the link flow x^l. We assume that, for all l, $C^l(\cdot)$ is convex. Its objective is like this:

$$\min_x C(x) = \sum_l C_l(x^l) \tag{3}$$

$$\text{subject to} \sum_{p \in P_s} x_{sp} = r_s \quad \text{for all} \;\; s \in S \tag{4}$$

$$x_{sp} \geq 0, \quad \text{for all} \;\; p \in P_s,\ s \in S \,. \tag{5}$$

A vector x is called a feasible rate if it satisfies Eqs. (4) and (5). A feasible rate x is called optimal if it is a minimum of the problem Eqs. (3)–(5). A standard technique to solve the constrained optimization problem, Eqs. (3)–(5) is the gradient projection algorithm. In such an algorithm routing is iteratively adjusted in opposite direction of the gradient and projected onto the feasible space defined by Eqs. (4) and (5). The complexity of this algorithm is $O(n^2)$. The designers of MATE have proved in [12] that it converges to an optimal routing when specific conditions are verified (see Theorem 2, page 4 in [12]).

3.2. Load Distribution in MPLS Network

Depending on the dynamic network status, LDM [13] selects a subset of the LSPs (candidate path set) for an ingress-egress pair, and distributes traffic load among those LSPs. Let L_{ij} denotes the set of all LSPs set up between an ingress node i and an egress node j, and let A_{ij} the corresponding candidate LSPs, then $A_{ij} \subseteq L_{ij}$. Initially, A_{ij} is set as follows:

$$A_{ij} = \{\text{LSPs from } i \text{ to } j \text{ with the smallest hop count and with the utilization rate lower than } \eta_0\} \,.$$

The utilization rate of an LSP, $u(l)$, is defined as the maximum of the utilization value of the links along the *LSP l*, and let $h(l)$ denotes the hop count of *LSP l*. The *utilization rate of a candidate paths set* A_{ij} is defined as following:

$$U(A_{ij}) = \min\left[u(l),\ \forall\, l \in A_{ij}\right]. \tag{6}$$

The LDM decides whether to expand the candidate LSP set based on the congestion level of candidate paths set. If $U(A_{ij}) \geq \rho$, then LDM further expands A_{ij}. The expansion of A_{ij} continues, considering LSPs in L_{ij} in the increasing order of hop count until $U(A_{ij}) < \rho$ or there is no LSP left in L_{ij} for further consideration.

Generally, an *LSP* $l \in L_{ij}$ with $h(l) = (h(\text{shortest } LSP) + m)$ should satisfy the following two conditions to be eligible for A_{ij}:

1. $u(l) < \max[u(k),\ \forall k \in A_{ij}]$,
2. $u(l) < \eta_m$, where $\eta_m < \eta_n$ for $m > n$.

The first condition means LDM utilizes the LSPs with more extra hops if they have lower utilization than the LSP that has the highest utilization among the LSPs in the current A_{ij}.

The second condition implies links with an utilization rate higher than η_m can only be used by the LSPs with less than m extra hops.

The candidate path set could either be pre-computed when there are some significant changes in the dynamic network status or be computed on demand for a new arriving user flow request. This is done in a $O(n^2)$ time in the worst case, and n refers here to the number of available paths between the ingress-egress pair of routers. For each incoming traffic flow, LDM randomly selects an LSP from the candidate LSP set according to a probability distribution function. This probability is inversely proportional to number of hops in the path. At the opposite, it is proportional to the utilization rate of the LSP. The complexity of the LDM splitting procedure is $O(n)$. Here n refers to the number of candidate paths selected at the end of the previous step and belonging to the set A_{ij}.

Let us notice here that instability can affect LDM because of oscillations due to candidate path selection. This oscillation problem can be solved using two thresholds. In [14] the authors propose a new version of LDM that corrects the instability of the original model. One of the disadvantages of LDM is to ignore the residual capacity of a path before assigning it a new traffic.

3.3. Load Balancing over Widest Disjoints Paths Algorithm

This model uses the selection path algorithm proposed by widest disjoint paths (WDP) algorithm [15] and a splitting algorithm called prediction of effective reparti-

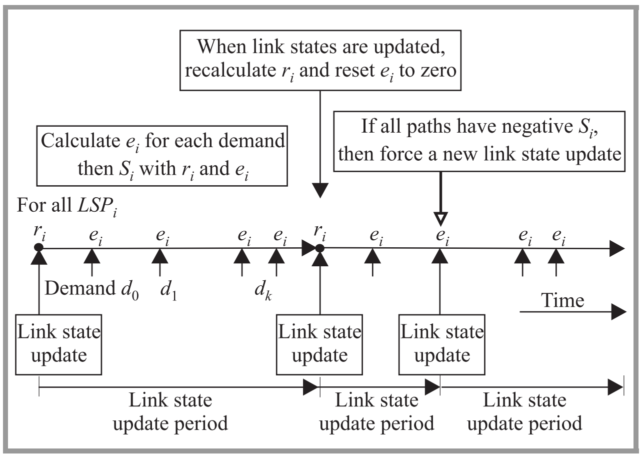

Fig. 1. Illustration of the principle of PER.

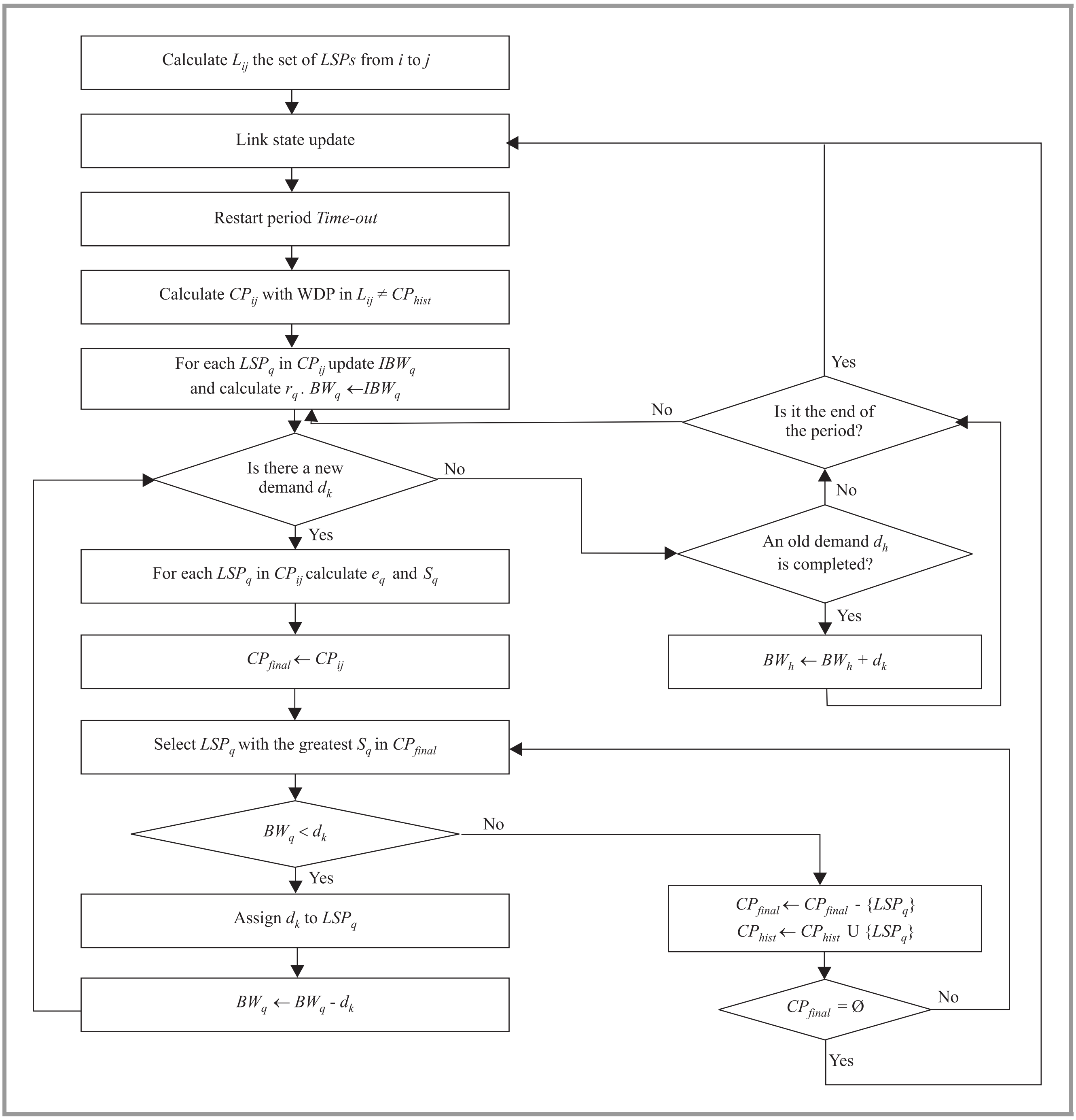

Fig. 2. Flowchart of PER algorithm.

tion (PER) [16]. PER is an improvement of LDM splitting algorithm. PER is designed to take into account the capacity of the selected path when it assigns a new traffic. The basic idea is that each ingress node takes into account its previous assignments of traffics to the different paths it manages. At each time, it must know the residual capacity of each of its paths to reach a given destination. However, local management made by each ingress node is necessarily partial. Indeed, an ingress node A is in competition with other nodes that can handle paths sharing links with the paths from A. Therefore the vision of the node A must reflect the actual state of the paths it manages. To do this, the idea developed by PER is to establish a periodic routing plan. Before beginning a given period, the node uses link state update to obtain the residual bandwidth of each path it manages. At the beginning of the period it has a perfect vision of the state of those paths. Then, during the period the state of its paths is updated in terms of assignments done. Knowing that there will be drifts, at the end of each period it performs a new update to prepare the routing plan of the next period. Figure 1 gives an illustration of the principle of PER.

During each period, the routing for a given destination is based on the calculation of the theoretical distribution of each path managed by the ingress router for a given destination. This calculation is based on Eq. (7). Let $A_{ij} = \{l_1, l_2, \ldots, l_n\}$ be the set of candidate paths from ingress node I to egress node J. It takes into account criteria like the hop count $h(k)$ of each path and the residual bandwidth capacity $b(k)$, where k is the index of a LSP in A_{ij}:

$$r_k = p_0 \frac{H}{h(k)} + p_1 \frac{b(k)}{B} \quad \text{with} \quad p_0 + p_1 = 1\,, \tag{7}$$

where: H is the constant to make the sum of the probabilities that are inversely proportional to the hop count of an LSP:

$$H = \frac{1}{\sum_{k=1}^{n} \frac{1}{h(k)}}\,, \tag{8}$$

coefficient B is the sum of residual bandwidth of all the LSPs in A_{ij}:

$$B = \sum_{k=1}^{n} b(k)\,, \tag{9}$$

p_0, p_1 are parameters of the model fixed by the network manager depending on its requirements.

During a period after each new request assignment, the ingress router computes the effective repartition rate e_k of each path using Eq. (10). This rate is calculated simply by considering the amount of traffic requests assigned to a path compared with the sum of all the requests routed to a destination by all paths in A_{ij} during the period:

$$e_k = \frac{\sum_{p=1}^{m(k)} d_p^k}{\sum_{q=1}^{m} d_q}\,, \quad \text{where} \quad \sum_{k=1}^{n} \sum_{p=1}^{m(k)} d_p^k = \sum_{q=1}^{m} d_q\,, \tag{10}$$

where: $m(k)$ is the number of flow traffics assigned to LSP number k between the n LSPs of set A_{ij},

m is the total number of flow traffics the considered ingress router has to route to router J: $m = \sum_{i=1}^{k} m(k)$,

d_p^k is the traffic amount of the p demand assigned to LSP number k,

d_q is the q traffic flow routed by the ingress node with a LSP of the set A_{ij}.

For each incoming flow, the ingress router calculates a relative distribution rate S_k for each k:

$$S_k = \frac{r_k - e_k}{r_k}\,. \tag{11}$$

This relative distribution rate enables selecting effectively the LSP which is assigned the flow. This LSP must verify the following 3 conditions:

1. S_k must be positive. This means that the effective distribution rate is below its theoretical rate. Therefore it is possible to increase its load.

2. The requested bandwidth $BW(d_k)$ must be less than $b(k)$ the residual bandwidth of the LSP.

3. There is no LSP verifying the conditions 1 and 2 with a greater S_k.

If there is no LSP to verify the conditions for delivering the demand then the router must force the update of data of path before the end of the period. This forced update enables to build a new set of candidate paths and consequently to establish a new routing plan based on this set. In case of failure, the demand must be distributed over several LSPs. Figure 2 summarizes how PER works.

3.4. Evaluation of Different TE Models Based on MPLS

In literature each of the presented models is said by the authors as being the best. Also to get an idea of the quality of the different models presented in this section, we have evaluated them by simulations. All simulations have been performed on the same architecture. For the sake of simplicity, let us consider the architecture given by Fig. 3 to compare their relative performances. The simulations have been conducted with the simulator NS2.

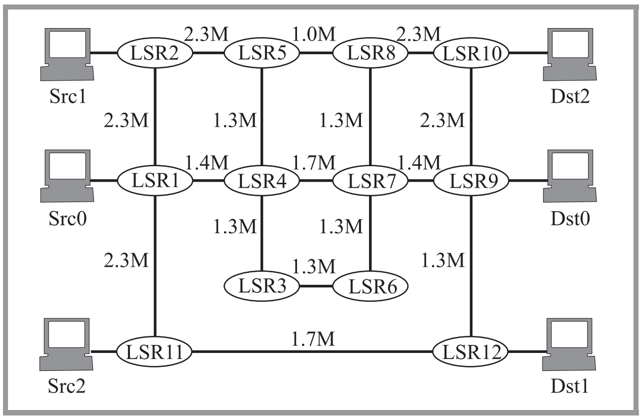

Fig. 3. Simulation topology. Explanations: LSR – label switch router, Src – source router, Dst – destination router.

For each model for TE we have used the same profile of traffic. This profile has the following characteristics:

– the volume of each individual demand is 300 kbit/s;

– the source and destination pairs are Src0-Dst0, Src1-Dst1 and Src2-Dst2, selected randomly;

– one flow generated in certain time is stopped in a random time;

– we adapt a time based triggering as a triggering policy and update link state every 3 s;

– the delay of each simulation is 150 s.

Figure 4 presents the results obtained by the different models. In order to have a reference one has represented on the same graph the curve corresponding to the theoretical model TB. Note that the curve of TB was not obtained by simulation in NS2 but by calculation in Matlab. The goal is to have a reference to compare with the proposed heuristic models. As we can see, MATE and LBWDP have comparable results, close to TB. At the opposite, LDM presents a utilization rate that may exceed 100%. This reflects the fact that LDM does not verify that the selected LSP owns a capacity of residual bandwidth enough to support the demand.

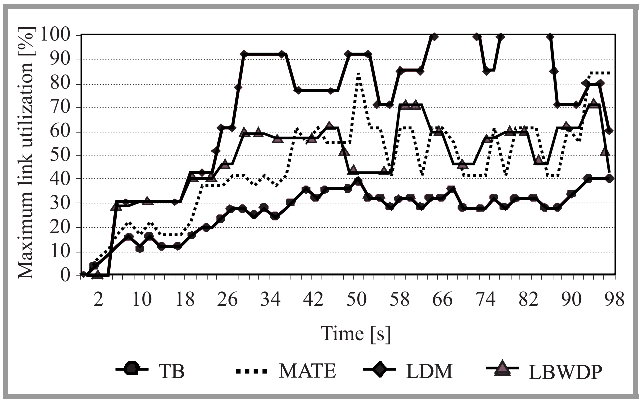

Fig. 4. Simulations results.

Our simulation results showed that LBWDP is one of the best algorithms for traffic engineering because with a priori decision its balance of flows is comparable with the results given by TB.

4. Periodic Multi-Step Routing Algorithm for DS-TE

In this section, we propose new DS-TE model for the intra-domain network, called PEMS [16], to give the differentiated services for the three classes defined in Diffserv.

The PEMS is composed of three phases. The preprocessing phase is achieved off-line and extracts good paths of all possible paths which can include every link at least once within them for each source-destination pairs using only topology information. These paths are kept until the topology is changed.

When a traffic demand arrives, it uses PER algorithm to select one LSP to carry current flow. Many QoS metrics such as hop-count, available bandwidth and delay constraints are considered before the path selection assignment. In PEMS, hop-count and disjointedness are used in the pre-processing phase together with available bandwidth and measured delay in the cost function to establish splitting ratios. PEMS basically aims to minimize the maximum link utilization like LBWDP algorithm and additionally to give different service quality to each class, especially to guarantee the low delay to EF class. But it has two differences in that PEMS uses measured delay $de(i)$ instead of hop-count and that it adapts different p_0, p_1 values according to the class, in contrast to LBWDP, which uses the same parameter values regardless of class. To establish the routing plan for each period, PEMS uses Eq. (12) that is an adaptation of Eq. (7) used by LBWDP:

$$r_i = p_0 \frac{D}{de(i)} + p_1 \frac{b(i)}{B} \quad \text{with} \quad p_0 + p_1 = 1\,. \tag{12}$$

In Eq. (12), D is a constant to make the sum of the probabilities that are inversely proportional to delay of an LSP_i, $de(i)$. Formally D is defined as it follows:

$$D = \frac{1}{\sum_{i=1}^{k} \frac{1}{de(i)}}\,. \tag{13}$$

In this model, bandwidth is associated with delay for differentiating the traffic at the flow level. Bandwidth has a bigger weight p_1 for AF class, while delay has a bigger weight p_0 for EF class. Adaptation of selective parameters is used to give different weight according to the metric important of each class. PEMS puts the weight parameters, p_0 and p_1, of each class as follows.

In Table 1, for EF class, p_0 is bigger than p_1 in order to give preference to LSP in BP_{ij} that owns the best delay than residual bandwidth because this class is for delay-sensitive traffic. For AF class, the criterion is inversed and so parameter p_1 is greater to express the preference of LSPs with important residual bandwidth.

Table 1
Example of parameter values for the three classes of traffic

Class	EF	AF	BE
p_0	0.7	0.3	0.5
p_1	0.3	0.7	0.5

This stage can be ameliorated by adapting dynamically the parameters of the splitting ratio equation depending on the network state.

Figure 5 gives PEMS flowchart to summarize how it works. The meaning of notations are as follows:

– $de(i)$: delay of LSP_i;

– $b(i)$: residual bandwidth of LSP_i;

– CP_{EF}, CP_{AF}, CP_{BE}: candidate path set for EF class, AF class and BE class, respectively;

– d^k_{cc}: kth demand with class cc;

– CP_{cc}: current class (one in CP_{EF}, CP_{AF} or CP_{BE});

– $CP^{cc}_{potential}$: subset of CP_{cc} corresponding to LSP_i that can process the requested demand d^k_{cc}.

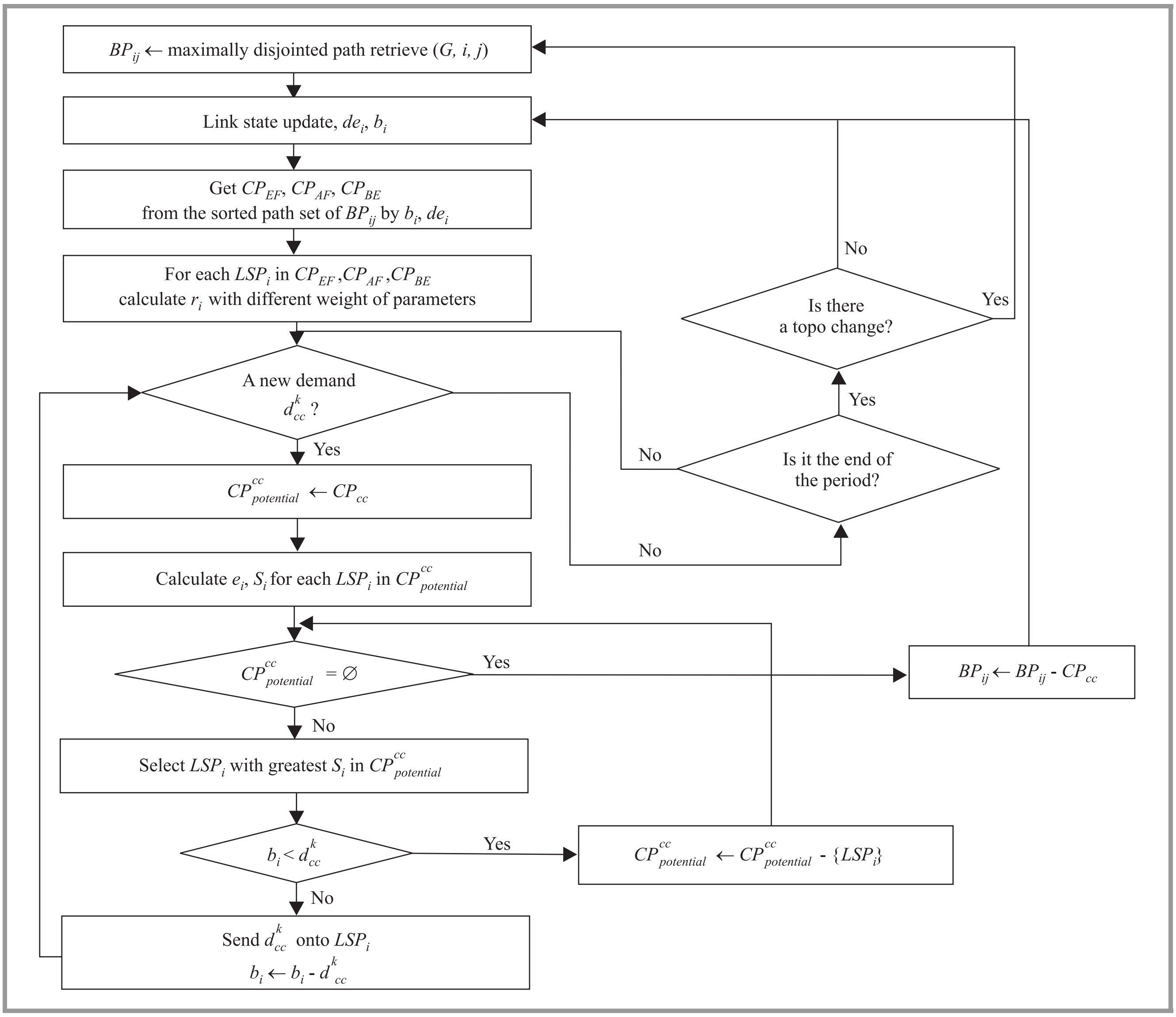

Fig. 5. PEMS flowchart.

In the online mode, when link state information are updated, new candidate paths for each class are calculated, based on updated information, such as measured delay and residual bandwidth. At this point, we use metric ordering by delay and residual bandwidth. This phase selects multiple low-delayed paths in the ordered paths set as candidate paths of delay-sensitive traffic and selects multiple paths having more residual capacity for the traffic to which the bandwidth is important for multipath routing to each traffic class.

Several simulations on multiple architectures have been done to assess PEMS in comparison with LBWDP. Different architectures have been generated using the generator BRITE, trying to be as close as possible to connectivity in a MPLS area. All simulations were conducted with MPLS network simulator for NS2 (MNS). In order to obtain comparable results for the two models, for each architecture we have defined traffic scenarios to apply to both models. In each simulation the goal is to transfer requested traffics between pairs of routers. Requested traffics are generated every 2 s and are all at a rate of 500 kbit/s. They belong to one of the three differentiation class (EF, AF or BE). The class is selected randomly but is the same for both models. Each traffic is stopped after a delay common for the two models. Every 3 s, each router performs its link state update to refresh the routing model parameter.

The first simulations were based on architectures of tens nodes in order to simultaneously verify the correctness of PEMS model and to compare it with LBWDP. Figure 6 illustrates the type of architecture generated by BRITE for 31 nodes. Figure 7 shows the obtained results with regard to delay criteria. These results shows that PEMS dealys differentiate the flows of the three classes. Indeed, for each architecture, the average delay obtained with PEMS for the class EF is smaller than for the delay of class AF traffic which is smaller than the delay experimented by class BE traffic. For LBWDP, one can see, for example, that for 10 or 20 nodes EF traffics results in a poorer delay.

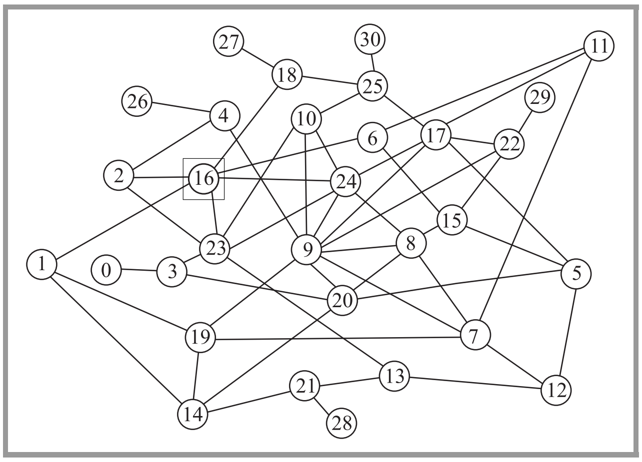

Fig. 6. Example of topology generated by BRITE for 31 nodes.

The second category of simulations where based on architectures of several hundred nodes. In this case, our main goal was to verify capacity to optimize traffic splitting in a dense architecture. Another goal was to verify the scalability of models, but this problem is out of the scope of this paper. For traffic splitting, simulations do not take care of the class of the traffic. In this case the comparison criterion is link utilization. The simulations give both maximum link utilization and average link utilization. Indeed, maximum link utilization indicates if a model privileges some paths. The average link utilization measures the average of utilization rate of all the links used in architecture. Thus if this average is low, many more links of the architecture have been used.

The results illustrated in Fig. 8 prove that LBWDP better balances the traffic in the network as it does not take account of each traffic class to route.

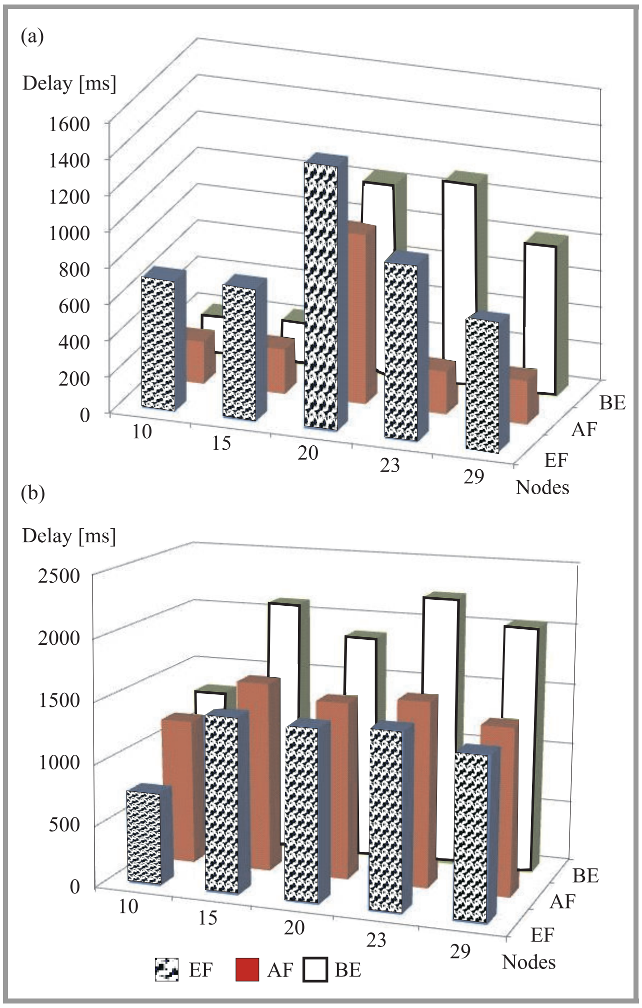

Fig. 7. Performance benchmarking between (a) LBWDP and (b) PEMS with regard to average delay.

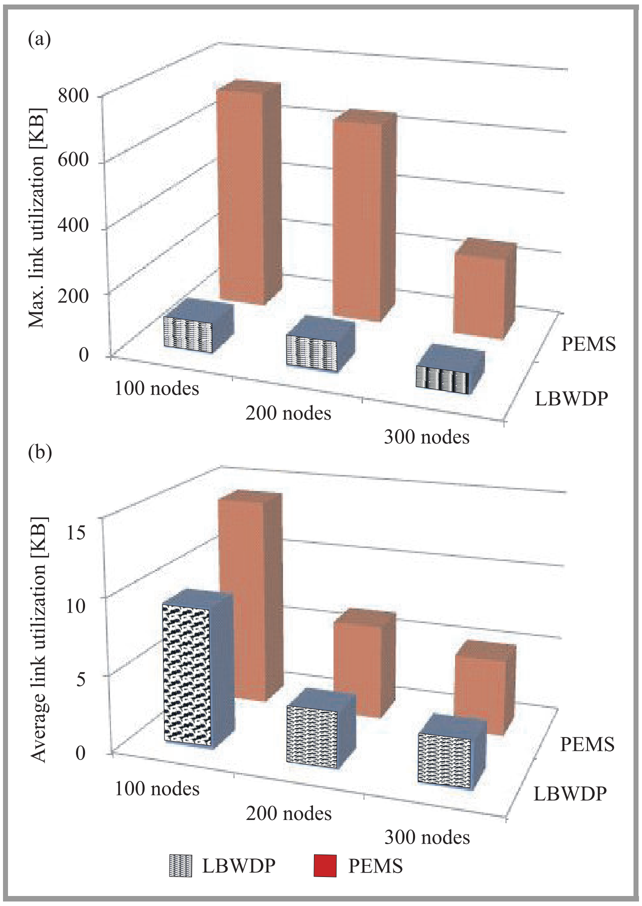

Fig. 8. Performance benchmarking between LBWDP and PEMS: (a) maximum and (b) average link utilization.

5. Conclusions

Multiprotocol label switching offers many advantages to service providers. In order to support today's various kinds of applications, the system needs to guarantee the quality of service. However, MPLS is incapable of providing differentiated service levels in a single flow. Hence MPLS and DiffServ seem to be a perfect match and if they can be combined in such a way to utilize strong points of each technology it can lead to a symbiotic association that can make the goal of end to end QoS feasible. DiffServ aware traffic engineering mechanisms operate on the basis of different Diffserv classes of traffic to improve network performance and extend the base capabilities of TE to allow route computation and admission control to be performed separately for different classes of service. Algorithms like PEMS seem to be a good compromise between improvement of resource utilization and the QoS required by end users.

A problem not addressed here is the comparison of PEMS to other models in terms of scalability. Our actual simulations results suggest that PEMS is scalable. This must be verified by simulations confirming a polynomial complexity of its algorithms. We think that PEMS must be scalable since this complexity concerns only the edge router of a MPLS network.

These models have yet to be assessed on real hardware architecture in order to confirm the performance illustrated by the simulations. Another important perspective is the ability to adapt models such as PEMS to the guarantee of quality of service of end-to-end communications. This poses the problem of application of DS-TE routing to inter-domains.

References

[1] A. Alles, "ATM internetworking", in *Proc. Eng. InterOp Conf.*, Las Vegas, USA, 1995.

[2] J. C. R Bennett and H. Zhang, "WF2Q: worst-case fair weighted fair queueing", in *Proc. IEEE Infocom'96 Conf. Comput. Commun.*, San Francisco, USA, 1996.

[3] R. Braden, D. Clark, and S. Shenker, "Integrated service in the Internet architecture: an overview", RFC 1633, June 1994.

[4] D. Black, M. Carlson, E. Davies, Z. Wang, and W. Weiss, "An architecture for differentiated service", RFC 2475, Dec. 1998.

[5] B. Fortz, J. Rexford, and M. Thorup, "Traffic engineering with traditional IP routing protocols", *IEEE Commun. Mag.*, vol. 40, no. 10, pp. 118–124, 2002.

[6] J. Ash and W. S. Lai, "Max allocation with reservation bandwidth constraints model for Diffserv-aware MPLS traffic engineering and performance comparisons", RFC 4126, June 2005.

[7] F. Le Faucheur, "Maximum allocation bandwidth constraints model for Diffserv-aware MPLS traffic engineering", RFC 4125, June 2005.

[8] F. Le Faucheur, J. Boyle, W. Townsend, D. Skalecki, K. Kompella, and T. D. Nadeau, "Russian dolls model for DS-TE", RFC 4127, June 2005.

[9] F. Le Faucheur, J. Boyle, W. Townsend, D. Skalecki, K. Kompella, and T. D. Nadeau, "Protocol extensions for support of Diffserv-aware MPLS traffic engineering", RFC 4124, June 2005.

[10] K. Lee, "Modèle global pour la qualité de service dans les réseaux de FAI: intégration de DiffServ et de l'ingénierie de trafic basée sur MPLS", Ph.D. thesis, Ecole Centrale de Lille, France, 2006.

[11] Y. Lee, Y. Seok, Y. Choi, and C. Kim, "A constrained multipath traffic engineering scheme for MPLS networks", in *Proc. IEEE ICC'2002 Conf.*, New York, USA, 2002.

[12] A. Elwalid, C. Jin, S. Low, and I. Widjaja, "MATE: MPLS adaptive traffic engineering", in *Proc. Infocom'2001 Conf.*, Anchorage, USA, 2001, pp. 1300–1309.

[13] J. Song, S. Kim, and M. Lee, "Dynamic load distribution in MPLS networks", in *Proceedings of ICOIN 2003*, Lecture Notes in Computer Science, vol. 2662. Heidelberg: Springer, 2003, pp. 989–999.

[14] K. Lee, A. Toguyéni, and A. Rahmani, "Hybrid multipath routing algorithms for load balancing in MPLS based IP network", in *Proc. AINA'2006 Conf.*, Vienna, Austria, 2006, pp. 165–170.

[15] N. Srihari and Z. Zhi-Li, "On selection of paths for multipath routing", in *Proc. IWQoS'01 Conf.*, Karlsruhe, Germany, 2001.

[16] K. Lee, A. Toguyéni, and A. Rahmani, "Periodic multi-step routing algorithm for DS-TE: PEMS", in *Proceedings of the CAiSE07 Workshops and Doctoral Consortium*, Lecture Series on Computer and Computational Sciences, vol. 2. Berlin/Heidelberg: Springer, 2006, pp. 1–4.

Armand Toguyéni was born in Dakar, Senegal, in 1964. He obtained in 1988 the engineer Diploma of the Institut Industriel du Nord (French Grande Ecole) and the same year his Master degree in computer sciences. He obtained a Ph.D. in automatic control for manufacturing and discrete events systems in 1992 and his Habilitation à Diriger des Recherches in 2001. He is a Professor of computer sciences and computer networks at the Ecole Centrale de Lille, France. He has in charge the Department of Computer Sciences of the Institut de Génie Informatique et Industriel de Lens. His research interests is the quality of service of D.E.S. More particularly one of his topic research is the design of new model to improve QoS in Internet. His research also concerns the development of networked control systems.

e-mail: Armand.Toguyeni@ec-lille.fr
LAGIS, Ecole Centrale de Lille, Cité scientifique – BP 48
59651 Villeneuve d'Ascq Cedex, France

Ouajdi Korbaa obtained in 1995 the engineering Diploma from the Ecole Centrale de Lille, France, and in the same year, the Master degree in production engineering and computer sciences. He is Ph.D. in production management, automatic control and computer sciences, of the University of Sciences and Technologies of Lille, France, since 1998. He also obtained, from the same university, the Habilitation à Diriger des Recherches degree in computer sciences in 2003. He is full Professor in the University of Sousse, Tunisia, and Director of the E-learning Department. He published around 70 papers (journals, plenary sessions, books chapters and conferences) on scheduling, performance evaluation, optimization, design, and monitoring. His current research field is the discrete optimization and more particularly cyclic scheduling, production planning, networks QoS optimization. He is reviewer for different journals and conferences. He is references by the "Who'sWho" in science and engineering editions of 2004, 2006, and 2008.

e-mail: ouajdi_korbaa@yahoo.fr
ISITC, Laboratory LI3, University of Sousse
5 bis, rue du 1er Juin 1955
Hammam Sousse 4011, Tunisia

Invited paper

100/1000 Gbit/s Ethernet and beyond

Marian Marciniak

Abstract—100 Gbit/s Ethernet is foreseen in metro and access by 2014, while 1 Tbit/s Ethernet is forecasted for trunk links before 1020. This paper reviews the advantages and constraints of the optical networking and discusses how they meet the 100 Gbit/s Ethernet needs.

Keywords*— *converged networks, dense wavelength division multiplexing, high-speed Ethernet, optical networking, transparent optical networks.

1. Introduction

Ethernet, being originally a computer networking protocol, nowadays is able to unify long distance, metro and access networking into a single network of the future [1]. The deployment of fibre-to-the-home (FTTH) in access observed in Japan, Korea, US and Europe will assure a broad bandwidth for the user at an affordable cost [2].

The previous decade has upgraded optical fibre transmission with the transparency of the links and with a possibility of long distance dense wavelength division multiplexing (DWDM) transmission with hundreds or thousands of independent transmission channels within a single fibre. However, while DWDM network application for voice and data transmission is already in a mature and highly sophisticated stage, novel kinds of traffic and services can be allocated to optical systems, and attempts to develop hybrid architectures for circuit and packet switched networks were reported recently [3]. Fixed and mobile communications will continue to converge coming years.

The next generation networking (NGN) initiative has been recently adopted by the International Telecommunication Union (ITU) as a goal to be achieved during study period 2005–2008 [4]. It is generally recognized that the Internet will support the majority of services offered by NGN both in access and in backbone, however a careful selection and separation of the services in the network is a necessary condition to assure the quality of service (QoS) and security. Consequently, the concept of NGN assumes the connectionless traffic be used for any kind of services even those that traditionally have been realized as a circuit switched connection traffic provided the average packet networks characteristics allow for satisfactory level of quality of service.

In parallel to classical point-to-point circuit switched connections, Internet traffic and packet services are globally and increasingly used for a variety of services. It is generally but apparently erroneously accepted that the packet traffic should replace the circuit-switched traffic everywhere, provided QoS and security issues are resolved satisfactorily. In fact that is criticized in this paper, and an optimal hybrid solution satisfying the needs and constraints of both real-time and packet services is proposed here. Indeed, the Internet as being based on a "best-effort" principle and carrying traffic of statistic nature is inherently vulnerable as QoS and security is concerned. The golden age of the Internet when it was a network connecting exclusive scientific community has passed for ever. Now everybody can access the Internet, and obviously not honest people also. In contrary, mass attacks towards the global Internet network or towards dedicated important targets seem to be inevitable in not a distant future.

The expansion of Internet traffic worldwide forces the global communication community to shift from classical circuit switched connection oriented networks to modern packet switched, connectionless transmission of data, with a strong interest in guarantees of the network reliability and availability as well as the security of the information and of the infrastructure, generalized mobility, etc. This revolutionary change is reflected in the International Telecommunication Union policy on the next generation networks. Consequently, NGN are expected to be deployed widely starting from the ITU study period 2005–2008, and this will be continued under the network of the future under the study period 2009–2012.

Consequently, communication networks target to transmit a variety of services. Those are not only classical voice telephony and facsimile transmission, but also the Internet traffic, data transmission, radio and digital television broadcasting (IPTV). Consequently, a variety of transmission media are used in access as metal and fibre cables, and microwave, millimeter wave, and optical free space communication links. However, owing to top performance of contemporary optical fibres there is a tendency to deploy fibres as far close to the end user as possible [5]. Thus fibres are used not only for digital voice or Internet traffic transmission, but also for expanding radio-over-fibre transmission applications that exploit the optical carrier wave amplitude modulation with a microwave carrier [6], [7], including analogue cable television transmission.

A question arises: why higher speed Ethernet? Fundamental bottlenecks are happening everywhere. Increased number of users together with increased access rates and methods and increased services results in explosion of bandwidth demand. Computing speed and system throughput doubles approximately every two years.

Networking is driven by the aggregation of data from multiple computing platforms. As the number of computing platforms grows fast, this results in a multiplicative effect on networking [8].

2. The 100 Gbit/s Ethernet Challenges

Ethernet is now widely adopted for communications in local area networks (LANs) and in metropolitan area networks (MANs). The Ethernet is facing the next evolutionary step towards 100 Gbit/s Ethernet (100GbE) [8]. As Ethernet becomes more prevalent, the issues related to the software, electronics, and optoelectronics need to be addressed. This becomes more evident for 100GbE, since that technology does not simply refer to high bit rate transmission at 100 Gbit/s, but also relates to switching, packet processing, and queuing and traffic management at 100 Gbit/s line rate. This is in parallel with a remarkable progress in transmission as 10 Gbit/s and recently 40 Gbit/s systems have become commercially deployed standards in optical networking, and multiplying the total aggregate capacity by an use of DWDM technology and transmitting simultaneously several wavelength channels. This has faced problems in view of fibre impairments, one of the most serious ones being fibre polarization mode dispersion (PMD). In particular, care has to be taken to minimize PMD coefficient when manufacturing the fibres and cables. As communication system throughput doubles roughly every 2 years, this implies the following network throughput roadmap [9]: 10 Gbit/s in 2007, 40 Gbit/s in 2011, 100 Gbit/s in 2014, 160 Gbit/s in 2015?, 640 Gbit/s in 2019?

It should be noted that industry experts claim a standard for 1 Tbit/s Ethernet will be needed by 2012 [10]! The IEEE Higher Speed Study Group (HSSG) objectives are:

- Support full-duplex operation only.
- Preserve the 802.3/Ethernet frame format utilizing the 802.3 MAC (media access control).
- Preserve minimum and maximum frame size of current 802.3 standard.
- Support a bit error rate (BER) better than or equal to 10^{-12} at the MAC/PLS (physical layer signalling) service interface.
- Support a MAC data rate of 40 Gbit/s.
- Provide physical layer specifications which support 40 Gbit/s operation over:
  - at least 100 m on OM3 multi-mode fibre (MMF) (i.e., 850 nm laser optimized),
  - at least 10 m over a copper cable assembly,
  - at least 1 m over a backplane.
- Support a MAC data rate of 100 Gbit/s.
- Provide physical layer specifications which support 100 Gbit/s operation over:
  - at least 40 km on single mode fibre (SMF),
  - at least 10 km on SMF,
  - at least 100 m on OM3 MMF,
  - at least 10 m over a copper cable assembly.
- Prior experience scaling IEEE 802.3 and contributions to the study group indicates:
  - 40 Gbit/s Ethernet will provide approximately the same cost balance between the LAN and the attached stations as 10 Gbit/s Ethernet,
  - the cost distribution between routers, switches, and the infrastructure remains acceptably balanced for 100 Gbit/s Ethernet.
- Given the topologies of the networks and intended applications, early deployment will be driven by key aggregation and high-bandwidth interconnect points. This is unlike the higher volume end system application typical for 10/100/1000 Mbit/s Ethernet, and as such, the initial volumes for 100 Gbit/s Ethernet are anticipated to be more modest than the lower speeds. This does not imply a reduction in the need or value of 100 Gbit/s Ethernet to address the stated applications.

Concerning compatibility the following actions have been performed:

- The IEEE 802 defines a family of standards. All standards shall be in conformance with the IEEE 802.1 *Architecture*, *Management*, and *Interworking* documents as follows: 802. *Overview* and *Architecture*, 802.1D, 802.1Q, and parts of 802.1f. If any of variances in conformance emerge, they shall be thoroughly disclosed and reviewed with 802. Each standard in the IEEE 802 family of standards shall include a definition of managed objects that are compatible with systems management standards. As an amendment to IEEE 802.3, the proposed project will remain in conformance with the IEEE 802 *Overview* and *Architecture* as well as the bridging standards IEEE 802.1D and IEEE 802.1Q.
- As an amendment to IEEE 802.3, the proposed project will follow the existing format and structure of IEEE 802.3 MIB (management information base) definitions providing a protocol independent specification of managed objects (IEEE 802.1F).
- The proposed amendment will conform to the full-duplex operating mode of the IEEE 802.3 MAC.
- As it was the case in previous IEEE 802.3 amendments, new physical layers specific to either 40 Gbit/s or 100 Gbit/s operation will be defined.

- By utilizing the existing IEEE 802.3 MAC protocol, this proposed amendment will maintain maximum compatibility with the installed base of Ethernet nodes.
- Bandwidth requirements for computing and networking applications are growing at different rates. These applications have different cost/performance requirements, which necessitates two distinct data rates, 40 Gbit/s and 100 Gbit/s.
- Substantially different from other IEEE 802 standards.
- One unique solution per problem (not two solutions to a problem).
- Easy for the document reader to select the relevant specification.

The technical feasibility of 100GbE has been already proven, as well as its confidence in reliability. The principle of scaling the IEEE 802.3 MAC to higher speeds has been already established within IEEE 802.3. Systems with an aggregate bandwidth of greater than or equal to 100 Gbit/s have been demonstrated and deployed in operational environment. The 100GbE project will build on the array of Ethernet component and system design experience, and the broad knowledge base of Ethernet network operation. Moreover, the experience gained in the deployment of 10 Gbit/s Ethernet might be exploited. For instance, parallel transmission techniques allow reuse of 10 Gbit/s technology and testing.

Economic feasibility study includes: known cost factors, reliable data, reasonable cost for performance, and consideration of installation costs [8]. Moreover, the costs of components and systems are defined. For the network aggregation market and core networking applications, the optimized rate offering the best balance of performance and cost is 100 Gbit/s.

3. Transparent Optical Transmission

Here we discuss the optical transparency and its fundamental limitations due to physical constraints as dispersion, polarization mode dispersion, and fibre nonlinearities, and we evaluate the achievable network performance [11].

Erbium-doped fibre amplifiers (EDFA) are nowadays widely exploited in optical transmission links, and their use results in the optical transparency of those links and networks. We understand transparency here as the feature allowing for the optical signal at the output of a link be proportional to the signal at the input. Thus the transparency is an analogue feature of a link.

The notion of transparency has already been applied also for metallic cable based electrical links: those links are so called transparent if the output signal is proportional to the signal at the input. Transparency in optical domain has also its common sense: the medium is transparent if the light goes through. The advent of erbium-doped fibre amplifiers resulted in transparency of optical link, thus in a possibility of wavelength division multiplexing (WDM) transmission.

Wavelength division multiplexing technology is one of the most promising and cost effective ways to increase optical link total throughput. In a WDM system many information channels are transmitted through one fibre using different optical wavelengths modulated by independent data streams. This method is analogous to frequency division multiplexing (FDM) which is widely exploited in other communication systems, especially in radio broadcasting. Using WDM we can easily increase the capacity of already existing fibre links that is particularly significant in the areas where placing new cables is impossible or too expensive. WDM is a technique compatible with the idea of all-optical networks, where one can create transparent optical paths connecting successive network nodes by switching optical channels organized at the different wavelengths.

Unfortunately, in real systems one is faced to the lack of the ideal transparency rather than to the transparency itself. Namely, the signal quality suffers from physical limitations of the fibre, which are the attenuation, chromatic dispersion, and nonlinear distortion. An ideal transparency is not realizable in an optical network, since even an ideal glass fibre exhibits attenuation, chromatic dispersion of the first and higher orders, and glass optical nonlinearities. Moreover, in real fibres polarization mode dispersion results from random local lack of circular symmetry of the fibre due to technology imperfections and local stresses caused by cable layout. Those analogue features of a fibre result in distortion, crosstalk, and noise of the transmitted optical signal. The term PMD is used both in the general sense of two polarization modes having different group velocities, and in the specific sense of the expected value of differential group delay $< \delta\tau >$ between two orthogonally polarized modes. PMD causes the spreading of a pulse in the time domain and it is actually the main transmission distance-limiting factor in 40 Gbit/s systems and above, and as such it became recently a subject of intense research both for fibre optimization and characterization as well [12].

Chromatic dispersion is an inherent feature of an optical link that severely limits the transmission distance of high bit rate data streams. Although dispersion compensating fibres (DCF) are commonly used in order to cope with the chromatic dispersion, they have a substantial drawback as they introduce additional power losses. Another way to combat dispersion effects is to use chirped fibre Bragg gratings as dispersion compensators. The transmission performance of a system with chirped Bragg gratings has been proven to be significantly superior to that of an equivalent DCF module [13].

Nonlinear impairments result directly from the optical nonlinearity of silica glass used as the row material for communication fibres. Modern high-speed DWDM systems are typically built of several transmission spans, each consisting of an erbium-doped fibre amplifier, a single-mode fibre transmission section, and the dispersion compensation section (typically a piece of dispersion compensating fibre or a chirped fibre-Bragg grating). Such cascaded configuration leads to accumulation of the products of nonlinear optical interactions. That in turn results in increase of the optical interchannel crosstalk and degrades the temporal and spectral characteristics of the signal, including the decrease of signal-to-noise ratio (SNR). Consequently, in real transmission links strong limitations for number of channels, channel spacing, bit rate and distance occur due to nonlinear interactions [14].

The most characteristic and essential problem for multichannel optical systems is interchannel crosstalk [15]. In WDM systems the interchannel crosstalk is caused by nonlinear interplay between many different spectral components of the aggregate optical signal. The nonlinear optical phenomena involved are self-phase modulation (SPM), cross-phase modulation (XPM), four-wave mixing (FWM), stimulated Raman scattering (SRS), and stimulated Brillouin scattering (SBS). In spite of the intrinsically small values of the nonlinearity coefficients in fused silica, the nonlinear effects in silica glass fibres can be observed even at low power levels because of very large interaction distances. This is possible because of important characteristics of single-mode fibres, a very small optical beam spot size, and extremely low attenuation.

Major problem of the network upgrade is to know to what extent the already existing infrastructure can be modernized. As a consequence, the network designers should know the limitations for number of channels, maximum transmission speed, as well as the distance between EDFAs. Those system parameters are determined by fibre attenuation, dispersion, and the optical noise level which results from the nonlinear optical phenomena in the silica fibre itself. The transmission system working on higher average optical power is more susceptible to signal distortion caused by nonlinear optical phenomena. Similarly, that problem occurs in multichannel systems because more channels mean higher total optical power in fibre. Signals co-propagating in neighbouring channels strongly interact producing unpredictable noises and decreasing signal-to-noise ratio for signals in different channels. Those phenomena are to be carefully investigated, especially in the case of utilizing new fibre types with decreased dispersion.

The transparent analogue nature of modern fibre communication systems provides a potential to modulate and detect the optical wave power with microwave or millimeter-wave envelope. Broadband wireless signal might be transmitted as an optical wave properly modulated in an analogue way. This works very well in a DWDM network with EDFA. In modern DWDM optical networks, one has to distinguish the physical network infrastructure (fibres and cables) from the virtual infrastructure (wavelengths). A question arises: do we really need separate networks for different services? Or separate fibres in a single network? Why do not use separate wavelengths for that?

An alternative approach to avoid the development of ultrafast electronic circuits is to use advanced modulation formats that achieve 100 Gbit/s information rate while allowing lower transmission rates. In such a case, the implementation will require components operating around 50 GHz and since electronic circuitry for 40 Gbits/s is already commercially available, there will be an easier migration to the development of say 50 Gbit/s capable silicon components.

Finally, for short reach interfaces there have been a number of implementations that provide 10 or 12 parallel 10 Gbit/s lanes for a total aggregate bit rate of 100 Gbit/s or 120 Gbit/s. Such solutions are being currently under discussion in IEEE's HSSG.

There have been a number of efforts to achieve higher data rates in optical communication systems. In the Information Society Technologies (IST) projects FASHION and TOPRATE have been shown that data rates of 160 Gbit/s can be transmitted using optical time division multiplexing (OTDM). Further IST projects address IP-based optical networks and develop concepts for optical packet switched networks, e.g., IST-LASAGNE and IST-IP NOBEL. In optical packet networks, the next logical step after 10GbE is 100GbE. In this regard another IST project is HECTO working on the development of photonic components, transmitter and receiver, for high-performance and high-speed but cost-efficient communication systems. Applications are time division multiplexed optical systems with up to 160 Gbit/s and optical packet networks based on serial 100GbE signals requiring about 110 Gbit/s. The focus of these projects has been in the optical domain rather than realization of cost-efficient components.

The next step in order to increase data rates and speed of the services is the introduction of services based on 100GbE. But 100 Gbit/s transmission is standing on the very beginning and the worldwide level of knowledge and know-how in the field of 100 Gbit/s is still low. A lot of research activities have to be done until the first test links can be prepared for commercial and field exploitation. First of all integrated circuits are necessary which enable transmission equipment, like, e.g., transceivers to provide this high-speed data signal with an adapted modulation technique. To make the technology suitable for exploitation basic physical effects must be investigated in order to use them for a future technology or to minimize or overcome them if they contribute impairments. Only then all the processes for the production of necessary components can be controlled with the desired and necessary reliability. Other challenges like the cost reduction of the components, the reduction of the operational expenses of the network operators and the minimization of the energy consumptions are also a big challenge and subject of research.

Furthermore, since it appears to be very challenging to build 100 Gbit/s transmission link with non-return-to-zero (NRZ) serial modulation of data at such ultra-high rates using current technology (due to the lack of suitable modulators, drivers, amplifiers, etc.), alternative electronic modulation formats could be explored as possible candidates for data multiplexing up to 100 Gbit/s, providing lower symbol rates, more easily handled by available components. Moreover, also parallel transmission approaches can be considered, although this brings along its share of problems, e.g., ensuring equal signal transit times through multiple paths in the cable or printed circuit board (PCB) being subject to bending, temperature variations and other factors expected during installation and operation, plus potentially lower reliability due to multiple interconnections and higher number of components. For network interface, parallel optical transmission schemes are not compatible with current 1GbE and 10GbE standards using single fibre per transmission direction in the network interface and shall be avoided. Use of parallel signal paths inside the 100GbE module and towards the backplane is free of such restrictions and can be considered. A possible solution for 100GbE modulation format can be a pure multi-level amplitude modulation, offering the advantage of lower clock frequency and required signal bandwidth of critical components, e.g., modulators. On the other hand, the robustness of multi-level modulation scheme against such common impairments in the transmission path as optical amplifier noise and fibre dispersion must be carefully analyzed.

The existing 802.3 protocol has to be extended to the operating speed of 40 Gbit/s and 100 Gbit/s in order to provide a significant increase in bandwidth while maintaining maximum compatibility with the installed base of 802.3 interfaces, previous investment in research and development, and principles of network operation and management. The joint IEEE & ITU work has been accelerated recently and a standard for 40/100GbE is expected in 2010 [16]. Nevertheless, advanced optical fibre infrastructure allows for realization of a ultra-high speed Ethernet, and a pioneering attempt towards a successful 100GbE link has been recently achieved in Japan [17].

4. Conclusions and Future Directions

Optical networks consisting of standard single-mode fibres are in principle suitable for transportation of data rates up to 100 Gbit/s and more, are to be widely deployed both in long distance and in metro/access. Physical limitations laid by the fibres themselves require new technologies to overcome these constraints. Noise accumulation, chromatic dispersion, polarization mode dispersion and nonlinear effects limit data rate and maximum transmission distance. Highly stable 100 Gbit/s Ethernet transmission over different distances through the network would require pushing state of the art in the limits towards optimization and development of new technologies and components for transmitters and receivers.

Therefore it is necessary to provide a solution for applications that have been demonstrated to need bandwidth beyond the existing capabilities. These include IPTV, downloading/uploading of large files at short time, Internet exchanges, high performance computing and video-on-demand (VoD) delivery. High bandwidth applications, such as video on demand and high performance computing justify the need for a 100 Gbit/s Ethernet. Indeed, even a personal computer will surpass 10 GHz computation speed in few years.

Bandwidth requirements for computing and core networking applications are growing at different rates, which necessitates the definition of two distinct data rates for the next generation of Ethernet networks in order to address these applications: servers, high performance computing clusters, storage area networks and network attached storage all currently make use of 1GbE and 10GbE, with significant growth of 10GbE in ’07 and ’08. The I/O bandwidth projections for server and computing applications indicate that there will be a significant market potential for a 40 Gbit/s Ethernet interface.

Dense wavelength division multiplexing technology allows to accommodate the high-speed Ethernet traffic with classical voice and emerging packet networks in a single access infrastructure, therefore reducing the costs of the 100GbE introduction.

Finally, we have to abandon the usual question “what in the hell will people do with the 100GbE access?” Twenty years ago, when the optical fibres were revolutionising long distance communications, conservative people asked “do we really need millions of phone calls at the same time?” In 1829 conservative people asked looking at George Stephenson’s “Rocket” “do we really need 13 tons of coal travelling with a speed of 12 miles per hour?” One can multiply such sort of questions: “Do we really need to fly at the 36 000 feet attitude?”, “What we have to do in the space?” The experience says the opening of new opportunities results in a prompt exploitation and novel applications.

Acknowledgments

The author acknowledges cooperation with the European COST (European Co-operation in the field of Scientific and Technical Research) projects: COST Action 291 Towards Digital Optical Networks (TDON) consortium, and with the International Telecommunication Union – Study Group 15 “Optical and Other Transport Networks”. Interactions with the International Electrotechnical Commission – Technical Committee 86 “Fibre Optics”, and the International Union of Radio Science – Commission D “Electronics and Photonics” are acknowledged. This research has been partially supported by the State Committee for Scientific Research under COST/51/2006 national grant.

References

[1] M. Marciniak, “100 Gb Ethernet over fibre networks – reality and challenges”, in *Proc. ICTON Conf.*, Sousse, Tunisia, 2007.

[2] P. Cochrane, “Fiber-to-the-home (FTTH) costs are now in!”, *Proc. IEEE*, vol. 96, no. 2, pp. 195–197, 2008.

[3] C. M. Gauger, P. J. Kühn, E. Van Breusegem, M. Pickavet, and P. Demeester, “Hybrid optical network architectures: bringing packets and circuits together”, *IEEE Commun. Mag.*, vol. 44, no. 8, pp. 36–42, 2006.

[4] "The World Telecommunication Standardization Assembly", Florianópolis, Brazil, 2004 [Online]. Available: http://www.itu.int/ITU-T/

[5] M. Marciniak, "Optical fibres – almost ideal transparent propagation medium?", in *Proc. 11th Int. Conf. Math. Meth. Electromag. Theory MMET'06 / Kharkiv Electromag. Photon. Week 2006*, Kharkov, Ukraine, 2006, pp. 358–362.

[6] A. Kaszubowska-Anandarajah and L. P. Barry, "Remote downconversion scheme for uplink configuration in radio/fibre systems", in *Proc. 7th Int. Conf. Transp. Opt. Netw. / 2nd Glob. Opt. Wirel. Netw. GOWN Sem.*, Barcelona, Spain, 2005, vol. 2, pp. 134–161.

[7] M. Marciniak, "Application of radio over fibre technology to enable converged optical and wireless next generation networking", in *Proc. Fourth IASTED Int. Conf. Anten., Radar, Propagat.*, Ed. J. Yao, Montreal, Canada, 2007, pp. 26–31.

[8] IEEE 802.3 Higher Speed Study Group tutorial: "An Overview: The Next Generation of Ethernet", IEEE 802 Plenary, Atlanta, Nov. 2007.

[9] S. Muller, A. Bechtolsheim, and A. Hendel, "HSSG speeds and feeds reality check", Jan. 2007 [Online]. Available: http://www.ieee802.org/3/hssg/public/jan07/muller_01_0107.pdf

[10] J. McDonough, "Moving standards to 100 GbE and beyond", *IEEE Appl. Pract.*, Online Mag., vol. 45, Suppl. 3, pp. 6–9, 2007.

[11] M. Marciniak, "Converged access networking with application of radio over fibre technology", in *Proc. Second Int. Conf. Access Netw. Worksh. AccessNets 2007*, Ottawa, Canada, 2007.

[12] K. Borzycki, M. Jaworski, and M. Marciniak, "Temperature dependence of PMD in tight buffered G.652 and G.655 single-mode fibres", in *Proc. 11th Eur. Conf. Netw. Opt. Commun. Worksh. Opt. Cabl. Infrastr.*, Berlin, Germany, 2006.

[13] H. Rourke *et al.*, "Fabrication and system performance of dispersion compensating gratings", in *Proc. Eur. Conf. Opt. Commun. ECOC'99*, Nice, France, 1999.

[14] M. Marciniak and A. Sedlin, "Numerical analysis of optical nonlinearities in multispan DWDM fibre transmission systems", in *COST P2 Worksh. Nonlin. Opt. Inform. Soc. NOIS 2000*, Enschede, The Netherlands, 2000.

[15] R. Sabella and P. Lugli, *High Speed Optical Communications*. Dordrecht/Boston/London: Kluwer, 1999, pp. 239–245.

[16] "The Ethernet Alliance® and the road to 100 G alliance announce intention to merge" [Online]. Available: http://www.ethernetalliance.org/press-room/press-releases/205-the-ethernet-alliancer-and-the-road-to.html

[17] "Japan's first 100-GbE demo", *Lightwave*, Jan. 2009 [Online]. Available: http://lw.pennnet.com/home.cfm

Marian Marciniak graduated in solid state physics from Marie Curie-Skłodowska University in Lublin, Poland, in 1977. He holds a Ph.D. degree in optoelectronics (1989), and a Doctor of Sciences (Habilitation) degree in physics/optics (1997). Actually he is the Head of Department of Transmission and Optical Technologies at the National Institute of Telecommunications in Warsaw. He authored and co-authored over 280 publications, including a number of invited conference presentations. He serves as a Honorary International Advisor to the George Green Institute for Electromagnetics Research, University of Nottingham, UK. He serves as the Chairman of the Management Committee of COST Action MP0702 "Towards functional sub-wavelength photonic structures".

e-mail: M.Marciniak@itl.waw.pl
e-mail: marian.marciniak@ieee.org
National Institute of Telecommunications
Szachowa st 1
04-894 Warsaw, Poland

Invited paper

All-Optical Techniques Enabling Packet Switching with Label Processing and Label Rewriting

Nicola Calabretta, Hyun-Do Jung, Javier Herrera Llorente, Eduward Tangdiongga, Ton Koonen, and Harm Dorren

Abstract—Scalability of packet switched cross-connects that utilize all-optical signal processing is a crucial issue that eventually determines the future role of photonic signal processing in optical networks. After reviewing several labeling techniques, we discuss label stacking and label swapping techniques and their benefits for scalable optical packet switched nodes. All-optical devices for implementing the packet switch based on the labeling techniques will be described. Finally, we present a 1×4 all-optical packet switch based on label swapping technique that utilizes a scalable and asynchronous label processor and label rewriter. Error-free operation indicates a potential utilization of the swapping technique in a multi-hop packet-switched network.

Keywords*— *label processor, optical flip-flop memory, optical packet switching, optical signal processing, wavelength converter.

1. Introduction

The increase of the traffic in the access networks makes it likely that future all-optical metro and core networks should be capable to handle tens of Tbit/s data traffic. Current networks are based on electronic circuit switching technology that has fundamental limits due to the scalability of multi-racks electronic switching fabrics and power consumption required by the optoelectronic conversions [1]–[3]. All-optical packet switching has been proposed as a technology to solve the bottleneck between the fibre bandwidth and the electronic router capacity by exploiting ultra-high speed and parallel operation of all-optical signal processing. Moreover, photonic integration of the optical subsystems potentially allows a reduction of volume and power consumption.

To exploit the benefit of photonic technology to miniaturize and decrease the power consumptions of the system, photonic integration of the all-optical packet switch depends on the capability to integrate the label processor and the optical delay related to the latency of the label processing. This imposes stringent constraints on the latency time of the label processor. High speed operation of the label processor (< 100 ps) must to allow photonic integration of the packet switch system. Moreover, scalability of the label processor with the number of labels (or the number of label bits) is crucial too. Indeed, the number of active components that can be integrated in the label processor is limited by the thermal crosstalk and heat dissipation which can prevent photonic integration of the circuit. Therefore, the choice of the labeling technique determines the architecture and then the scalability of the node.

All-optical packet switch employing all-optical label processor were investigated in [1]–[10]. Mainly these works employed optical correlators, which recognize the labels, and set/reset optical flip-flops to store the information for the duration of the packet. However, as the number of addresses of the wavelength division multiplexing (WDM) channels carried by each fiber, and of the packet data rate increase, photonic integration, high speed operation, low latency, and scalability of the label processor remain key-issues to be solved.

Our research focuses on the realization of an all-optical packet switching system that is scalable and suitable for photonic integration. In this paper, first we give a comparison between several labeling techniques in terms of scalability and photonic integration of the node. Then, we discuss in detail the label stacking and label swapping techniques and their benefits for scalable optical packet switched nodes. Thus, we review the main subsystems blocks that enable the practical implementation of an optical packet switching (OPS) network based on the mentioned label techniques. Finally, we present a 1×4 all-optical packet switch based on label swapping technique that utilizes a scalable and asynchronous label processor and label rewriter.

The paper is organized as follows. In Section 2, the all-optical signal processing functionalities required to implement an all-optical node are described and a comparison of the labeling technique is reported. In Section 3, we review existing all-optical devices enabling all-packet switching, and in Section 4, we provide experimental results on a 1×4 packet switch in which all the functionalities were implemented in all-optical manner. Finally, we sum up and discuss the main results in the conclusion Section 5.

2. Labeling Techniques for All-Optical Packet Switch

A typical core network overlay is shown in Fig. 1(a). The edge router aggregates IP packets with common destination address to form the optical payload of the packet. An optical label is attached to the payload. Several labeling techniques can be used to generate the packet label. The choice of the labeling technique determines the scalability of the node. The generated optical packet is routed by the OPS nodes based on the assigned label, up to the destination. A typical $N \times N$ packet switched cross-connect node is schematically shown in Fig. 1(b). Each of the N inputs carries M the WDM channels are demultiplexed by an arrayed waveguide grating (AWG) before to be processed. The switching fabric performs the label processing and forwarding of the packets, while the synchronization and buffering stages are used to solve the contention resolution between packets leaving the same output port at the same wavelength.

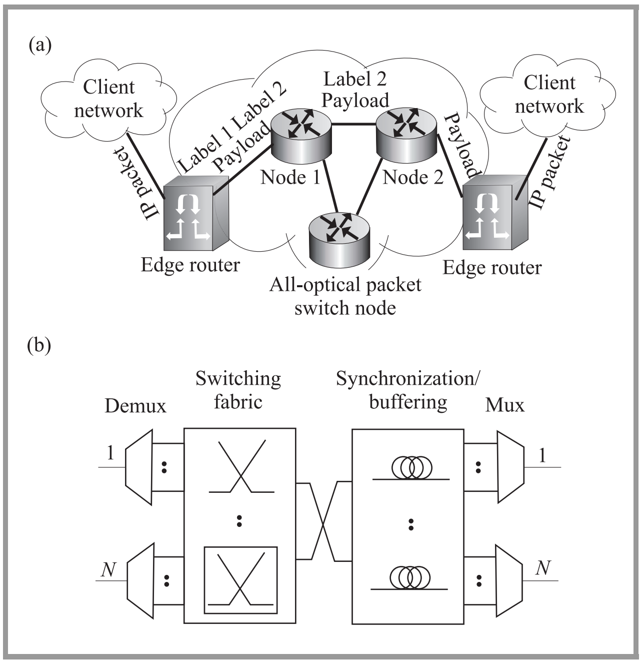

Fig. 1. (a) A general core network overlay. (b) Schematic of optical packet switch node.

The switching fabric consists of three main blocks as shown in Fig. 2: a label processor, a control signal generator and a routing switch. The optical label processor recognizes the optical label that, in combination with an optical control generator, provides the optical control signal to the routing switch to forward the packet. We use a wavelength routing switch as switching strategy, where the packet is routed to a proper output based on the wavelength's packet. Some crucial issues for practical realization of a scalable, all-optical and cost-effective switching fabric are low-power operation and limited amount of components. For practical applications we would also ask for photonic integration on a single chip. Furthermore, it is highly desirable that the label processing operation could be asynchronous, so that the label processor does not require any external synchronization of packets. Given the general cross-connect architecture, the scalability of the node, in terms of number of components and power, will depend on the label technique and the all-optical technology adopted.

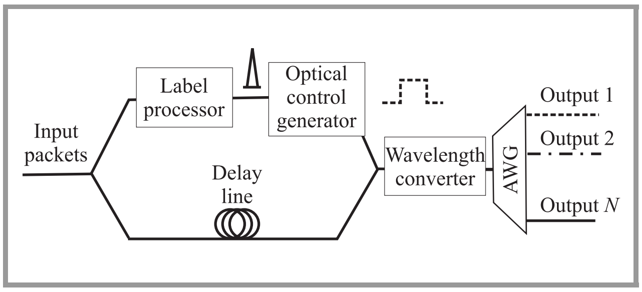

Fig. 2. Optical packet switching fabric.

In all-optical packet switching, the optical label provides information on the packet forwarding. Several techniques have been developed for labeling the optical packets which can be grouped in three main classes: end-to-end label, label swapping, and label stacking.

In the end-to-end label, a distinct label uniquely identifies a distinct node. Thus, the number of end-to-end labels increases linearly with the number of nodes. Moreover, the label does not change along the optical paths to the destination. In the label stacking technique, the label is composed by several sublabels. The number of sublabels is determined by the number of hops required to forward the packet from the source to the destination node. The size of each sublabel is determined by the number of optical output links of the node. As an example, we consider as case study the USA and European Union (EU) IP network backbones depicted in Fig. 3. In those two topologies, the maximum number of output ports that can occur in a node, which determines the size of the sublabel, is 7 in both topologies. The maximum number of hops, which determines the number of sublabels, required for a packet to reach the destination node is 8 and 5 for USA and EU, respectively. In the label swapping technique the labels have a local meaning, but instead to contain several sublabels for packet forwarding at each node, each node rewrites a new label containing the forwarding information for the next node. Thus, each node requires in addition an optical rewriting function.

In terms of scalability and power consumption of the OPS node, the label stacking technique seems to be the most efficient because it decreases the amount of active components required by the node, at the price of having a larger packet overhead. Indeed, in the end-to-end label, the OPS node requires $2 \times N \times M \times L$ active devices (the 2 accounts the label processors based on optical correlators and the optical control generators), N is the inputs port, M the WDM channels and L is the number of nodes of the considered network. Note that this number increases linearly with the network nodes because the label has a global meaning and therefore each node has to be capable to process all possible labels. On the contrary, the label stacking technique requires a number of active devices that is given by $2 \times N \times M \times H$, where H is the size of the sublabel, which is determined by maximum number of output ports of the node. As $H < L$, the label stacking technique requires a lower number of components than the end-to-end label one. The label swapping technique provides the same scalability as the label stacking, but at the price of an additional rewriting function that costs an increase of components. This makes label swapping more complicate of the simple forwarding processing as in the label stacking technique.

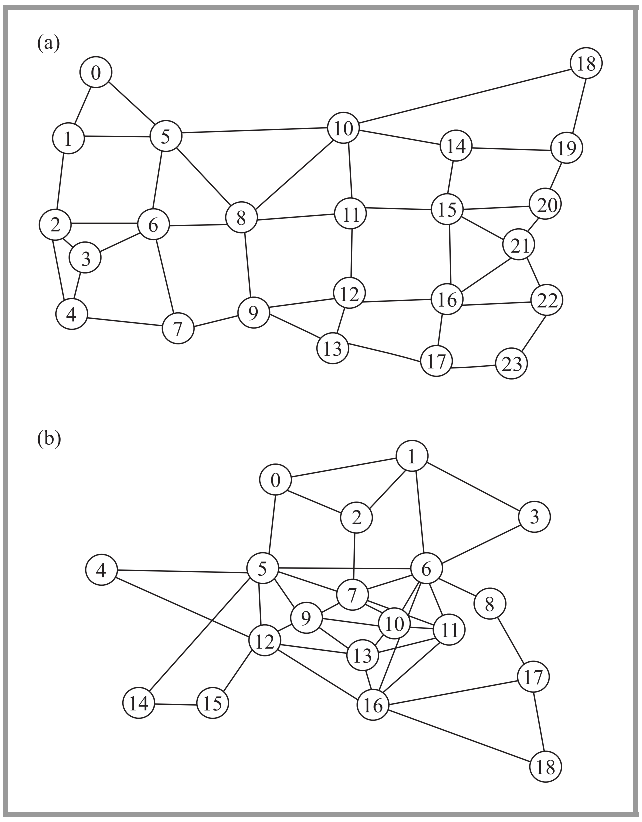

Fig. 3. (a) USA and (b) EU IP network backbones.

A possible disadvantage of the label stacking technique is the increasing of the packet overhead. However, if we consider the topologies depicted in Fig. 3, the number of nodes are 24 and 19 for the USA and EU networks, respectively, while the maximum number of output ports is 7 in both topologies and the maximum number of hops is 8 and 5 for USA and EU, respectively. As a result, considering a typical packet payload size of 1500 bits, the additional packet overhead introduced by the label stacking technique is less than 1%.

The label stacking and label swapping techniques present also other advantages. Those techniques can be applied either for an OPS network or optical burst switching (OBS) network. In the OBS case, implementation of the optical buffering, mandatory in the OPS node, can be done at edge-router stage, alleviating the node architecture. Moreover, some important function such as time-to-live processing are not required anymore but the expiring time of the packet is intrinsically calculated by decreasing one of the sublabels at the time after each hop.

Discussed the potential benefits of the label stacking and label swapping techniques, we will consider in the following section the required physical layer subsystems for the realization of the optical switching nodes.

3. All-Optical Devices Enabling Optical Packet Switching

A schematic example on the operation of the label stacking and label swapping techniques are represented Fig. 4(a) and Fig. 4(b), respectively. In the label stacking operation, the edge router, after consulting the network look-up table, generates the sublabels (label B and label C in the Fig. 4)

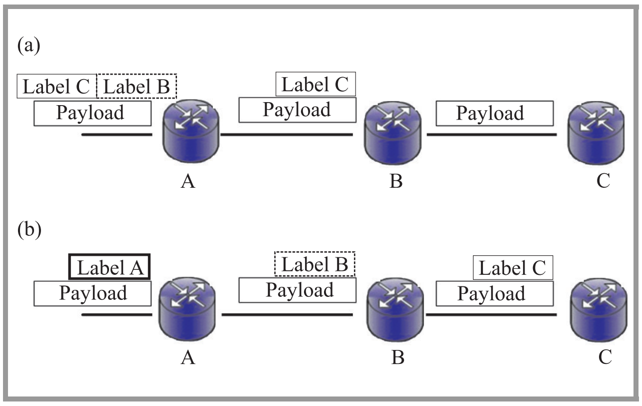

Fig. 4. Schematic of the operation of the (a) label stacking and (b) label swapping techniques.

necessary to route the packet to the destination. Each node processes only the front label, namely node A processes label B and node B processes label C. In the label swapping operation, the edge router, similar to the previous case, consults the network look-up table and generates the label necessary for routing the packet at the next node. Each node routes the packet to the next node based on the processed label, and inserts a new label.

Figure 5 shows schematically the optical packet switching and the subsystems blocks required to perform switching operation based on label stacking or label swapping technique. The switching fabric consists of three main blocks: a label processing subsystem, a control signal generator and a routing switch. The label processing subsystems may include the label extractor/eraser, the label recognizer and the label rewriter. The optical packets are first processed by the label processing subsystem. The label extractor/eraser separates the label from the payload packet. The payload is delayed for the time required to the label processor and optical control signal generator to provide the routing signal before to be fed into the wavelength routing switch. The extracted label is fed into the label recognizer, which provides the control signal for setting the optical signal generator. The optical control signal generator produces a routing signal for driving the wavelength routing switch. Simultaneously, the label rewriter produces the new label to be at-

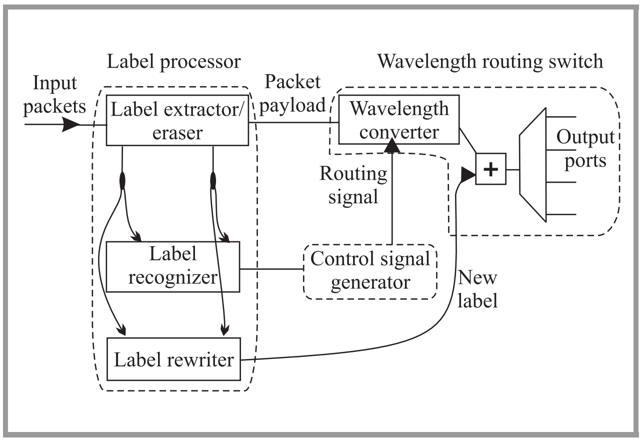

Fig. 5. The all-optical packet switch fabric including the three main blocks.

tached to the switched payload. We use a wavelength routing switch as switching strategy, where the packet is routed to a proper output based on the wavelength's packet. The wavelength routing switch can be implemented by a wavelength converter followed by an AWG. An alternative solution as routing switch can be a space routing switch. Here the packet is routed spatially to the output switch and can be implemented by using all-optical switches. In the following, we report some of the implementations of the single subsystem required to realize the all-optical packet switch. Although several solutions can be found in literature based on different technologies, our research focus is on the realization of an all-optical packet switching system suitable for photonic integration, and thus we have considered semiconductor based all-optical signal processing subsystems.

Label extractor/eraser. Demonstrations of several schemes capable to extract the label information are reported in [9]–[13]. The reported solutions are mainly based on the coding of the label. In [11]–[13] the in-band label bits separated in time from the payload were successfully extracted. The label extractor employed nonlinear gain and index dynamics in semiconductor optical amplifiers. In [9], [10], the label was also in-band with the payload but at different wavelength. The label extraction was achieved by using a passive filter.

Label recognizer. The proposed solutions are based on three different paradigms. One is based on classical optical correlators; therefore an optical pulse is produced only at the correlator output that matches the label pattern [14]–[16]. The second paradigm is based on time-to-wavelength conversion, and in this case the address information is converted into a pulse at distinct wavelength univocally determined by the label [17]. In both cases, the address information employed in both strategies is encoded by using pulse position modulation (PPM) [2]. The main advantage to code the label information with PPM is the simplicity and feasibility of all-optically label matching that can be realized by using pulse position correlators, with very fast processing time. Furthermore there is no need to generate any local pattern for pattern-matching purposes. The disadvantage of those two techniques is that the number of optical correlators scales linear with the number of labels to be recognized. The third paradigm is based on binary processing of the label [10]. The advantage of the binary processing is that it scales logarithmic with the number of labels. Therefore it will require much less active components. Explanation on the operation of the binary processing will be discussed in the next section.

Optical control signal generator. Mainly the output of the label processor consists of a single pulse that identifies distinct routing information. The optical control generator, mainly acting as an optical flip-flop memory, converts the short pulse in a continuous wave (CW) control signal at a defined wavelength. The CW control signal is used in combination with the wavelength converter to route the packet to the proper output. Demonstrations of several optical flip-flop memory techniques can be found in [18], [19]. Generally speaking, the all-optical flip-flop memories are based on two coupled laser diodes (or two coupled switches biased by two distinct CW light-waves). The system can have two possible states. In state one, light from laser 1 suppresses lasing in laser 2. Conversely, in state 2, light from laser 2 suppresses lasing in laser 1. To change states, lasing in the dominant laser is stopped by injecting light (set and reset), not at the dominant laser's lasing wavelength, into the dominant laser. The output pulse of the label processor (and its delayed copy) is used as set (reset) pulse for setting (resetting) one of the optical flip-flop memories.

Wavelength routing switch. We employed as switching strategy for routing the packet the wavelength routing switch. The main device in this operation is a very fast, broadband operation non inverting wavelength converter. Non-inverted wavelength conversion based on a semiconductor optical amplifier (SOA) and an optical band pass filter (BPF) has been demonstrated in [20]. Typically the recovery time of the SOA employed is in the order of 100's of picoseconds, which means a maximum speed conversion up to 10 Gbit/s. The use of the optical BPF with a central wavelength that is blue shifted compared to the central wavelength of the converted signal shortens the recovery time of the wavelength converter. Wavelength conversion operation at bit rates up to 320 Gbit/s has been demonstrated [21]. Moreover, a monolithically integrated version has been also demonstrated showing the potential integration of this subsystem with the other ones [22].

4. All-Optical Label Swapping Implementation

In this section we present a 1×4 all-optical packet switch based on label swapping technique [23]. We demonstrate

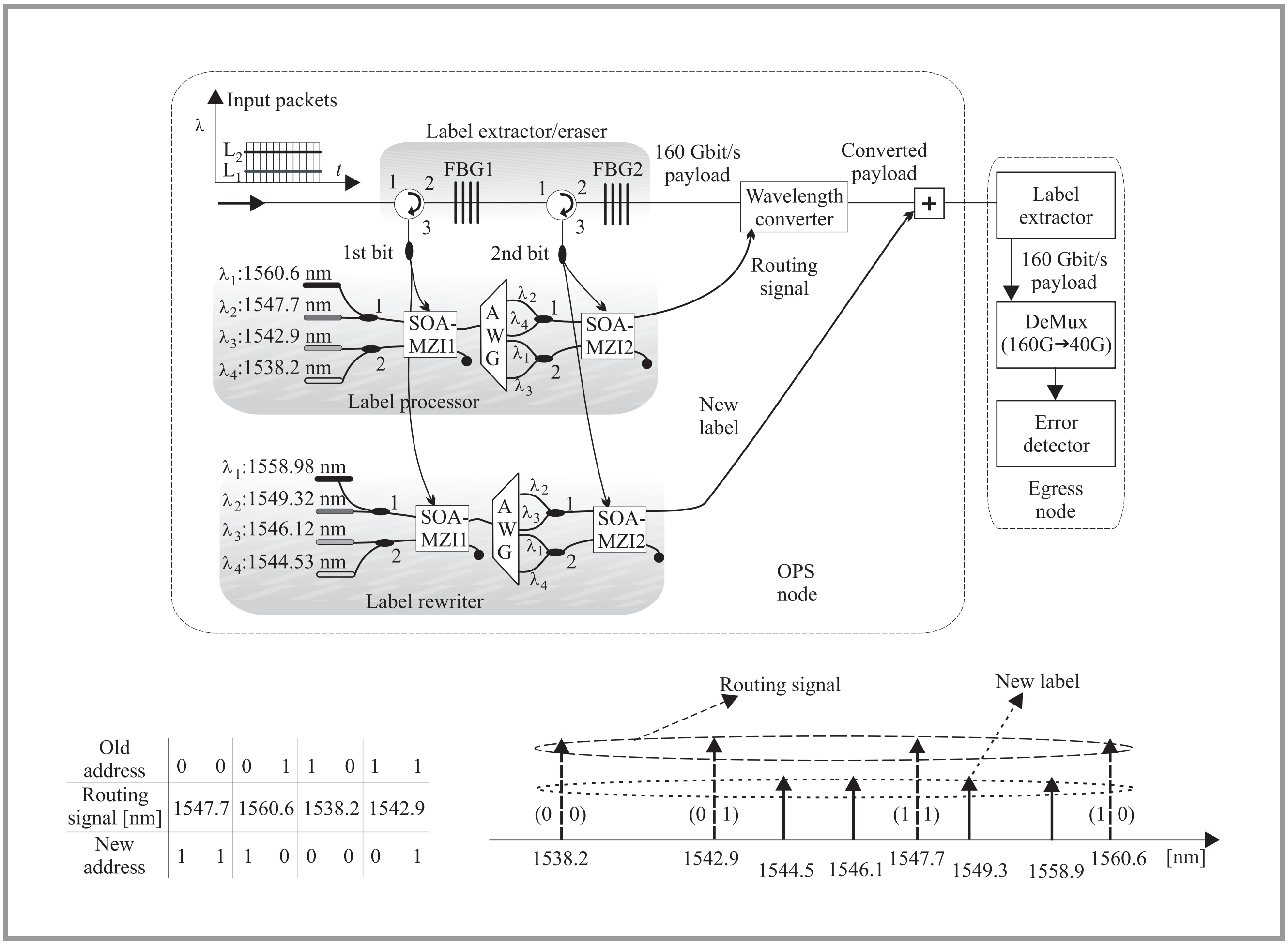

Old address	0 0	0 1	1 0	1 1
Routing signal [nm]	1547.7	1560.6	1538.2	1542.9
New address	1 1	1 0	0 0	0 1

Fig. 6. Experimental set-up employed to demonstrate the all-optical packet switch based on the label processor and label rewriter. Self-routing table employed in the label swapping experiments.

a label processor for processing in-band labeling addresses and an all-optical label rewriting function that provides a new address according to the old one. The label processor and label rewriter processes "on the fly" the optical labels, operates in asynchronous fashion and can handle packets with variable length.

Figure 6 illustrates the all-optical packet switch based on label swapping technique and the label swapping table. The input packets consist of a 160 Gbit/s payload, with a pulsewidth of 1.6 ps making the 20 dB bandwidth of the payload to be 5 nm. The packet address information is encoded by in-band labels. With this we mean that the wavelengths of the labels are chosen within the bandwidth of the payload. We encode addresses by combining different labels. The label has a binary value: the label value is 1 if the label is attached to the payload, the label value is 0 if no label is attached to the payload. Thus, by using N in-band label wavelengths, 2^N possible addresses can be encoded, which makes this labelling technique highly scalable within a limited bandwidth.

To perform the label swapping and routing of the packet, we utilize four all-optical functions as shown in Fig. 6: label extraction/erasing, label processing, label rewriting, and wavelength conversion. The packet address encoded by the in-band labels is separated from the data payload by the label extractor/eraser which consists of (reflective) fiber Bragg gratings (FBG) centered at the labels wavelengths. While the labels are reflected by the FBGs, the packet payload can pass through the label extractor/eraser before to enter the wavelength converter. The data payload is optically delayed for the time required to the label process to provide a routing signal, before being fed into the wavelength converter.

The optical power of the extracted labels is used to drive the label processor and label rewriter. The label processor receives also as input 2^N CW bias signals at different wavelengths $\lambda_1 \ldots \lambda_2^N$. The wavelengths of the CW-signals are chosen according to the self-routing table and represent the wavelengths at which the payload will be converted. An example of self-routing table for addresses composed by two labels is reported in Fig. 6. For each input labels combination, a routing signal at distinct wavelength and a new combination of labels should be provided by the label processor and the label rewriter, respectively. Thus, the label processor provides a routing signal according to the input labels. The label processor consists of a cascaded of periodic filter and optical switch. The periodic filter has one input and two outputs. The optical switch has two inputs and one output. Each of the 1×2 periodic filter separates (in wavelength) half of the input CW-signal to output port 1 and the other half of the input CW-signals at the output port 2. The 2×1 optical switch selects the CW-signals of port 1 or port 2 based on the value of the label information. Therefore, the output of each pair of periodic filter and optical switch consists of half the number of CW-signals. Thus, after the first stage, the 2^N CW-signals becomes $2^N/2 = 2^{N-1}$. Therefore, after cascading N pairs in which each optical switch is driven by the corresponding label, a distinct CW-signal is selected. This CW-signal at distinct wavelength has a time duration equal to the packet time duration and represents the routing signal to which the payload will be converted. The wavelength of the routing signal represents the central wavelength at which the 160 Gbit/s data payload will be converted by means of wavelength conversion.

Simultaneously, the label rewriter provides the new labels, which have a time duration equal to the packet duration. The label rewriter has the same structure as the label processor discussed previously. The principle of operation of the label rewriter is similar to the label processor. In the case of label rewriter, the CW-signals and the periodic filters are set to provide the new label combinations according to the self-routing table shown in Fig. 6. The wavelengths of the CW-signals are set to be in-band with the switched payload (the central wavelength of the payload is set by the label processor). Thus, for a given old labels combination,

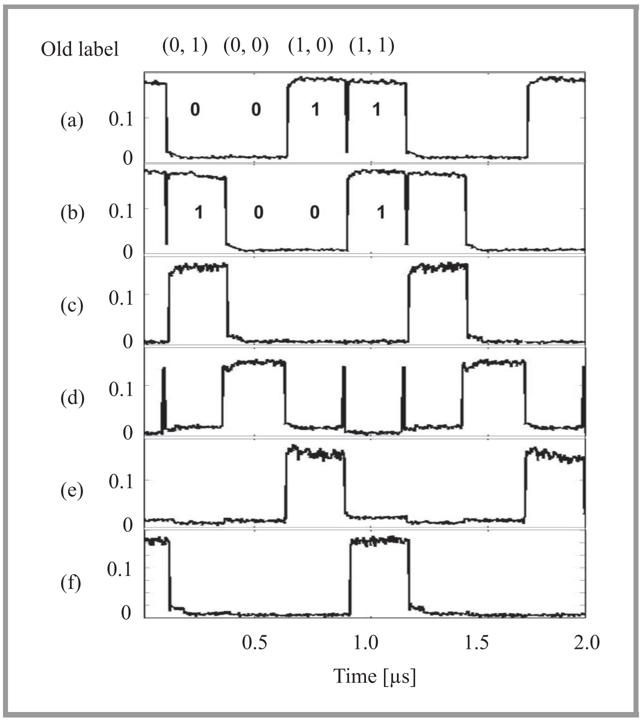

Fig. 7. Measured traces. Extracted labels: (a) label 1; (b) label 2. Output traces of the label processor: (c) 1560.6 nm; (d) 1547.7 nm; (e) 1538.2 nm; (f) 1542.9 nm.

the routing signal is provided by the label processor, and the new labels are provided by the label rewriter. Moreover, the wavelengths of the new labels are selected so that they are in-band with the bandwidth of the converted payload. The new labels are attached to the wavelength converted payload (see Fig. 6). The packet with the new labels is routed by means of an AWG to distinct output ports of the packet switch, according to the central wavelength of the converted payload.

The experimental results of the 1×4 packet switch based on label swapping technique by using two labels address. The extracted labels are shown in Fig. 7(a),(b). The measured optical signal to noise ratio (OSNR) at the SOA-MZI2 output was 32 dB, and the dynamic extinction ratio was 13 dB. The wavelength converter is based on ultrafast chirp dynamics in a single SOA [20]. We set the CW-signals according to the label swapping table. The label processor output traces are shown in Fig. 7(c)–(f), while in Fig. 8(c)–(f) it is shown the output traces of the label-rewriter. The new labels were then combined with

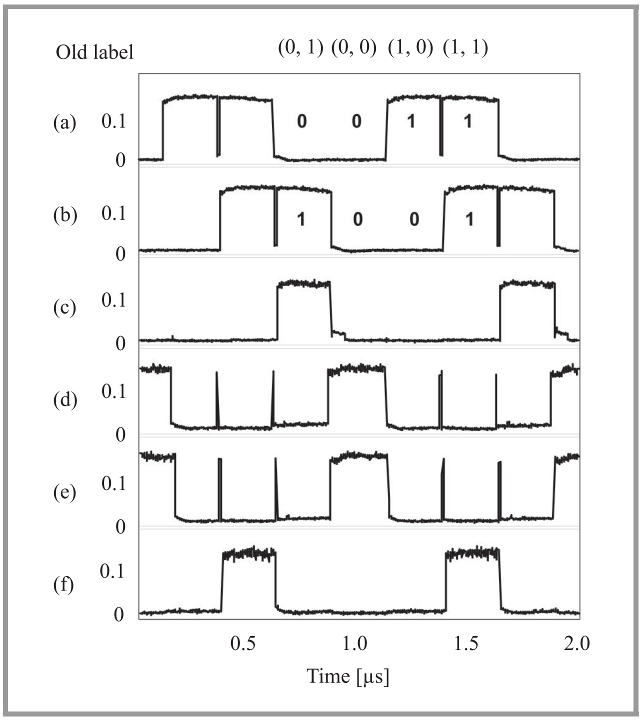

Fig. 8. Measured traces. Extracted labels: (a) label 1; (b) label 2. Output traces of the label rewriter: (c) 1558.9 nm; (d) 1549.3 nm; (e) 1546.1 nm; (f) 1544.5 nm.

the 160 Gbit/s wavelength converted payload. At the receiving node, the packet was processed by the label extractor /eraser, and the resulting 160 Gbit/s payload was evaluated.

Figure 9 shows the bit error rate (BER) performance at different position of the two nodes system. The BER measurements were performed in a static operation by using a 160 Gbit/s pseudorandom bit sequence (PRBS) $2^{31} - 1$ data payload and fixing one address (old label (0.1)). The label extractor in node 1 causes a penalty of less than

0.5 dB compared to the back-to-back payload. After the wavelength conversion, error-free operation was obtained with 5.5 dB of penalty. As reference we also reported the 160 Gbit/s back-to-back wavelength converted, which has 4 dB of penalty. The additional 1.5 dB penalty compared with 160 Gbit/s back-to-back wavelength conversion can be ascribed to the pulse broadening by the label extractor which affects the wavelength conversion performance. The switched packet was then fed into the receiving node 2.

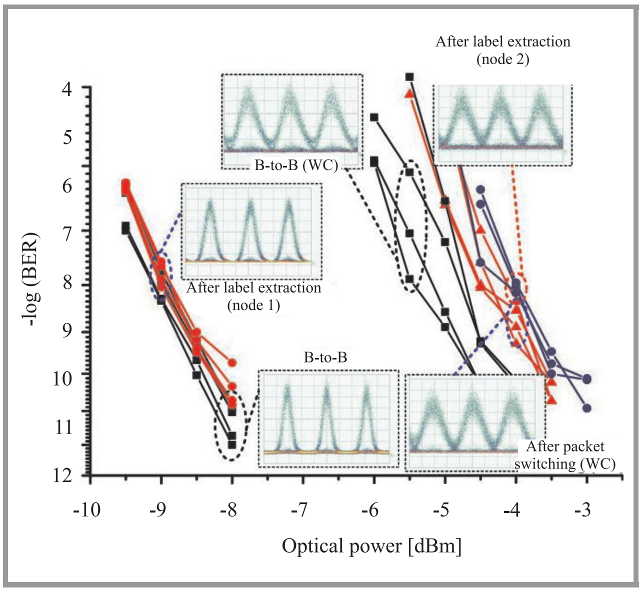

Fig. 9. BER measurements and eye diagrams at different points of the system (time scale: 2 ps/div).

The power penalty after the label extractor is 0.5 dB. This results in a limited power penalty caused by the extraction/insertion of the new labels.

5. Conclusions

We have discussed several all-optical building blocks that potentially can enable the realization of an all-optical packet switching node based on different labelling techniques. It has been discussed that label swapping and label stacking can improve the scalability of the cross-connect node by reducing significantly the number of active devices. The reviewed all-optical building blocks operate asynchronously, with low optical power and at high bit rate, and could be potentially monolithically integrated.

We demonstrated an all-optical 1×4 packet switch by using a scalable and asynchronous label processing and rewriting function. Experiments performed in two-cascaded nodes configuration show error-free packet switching operation at 160 Gbit/s, while the label erasing and new label insertion operation introduces only 0.5 dB of power penalty. Those results indicate a potential utilization of the presented technique in a multi-hops packet switched network.

References

[1] D. J. Blumenthal, “Optical packet switching”, in *Proc. 17th Ann. Meet. LEOS 2004*, Puerto Rico, USA, 2004, vol. 2, pp. 910–912.

[2] H. J. S. Dorren *et al.*, “Optical packet switching and buffering by using all-optical signal processing methods”, *J. Lightw. Technol.*, vol. 21, pp. 2–12, 2003.

[3] S. J. B. Yoo, “Optical packet and burst switching technologies for future photonic internet”, *J. Lightw. Technol.*, vol. 24, pp. 4468–4492, 2006.

[4] J. P. Wang *et al.*, “Demonstration of 40-Gb/s packet routing using all-optical header processing”, *IEEE Photon. Technol. Lett.*, vol. 18, pp. 2275–2277, 2006.

[5] F. Ramos *et al.*, “IST-LASAGNE: towards all-optical label swapping employing optical logic gates and optical flip-flops”, *J. Lightw. Technol.*, vol. 23, pp. 2993–3011, 2005.

[6] M. Takenaka *et al.*, “All-optical packet switching by MMI-BLD optical flip-flop”, in *Proc. OFC/NFOEC 2006 Conf.*, Anaheim, USA, 2006, OThS3.

[7] P. K. A. Wai *et al.*, “1×4 all-optical packet switch at 10 Gb/s”, *IEEE Photon. Technol. Lett.*, vol. 17, pp. 1289–1291, 2005.

[8] P. Seddighian *et al.*, “All-optical swapping of spectral amplitude code labels for packet switching”, in *Proc. Conf. Photon. Switch. 2007*, San Francisco, USA, 2007, pp. 143–144.

[9] J. Herrera *et al.*, “160-Gb/s all-optical packet switching over a 110-km field installed optical link”, *J. Lightw. Technol.*, vol. 26, pp. 176–182, 2008.

[10] N. Calabretta *et al.*, “1×4 all-optical packet switch at 160 Gb/s employing optical processing of scalable in-band address labels”, in *Proc. OFC 2008 Conf.*, San Diego, USA, 2008, Paper 33.

[11] N. Calabretta *et al.*, “Bragg grating assisted all-optical header preprocessor”, *Electron. Lett.*, vol. 38, pp. 1560–1561, 2002.

[12] N. Calabretta *et al.*, “Optical signal processing based on self-induced polarization rotation in a semiconductor optical amplifier”, *J. Lightw. Technol.*, vol. 22, pp. 372–381, 2004.

[13] N. Calabretta *et al.*, “All-optical signal processing based on self-induced effects in a vertical cavity semiconductor switch”, in *Proc. OFC/NFOEC 2006 Conf.*, Anaheim, USA, 2006, OThS8.

[14] N. Calabretta *et al.*, “All-optical header processor for packet switched networks”, *IEE Proc. Optoelectron.*, vol. 150, no. 3, pp. 219–223, 2003.

[15] N. Calabretta *et al.*, “Ultrafast asynchronous multi-output all-optical header processor”, *IEEE Photon. Technol. Lett.*, vol. 16, pp. 1182–1184, 2004.

[16] N. Calabretta *et al.*, “All-optical label processing techniques for pure DPSK optical packets”, *J. Select. Top. Quant. Electron.*, vol. 12, pp. 686–696, 2006.

[17] N. Calabretta *et al.*, “Exploiting time-to-wavelength conversion for all-optical label processing”, *IEEE Photon. Technol. Lett.*, vol. 18, pp. 436–438, 2006.

[18] M. T. Hill *et al.*, “A fast low-power optical memory based on coupled micro-ring lasers”, *Nature*, vol. 432, pp. 206–209, 2004.

[19] Y. Liu *et al.*, “Packaged and hybrid integrated all-optical flip-flop memory”, *Electron. Lett.*, vol. 42, pp. 112–114, 2006.

[20] Y. Liu *et al.*, “Error-free all-optical wavelength conversion at 160 Gb/s using a semiconductor optical amplifier and an optical band pass filter”, *J. Lightw. Technol.*, vol. 24, pp. 230–236, 2006.

[21] Y. Liu *et al.*, “Error-free 320 Gb/s all-optical wavelength conversion using a semiconductor optical amplifier”, *J. Lightw. Technol.*, vol. 25, pp. 103–108, 2007.

[22] E. Tangdiongga *et al.*, “Monolithically integrated 80-Gb/s AWG-based all-optical wavelength converter”, *IEEE Photon. Technol. Lett.*, vol. 18, pp. 1627–1629, 2006.

[23] N. Calabretta *et al.*, "All-optical label swapping of 160 Gb/s data packets employing optical processing of scalable in-band address labels", in *Proc. ECOC 2008 Conf.*, Brussels, Belgium, 2008, Th2.E.3.

Nicola Calabretta received the Bachelor's degree and the M.Sc. degree, both in telecommunications engineering, from the Turin University of Technology, Italy, in 1995 and 1999, respectively. In 1995, he visited the RAI Research Center, Turin. In 2004 he received the Ph.D. degree from the COBRA Research Institute, Eindhoven University of Technology, The Netherlands. From 2004 to 2007 he was working as researcher at the Scuola Superiore Sant'Anna University, Pisa, Italy. He is currently with COBRA Research Institute. Dr. Calabretta co-authored more than 80 papers published in international journals and conferences and holds 3 patents. He is currently acting as a Referee for several IEEE and IEE and OSA Journals. His fields of interest are all-optical signal processing for optical packet switching, semiconductor optical amplifier, all-optical wavelength conversion and regeneration, and advanced modulation formats for optical packet switching.

e-mail: n.calabretta@tue.nl
COBRA Research Institute
Eindhoven University of Technology
P.O. Box 512, 5600MB, Eindhoven, The Netherlands

Hyun-Do Jung received the B.Sc. degree in radio sciences and engineering from the Kyunghee University, Korea, in 1999, and the Ph.D. degree in electrical and electronic engineering from the Yonsei University, Korea, in 2005. Since 2005, he has been with the Department of Electrical Engineering, Eindhoven University of Technology, The Netherlands, as a senior researcher, where he is involved in EU-Project (MUFINS and ALPHA) related to optical packet switching and in-building/access networks. His current research interests include optical systems for communications, optical packet switching network, WDM-PON network and microwave photonics technologies.

e-mail: h.d.jung@tue.nl
COBRA Research Institute
Eindhoven University of Technology
P.O. Box 512, 5600MB, Eindhoven, The Netherlands

Javier Herrera Llorente received the M.Sc. and Ph.D. degrees in 2000 and 2005, respectively, from the Valencia University of Technology, Spain. From 2006 he was a postdoctoral researcher at the COBRA Research Institute, Eindhoven University of Technology, The Netherlands. Currently he is a postdoctoral researcher at the Nanophotonics Technology Center, Valencia University of Technology. He has co-authored more than 50 papers in technical journals and conferences, holds one patent, and acts as a peer reviewer for several IEEE, IEE, and OSA journals. His research topics are all-optical signal processing, microwave photonics, nonlinear optical devices, and integrated photonics.

e-mail: j.herrera.llorente@tue.nl
COBRA Research Institute
Eindhoven University of Technology
P.O. Box 512, 5600 MB, Eindhoven, The Netherlands

Eduward Tangdiongga received his M.Sc. degree in electrical engineering in 1994 from the Eindhoven University of Technology, The Netherlands, and his Ph.D. degree in 2001. From 2001 to 2009 he participated in the European Union sponsored project FASHION and the EU research projects: ALPHA, POF-PLUS, BOOM, and EURO-FOS. In 2005 he was on a sabbatical leave at Fujitsu Research Labs in Japan working on the topic of pulse compression using nonlinear fibers and nonlinear switching using quantum-dot semiconductor optical amplifiers. He currently works as Assistant Professor in Eindhoven University of Technology in the field of access and short-to-medium range optical networks.

e-mail: e.tangdiongga@tue.nl
COBRA Research Institute
Eindhoven University of Technology
P.O. Box 512, 5600 MB, Eindhoven, The Netherlands

Ton (A. M. J.) Koonen received the M.Sc. (*cum laude*) degree in electrical engineering from the Eindhoven University of Technology, The Netherlands, in 1979. He was with Bell Laboratories in Lucent Tech as a Technical Manager of applied research for more than 20 years. He was a part-time Professor at the Twente Univer-

sity, Enschede, The Netherlands, from 1991 to 2000. Since 2001, he is a Full Professor at the Eindhoven University of Technology in the Electro-Optical Communication Systems Group at the COBRA Institute, where he is the Chairman of this group since 2004. His current research interests include broadband fiber access and in-building networks, radio-over-fiber networks, and optical packet-switched networks. He has initiated and led several European and national R&D projects in this area on dynamically reconfigurable hybrid fiber access networks, fiber-wireless, packet-switched access, and short-range multimode (polymer) optical fiber networks, and label-controlled optical packet routed networks. Currently, he is involved in a number of access/in-home projects in the Dutch Freeband program, the Dutch IOP Generieke Communicatie program, and the EC FP6 IST and FP7 ICT programs. Prof. Koonen is a Bell Laboratories Fellow since 1998, and a member of the LEOS Board of Governors since 2007.
e-mail: a.m.j.koonen@tue.nl
COBRA Research Institute
Eindhoven University of Technology
P.O. Box 512, 5600 MB, Eindhoven, The Netherlands

Harm J. S. Dorren received his M.Sc. degree in theoretical physics in 1991 and the Ph.D. degree in 1995, both from the Utrecht University, The Netherlands. After postdoctoral positions he joined the Eindhoven University of Technology, The Netherlands, in 1996, where he presently serves as a Professor and as the Scientific Director of the COBRA Research Institute. In 2002 he was also a visiting researcher at the National Institute of Industrial Science and Technology (AIST) in Tsukuba, Japan. His research interests include optical packet switching, digital optical signal processing and ultrafast photonics. Prof. Dorren co-authored over 250 journal papers and conference proceedings and currently serves as an associate editor for the "IEEE Journal of Quantum Electronics".
e-mail: h.j.s.dorren@tue.nl
COBRA Research Institute
Eindhoven University of Technology
P.O. Box 512, 5600 MB, Eindhoven, The Netherlands

Invited paper

Features of Formation of Radar-Tracking and Optical Images in a Mobile Test Stand of Radio-Vision Systems of a Car

Andrey Ananenkov, Anton Konovaltsev, Alexey Kukhorev, Vladimir Nujdin, Vladimir Rastorguev, and Pavel Sokolov

Abstract—In the report the features of formation of radar images (RI) and optical images (OI) in the mobile test stand of radio-vision systems (RVS) of a car are presented. The radio-vision system of a car (CRVS) of the millimeter-wavelength with frequency modulation is considered. Features of formation and processing of the radar-tracking image in CRVS are discussed, in particular: the sizes of the image, system of coordinates, primary and secondary processing of RI, requirements for speeds of transfer of figures in real time of processing, for subsystem of display of RI and synchronization. The structure of the mobile test stand of CRVS is described. This stand consists of: CRVS, a video camera, the module of formation, recording and display of RI and of optical images, the module of control of a stand, the power supply unit. Features of formation and display OI are considered, in particular: the coordination of scale and shortening of images, creation of time synchronization at display and records of OI, and questions of synchronous fusion of RI and OI also.

Keywords—features of formation and fusion of radar and optical images, mobile test stand, radar image, radio-vision system of a car.

1. Introduction

The development of motor industry in the world constantly increases and the intensity and density of transport movement on road increase also. As a result quantity of road and transport incidents (road accident) increases also.

The reasons of road accident are various. So, according to American Agency NHTSA (National Highway Traffic Safety Administration), besides malfunction of a vehicle, 68% of road accidents are connected with a carelessness and insufficient knowledge of the driver of a road situation. Thus, insufficient knowledge of the driver is in direct dependence on conditions of optical visibility such as: light exposure of road and a roadside, visibility of a marking and indexes, a degree of windscreens impurity cabins, presence in air of a fog, a snow, a rain, a dust, a smoke and other preventing factors.

In works [1]–[3] it is shown, that the core by the decision of an actual problem of increase of traffic safety of vehicles in conditions of absence or the limited optical visibility is use on the car of the radio-vision system (CRVS). This system is working in millimeter range of wavelengths and does not depend on any weather conditions: a smoke, a dust, etc. The CRVS is the small-sized, all-weather, information-measuring system representing new generation of panoramic radar stations (RS) of the forward review for modern vehicles. This system has not analogues in the world market.

Several years ago the experimental sample of CRVS has been developed by experts of Moscow Aviation Institute (MAI) and produced. This radar is intended for formation radar images (RI) of road conditions in front of a car. The driver in conditions of absence of optical visibility can observe on the screen the indicator in the interior of the automobile an obstacle a border of the road, traffic signs, obstacles and vehicles parked on a roadside within the working range of CRVS in view of dynamics of movement of own automobile also.

2. Features of Formation and Processing of RI

In Fig. 1 the block diagram CRVS designed is presented. The CRVS is constructed as panoramic RS of millimeter-wave length with linear frequency modulation (LFM) of a signal of the transmitter. The antenna of CRVS is a rotating wave-slot-hole antenna array. The antenna of CRVS scans space in front of the car in the set of working sector. The information about conditions of movement in front of the car is incorporated on the receiver output of CRVS in the mixed signal of transmitted and reflected from the purpose of signals. From an output receiver of CRVS the mixed signal transfer on input of analog to digital converter (ADC) – a part of block of digital signal processing (DSP).

The further primary processing of the digitized mixed signal includes following basic stages: digital filtration with application of procedure of decimation; intermediate buffering; formation of information packages and transfer of the generated data files on the operating HOST-computer; fast Fourier transform (FFT) by program methods on a personal computer (PC); addition on RI the demanded service information (a coordinate grid); a conclusion received RI on the screen of the indicator (the monitor of the PC).

One of serious problems which limits wide introduction of CRVS in modern automobiles is the creation of secondary algorithms of processing of RI for formation of the radar image adequate for the driver. In experimental sample of CRVS secondary processing of the information consists in elementary formation on the final radar image of the additional information such as drawing a grid of a range of distances in a mode of real time.

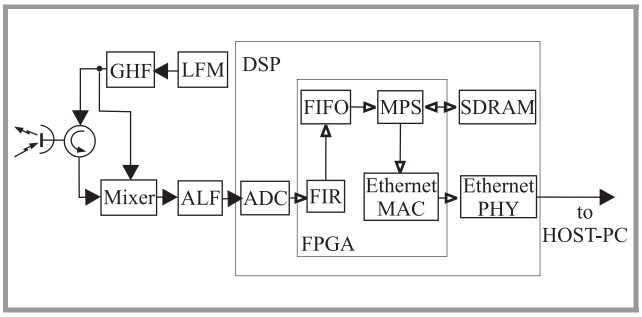

Fig. 1. The block diagram of CRVS. Explanations: GHF – generator of high frequency, ALF – amplifier of low frequency, FIFO – first in first out, FIR – finite impulse response, FPGA – field programmable gate array, MPS – microprocessor system, MAC – media access control, SDRAM – synchronous dynamic random access memory.

However, the part of tasks of secondary processing of RI is solved by developers of CRVS in a model variant on PC only. Among these tasks: definition of a range up to obstacles and taking place vehicles (VC), properly informing the driver about a critical range up to objects of an artificial origin (AO) in lane of VC, and automatic definition of width of road and distances from the automobile with CRVS, up to left and right roadsides also.

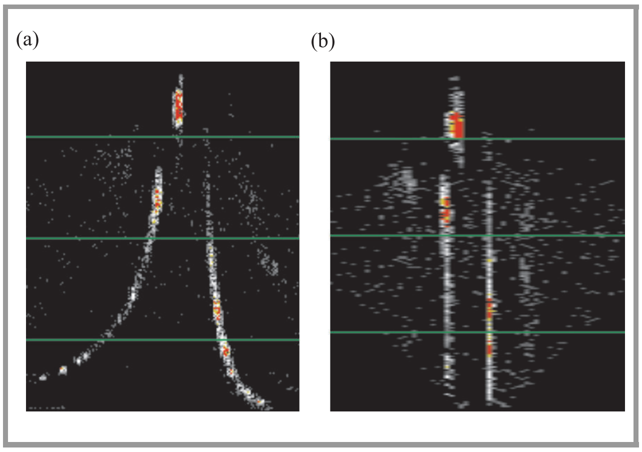

Fig. 2. Radar image in coordinates: (a) range-azimuth; (b) range-range.

In Fig. 2(a) the example of the staff of the radar image which is observed by the driver on the screen of indicator of system of radio-vision (SRV) is submitted.

One staff of RI represents a spatial spectrum of road conditions in front of VC in coordinates range – an azimuth corner. On presented RI staff (Fig. 2) borders of road, a roadside and a vehicle (on distance of the order of 170 m), moving on a counter lane clearly differ also.

Additional task of secondary data processing is transformation of coordinates received RI from coordinates range-azimuth in coordinates range-range. The given mode is organized in existing experimental sample CRVS (Fig. 2(b)) in real time.

In Fig. 3 the principle of formation of radar file data in CRVS is shown. The working sector of scanning antenna

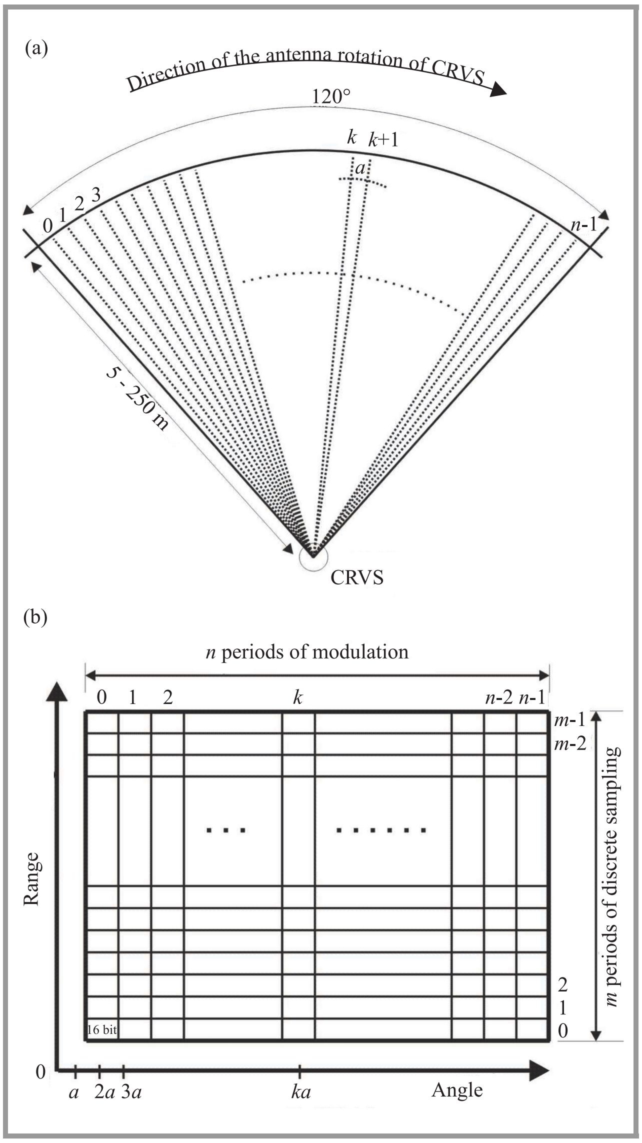

Fig. 3. The principle of formation of radar file data in CRVS: (a) working sector; (b) structure of the staff of radar image (array $m \times n$ 16-bit words).

of CRVS makes 120°. At an input of the antenna in working sector, on a signal from the gauge of the antenna position, ADC starts to digitize the mixed signal from the receiver

output. Word length of ADC is equal 10, frequency of digitization: $f_d = 20$ MHz. In operating mode of CRVS with frequency of antenna rotation: $f_{ar} = 8$ Hz, with modulating frequency of LFM signal $F_M = 8$ kHz and decimation factor: $d = 4$, the RI staff of CRVS it is possible to present as a two-space file $(m \times n)$ 16-bit words in the size: size = 832500 byte.
The work of CRVS is organized in real time with frequency of reproduction of RI staff: not less than 8 Hz. Such work means high-speed data transmission with DSP on a HOST-computer for the further processing.
The size of a network used datagram protocol (UDP)-package is limited by requirements of the standard of transfer Ethernet or of standard USB 2.0 (Universal Serial Bus) which has high throughput and makes up to 480 Mbit/s. On the end of a cycle of the receiving, corresponding one pass of working sector, to accepted data radar file, FFT procedure is applied to formation of a spatial spectrum – staff of RI.

3. The Mobile Test Stand

For research of the statistical characteristics of RI received on CRVS output, at a stage of natural tests it is necessary to provide synchronous record of optical and radar images of road conditions. In the further, at a stage of the laboratory analysis of the real experiment, the received record enables the comparing of these images and in more details to check up conformity of RI to real conditions.
In Fig. 4 the block diagram of mobile test stand of CRVS is shown. Basic module of CRVS – radar is installed on a roof of a car. In the same place, with the purpose of fixing of the optical image, the portable video camera is installed also.

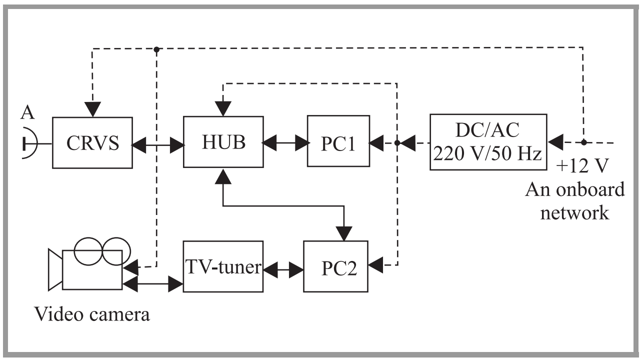

Fig. 4. The block diagram of mobile test stand of CRVS.

At the organization of an operating mode with a synchronous conclusion to indicator RI and OI (optical images), and simultaneous fixing of these data on a hard disk also, has arisen a problem of shortage of speed of the PC applied as an operating HOST-computer. To maintenance of synchronous record OI it has been decided to apply the second personal computer (PC2 in Fig. 4).

4. Main Design Activities for Synchronous Fusion of RI and OI

For synchronous record optical and radar images on a hard disk both of computer PC1 and PC2, and radar also, are incorporated by means of network HUB in a local network. By inquiry of the operating program with PC1, radar begins data gathering in working sector. Simultaneously with inquiry to radar on reception of data from radar, PC1 sends on PC2 a command on fixing of the optical image from a video camera. Received from RI it is fixed on hard disk PC1 and then it is deduced on the indicator – screen PC1. Thus the staff of the optical image from a video camera, it is fixed in a corresponding file of experiment on PC2.
Requirements to synchronous fusion of radar and optical images:

- time synchronization during formation of images on the interface of a stand;
- coordination of the aperture and quantity of information pixels of images at an azimuth;
- coordination of information velocity: the optical image – 24 Hz, radar-tracking: 10–15 Hz.

In Fig. 5 the staff of optical and radar images who has been written down synchronously during natural tests of CRVS are presented.

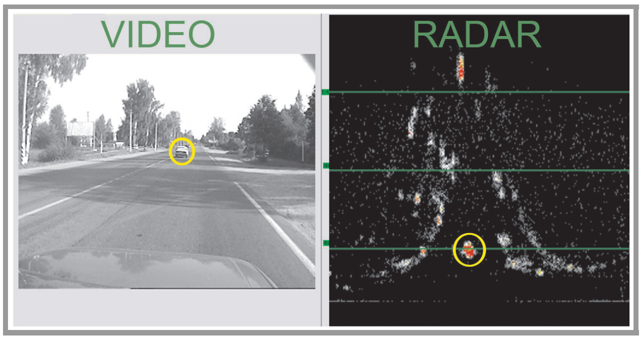

Fig. 5. Synchronous record optical and radar images.

Taking into account increase of requirements of traffic safety of vehicles in conditions of absence or the limited optical visibility establish the increasing quantity of various information sensors: optical, radar, infra-red. In result there is an opportunity to realize of fusion sensors. This problem is known for a long time and successfully is solved at construction of navigation systems of modern planes and helicopters. The essence of a problem of fusion consists in use of the several sensors measuring identical parameters or forming identical images, in aggregate, to receive more exact measurement of parameter or the best image.
The basis of an advantage at fusion consists that each sensor has the advantages and lacks. Therefore, using ad-

vantages of each sensor, at fusion will be received "more exact" results or the better informative image on an output of a complex.
With reference to our task on the automobile is possible fusing of the following sensors:

– homogeneous (same) sensors, for example, radar-tracking sensors of long and small range;

– heterogeneous (diverse works by a physical principle) sensors, for example, the radar-tracking sensor of long distance and the infra-red or optical gauge.

It is represented to the most effective fusing of panoramic radar of forward review (CRVS) and a video camera.

5. Conclusion

The considered features of formation and processing of RI in CRVS have allowed to formulate requirements concerning the size of the image, system of coordinates, speed of transfer of figures and creation of processing in real time, system of display of RI and synchronization.
On the basis of analysis RI, received as a result of natural tests CRVS, tasks of secondary processing RI for formation of the radar image adequate for the driver of the received image has been determined. For creation of algorithms of secondary processing RI on the basis of test stand CRVS requirements to the module of time synchronization has been determined at display, record and overlapping RI and OI.

References

[1] V. V. Rastorguev *et al.*, "A front survey automobile radar with frequency modulation", in *Proc. Seventh Sci. Exch. Sem. Radio Tech. Syst. Dev. UHF*, Munich, Germany, 2000.

[2] A. E. Ananenkov, E. V. Voronkov, A. V. Konovaltsev, V. M. Nujdin, and V. V. Rastorguev, "The field tests of radio-vision system for ships navigation", in *Proc. Eighth Sci. Exch. Sem. Radio Tech. Syst. Dev. UHF*, Moscow, Russia, 2003.

[3] A. E. Ananenkov *et al.*, "Features of dispersion of wideband probing signals in radio-vision systems of the MM – wavelength", in *Proc. Symp. Sens. Driv. Assist. Syst.*, Heilbronn, Germany, 2006.

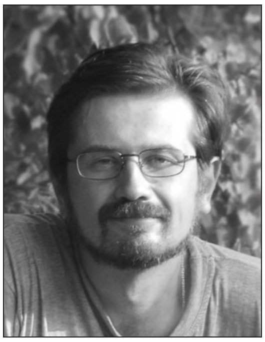

Andrey Evgenjevich Ananenkov is the senior scientific employee of the Radio-Receiver Subsystem Department of the Moscow Aviation Institute (MAI), State Technical University, Russia. He got his Ph.D. from the MAI in 1997. He is the author of more than 20 scientific works in the area of signal processing in radar systems.

e-mail: kaf407@mai.ru
Moscow Aviation Institute
State Technical University
4, Volokolamskoye shosse
125993 Moscow, Russia

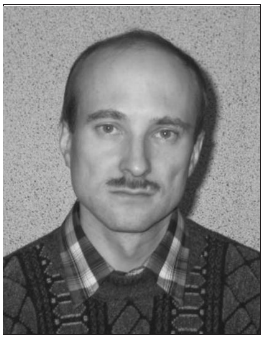

Anton Vjacheslavovich Konovaltsev is the leading engineer of the Radio-Receiver Subsystem Department of the Moscow Aviation Institute (MAI), State Technical University, Russia. He is the author of 7 scientific works in the area of hardware and software of signal processing in radio-electronic systems.

e-mail: kaf407@mai.ru
Moscow Aviation Institute
State Technical University
4, Volokolamskoye shosse
125993 Moscow, Russia

Alexey Aleksandrovich Kukhorev is the post-graduate student of the Moscow Aviation Institute (MAI), State Technical University, Russia. He is the specialist in the area of hardware and software of signal processing in radio-electronic systems.

e-mail: kaf407@mai.ru
Moscow Aviation Institute
State Technical University
4, Volokolamskoye shosse
125993 Moscow, Russia

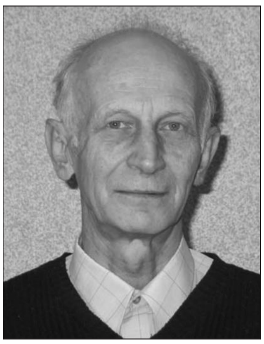

Vladimir Mihajlovich Nujdin works as a Docent of the Radio-Receiver Subsystem Department of the Moscow Aviation Institute (MAI), State Technical University, Russia. He got his Ph.D. from the MAI in 1983. He is the specialist in the area of radar and radio-navigation systems, and the author of more than 50 scientific works.

e-mail: kaf407@mai.ru
Moscow Aviation Institute
State Technical University
4, Volokolamskoye shosse
125993 Moscow, Russia

Vladimir Viktorovich Rastorguev works as a Professor of the Radio-Receiver Subsystem Department of the Moscow Aviation Institute (MAI), State Technical University, Russia. He got his Ph.D. from the MAI in 1978. He is the specialist in the area of the optimal signal processing in radar and radio-navigation systems, and the author of more than 90 scientific works.

e-mail: rast@mai.ru
Moscow Aviation Institute
State Technical University
4, Volokolamskoye shosse
125993 Moscow, Russia

Pavel Vladimirovich Sokolov is the post-graduate student of the Moscow Aviation Institute (MAI), State Technical University, Russia. He is the specialist in the area of the applied software of signal processing in radio-electronic systems, and the author of 7 scientific works.

e-mail:kaf407@mai.ru
Moscow Aviation Institute
State Technical University
4, Volokolamskoye shosse
125993 Moscow, Russia

Invited paper

Setting an Upper-Wavelength Limit to the Supercontinuum Generated in a Photonic Crystal Fibre

Luca Tartara, Vittorio Degiorgio, Rim Cherif, and Mourad Zghal

Abstract—We report about a novel kind of supercontinuum generation in a photonic crystal fibre in which the spectral broadening occurs only on the blue side of the pump wavelength. As a consequence a limit to the extent of the supercontinuum is set and thus a way for tailoring the broadened spectrum according to a peculiar application is provided. We present a theoretical explanation along with experimental data which are supported by the results of a set of numerical simulations.

Keywords— nonlinear optics, photonic crystal fibres, supercontinuum generation.

1. Introduction

Supercontinuum generation (SCG) has attracted a great deal of attention in recent years thanks to the development of photonic crystal fibres (PCFs) which have proven to be ideal media for nonlinear optical interactions [1]. In fact the tight confinement of light provided by the high refractive-index contrast makes high intensities available for long propagation lengths even at moderate power levels. Moreover, the unusual dispersion characteristics of PCFs allow for the fulfilment of the phase-matching condition for several nonlinear processes. Many phenomena contribute thus to the broadening of the input spectrum generating new spectral components which are commonly both red- and blue-shifted for hundreds of nanometers. Such a broadened spectrum can be profitably exploited in several applications with many examples coming from the field of optical communications. A multi-wavelength source covering all the telecom spectral range can be easily obtained from one single-line laser diode by broadening its spectrum. All-optical signal processing also can be performed by means of SCG: in a wavelength division multiplexed system a signal at a given carrier wavelength can be switched to a single destination or multicast to several destinations exploiting the wavelength-conversion capability offered by the filtering of the broadened spectrum of the input signal.

However, the many processes leading to SCG make it impossible to control the evolution of the spectrum in order to generate only the components to be effectively employed. As a consequence a certain amount of spectral power gets wasted falling outside the wavelength range of interest particularly when a given flatness is required. In this work we present a novel kind of SCG in a PCF in which the spectral broadening occurs only on the blue side of the pump wavelength thus setting a limit to the continuum on the long-wavelength side.

2. Theoretical Background

The physics behind SCG in a PCF by means of ultrashort pulses has been the subject of several works focusing on the regime of anomalous dispersion where solitonlike dynamics play a major role. It has indeed been shown that SCG arises from the Raman-induced fission of higher-order solitons. The driving phenomena are the perturbation suffered by the input pulse because of intra-pulse Raman scattering and the following decay into fundamental solitons. Such pulses are then progressively shifted towards longer wavelengths emitting at the same time a resonantly-coupled blue-shifted dispersive wave [2]. Both the theoretical investigations and the experimental demonstrations have considered only the propagation of the fundamental mode of a PCF for which there exists no cut-off wavelength. However, when the launch conditions at the fibre input tip enable the excitation of a higher-order mode, the propagation at wavelengths longer than the cut-off wavelength is no longer possible and therefore the spectral broadening towards the red side due to the Raman effect is prevented. Because of the resonant coupling to the spectral components generated at shorter wavelengths, also the broadening of the spectrum to the blue side is expected to be affected but it is not clear to which extent.

In fact other sources of perturbation such as higher-order linear and nonlinear dispersion have been shown to be responsible for the generation of dispersive waves at shorter wavelengths by solitonlike pulses [3]. Then the broadening of the spectrum would not be prevented and the cut-off wavelength would act as a boundary to the continuum at least on the long-wavelength side. If the input wavelength is tuned very close to the cut-off wavelength a single-sided SCG would occur with new spectral components arising only on the blue side.

We have also carried out a set of numerical simulations about the propagation in a higher-order mode of a femtosecond pulse in a PCF in order to strenghten our theoretical conclusions.

The model we have adopted is based on the generalized nonlinear Schrödinger equation as described in [4]. However, we have introduced a wavelength-dependent loss for keeping into account the effect of the modal cut-off. Loss is set to zero for wavelengths well below the cut-off wavelength and is very high for wavelengths far above. In the region around the cut-off wavelength the loss coefficient varies continuously from the low to the high value. Such a model allows us to clarify the contribution of the several mechanisms playing a role in the spectral evolution by running the numerical simulation excluding certain terms of the nonlinear Schrödinger equation.

The spectrum displayed in Fig. 1(a) is obtained by plugging in the simulation the whole nonlinear response made up of self-phase modulation, stimulated Raman scattering and self-steepening. The cut-off wavelength is set at 830 nm and the pump wavelength at 810 nm, while the zero-dispersion wavelength is 700 nm. The propagation length is 50 cm. Even if the modal cut-off prevents the spectrum from broadening towards longer wavelengths, a white-light radiation is clearly generated on the blue side of the pump wavelength. In such a way it is thus possible to control the extent of the supercontinuum spectrum simply by tuning the input wavelength close to the cut-off wavelength and choosing appropriate values of the input power and the fibre length fixing the short-wavelength edge.

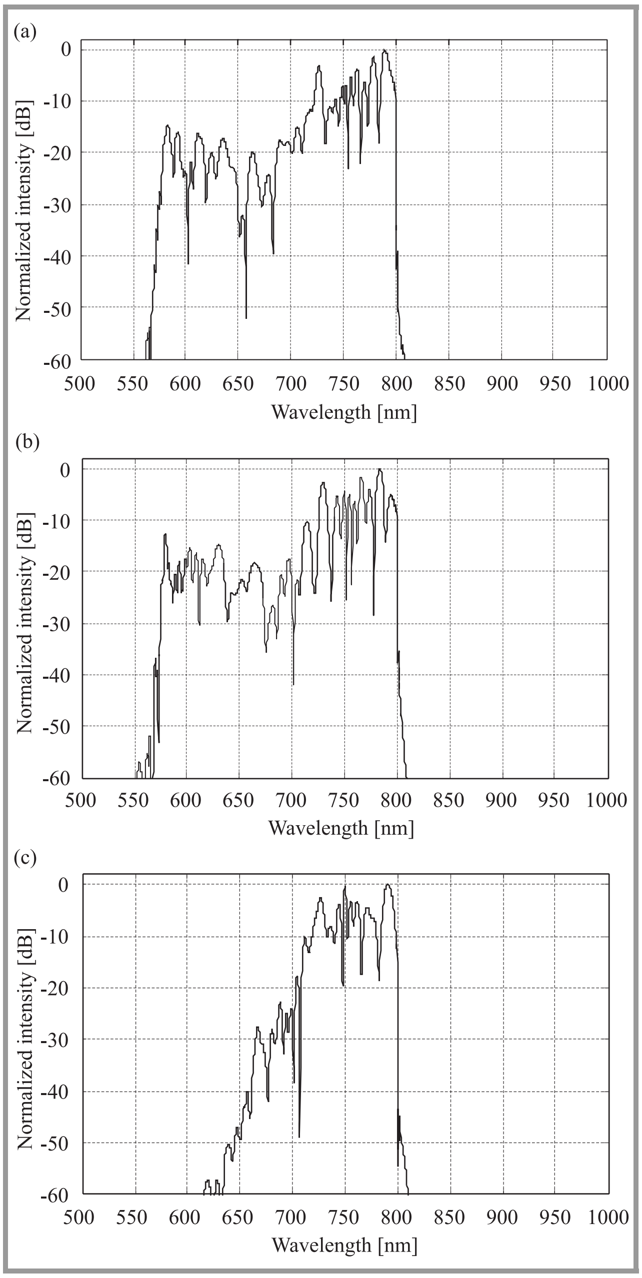

Fig. 1. Numerically computed supercontinuum spectrum: (a) by employing the whole model; (b) by excluding nonlinear perturbations; (c) by isolating the contribution of Raman scattering.

The numerical tool we have developed allows then to identify which kind of perturbation turns out to be mainly responsible for the generation of the blue-shifted continuum. Figure 1(b) shows the spectrum obtained when the nonlinear perturbations are neglected, that is to say, when the terms accounting for the stimulated Raman scattering and the self-steepening effects are not included in the nonlinear Schrödinger equation. The contribution of the higher-order linear dispersion is instead working. The values of the excitation and of the fibre parameters are kept constant. The result is highly similar to the one reported in Fig. 1(b) suggesting that the main reason for the growth of dispersive waves leading to SCG is the effect of the differential dispersion. As a proof of that one can consider the spectrum displayed in Fig. 1(c), which is the result provided by the numerical tool when the only active perturbation is the one coming from the Raman effect. In such a case the broadening to the blue side has a much smaller extent as the impossibility for the Raman solitons to propagate hinders the resonant coupling to the shorter-wavelength dispersive waves.

3. Experimental Set-up

The photonic crystal fibre used in our experiments is shown in Fig. 2. The air-silica microstructure is made up of holes with a 2.5-μm average diameter which are arranged in a hexagonal pattern with a 2.7-μm pitch. The linear dimension of the solid core is about 2.2 μm.

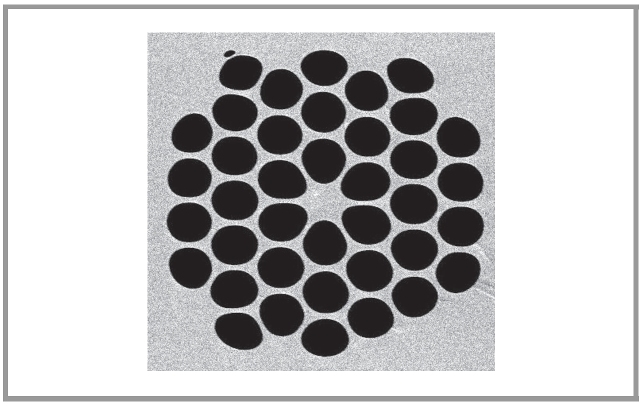

Fig. 2. Image of the cross section of the fibre taken by a scanning electron microscope.

We have performed a numerical investigation about the modal properties of the fibre. The spatial patterns of the fundamental mode and of the first two higher-order modes are depicted in Fig. 3. We will refer to them as mode 0, mode 1 and mode 2. The zero dispersion wavelengths are 840 nm, 660 nm and 600 nm, respectively. The cut-off wavelength of mode 1 is around 1300 nm and the cut-off wavelength of mode 2 is 830 nm.

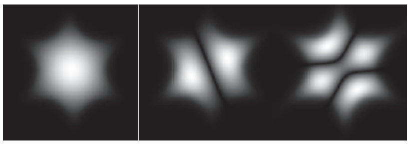

Fig. 3. Spatial patterns for mode 0 (left), mode 1 (centre), and mode 2 (right).

The light source is a cw-mode locked Ti:Sapphire laser delivering a train of femtosecond pulses at the repetition rate of 80 MHz. The wavelength can be tuned from 700 nm to 900 nm. In order to avoid harmful backreflections from the input tip of the fibre we employ a Faraday isolator which broadens the pulsewidth up to 190 fs.
The laser beam is coupled into a PCF span of 50-cm length by means of an aspheric lens having a numerical aperture of 0.65. The fibre is mounted on a three-axes translation stage allowing the positioning of the fibre with a resolution of 20 nm. Thanks to this kind of set-up we can exploit an offset pumping technique moving the input tip of the fibre in the focal plane. We are thus able to obtain a selective excitation of different fibre modes at the expense of the coupling efficiency: the higher the order of the mode, the lower the coupled power.
At the output end of the fibre the light is collected by a 100 x objective with a numerical aperture of 0.95. The spectral properties of the output radiation are monitored by an optical spectrum analyzer having a resolution of 0.1 nm.

4. Experimental Results

For input wavelengths above 810 nm only mode 0 can be excited regardless of the positioning of the fibre in the focal plane. By increasing the input power, we can record a progressive broadening of the output spectrum occurring in quite a symmetrical fashion as no limitations to the propagation occur. We will not discuss this case any longer as it represents the usual situation described in many other works. A further insight is nevertheless reported in [5].
When the pump wavelength is tuned below 810 nm we are able to excite several modes. By a proper positioning of the fibre in the focal plane the excitation turns out to be highly selective so that at the output of the fibre we can easily detect either mode 0 or mode 1, or mode 2.
Mode 1 can be easily excited and the coupling efficiency is not severely degraded in comparison to the fundamental mode. Soliton dynamics play a fundamental role as the propagation occurs in the anomalous dispersion regime. Therefore the spectral evolution leading to SCG is characterized by the appearance of new components on both sides of the input wavelength. However, it is important to notice that the generation of red-shifted spectral components stops at wavelengths shorter than 1300 nm with a progressive decaying intensity above 1100 nm. The explanation for such a behavior is the influence of the cut-off wavelength making the propagation at wavelengths longer than 1300 nm impossible.
The excitation of mode 2 is instead rather difficult. The focal spot of the pump beam has in fact to be carefully positioned on the input cross section of the fibre far away from the point yielding the highest coupling efficiency. Such a strong offset severely affects the available power inside the fibre, which results very low in comparison to mode 0 and even mode 1. The maximum average power we can record at the output of the fibre span is indeed below 20 mW even if the exact value could be slightly higher because of the limited collection efficiency provided by the objective. Nevertheless the spectrum broadens down to the blue region as in the previous cases. However, no spectral components on the long wavelength side are generated. An example of such a kind of supercontinuum spectrum is shown in Fig. 4. Even when the pump wavelength is tuned down to 705 nm, the spectrum broadening is exclusively towards shorter wavelengths except for an isolated peak arising near 800 nm with a very weak intensity.

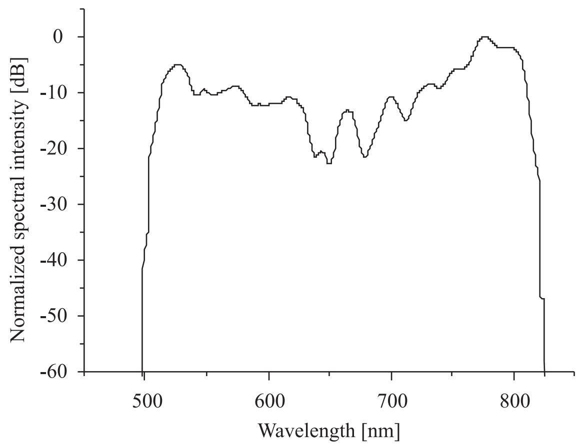

Fig. 4. Supercontinuum spectrum obtained for mode 2 when the pump wavelength is 785 nm and the output power is 5 mW.

This spectrum shown in Fig. 4 is a clear demonstration of the possibility of controlling and limiting the extent of the supercontinuum by exploiting the cut-off wavelength of a higher-order mode.

5. Conclusions

We have studied both numerically and experimentally the role played by the cut-off wavelength in the dynamics of supercontinuum generation in a photonic crystal fibre. It has been shown that its effect does not hinder the spectrum from broadening towards shorter wavelengths. On the contrary it can be exploited to tailor the extent of the supercontinuum setting a limit on the long-wavelength edge.

References

[1] J. M. Dudley, G. Genty, and S. Coen, "Supercontinuum generation in photonic crystal fibers", *Rev. Mod. Phys.*, vol. 78, no. 4, pp. 1135–1184, 2006.

[2] L. Tartara, I. Cristiani, and V. Degiorgio, "Blue light and infrared continuum generation by soliton fission in a microstructured fiber", *Appl. Phys. B*, vol. 77, no. 2–3, pp. 307–311, 2003.

[3] Y. Kodama and A. Hasegawa, "Nonlinear pulse propagation in a monomode dielectric waveguide", *IEEE J. Quant. Electron.*, vol. 23, no. 5, pp. 510–524, 1987.

[4] I. Cristiani, R. Tediosi, L. Tartara, and V. Degiorgio, "Dispersive wave generation by solitons in microstructured optical fibers", *Opt. Expr.*, vol. 12, no. 1, pp. 124–135, 2004.

[5] R. Cherif, M. Zghal, L. Tartara, and V. Degiorgio, "Supercontinuum generation by higher-order mode excitation in a photonic crystal fiber", *Opt. Expr.*, vol. 16, no. 3, pp. 2147–2152, 2008.

Luca Tartara received his "Laurea" degree in electronics with honours in 1999 and his Ph.D. in electronics and computer sciences in 2004 both from the Faculty of Engineering at the University of Pavia. He is Assistant Professor in physics of matter at the same university, since 2005. He is the author or co-author of more than 50 publications on international peer-reviewed journals and contributions to international conferences in the following fields: nonlinear optics and nonlinear optical materials, fiber optics, lasers and parametric light sources, characterization of ultrashort light pulses.
e-mail: luca.tartara@unipv.it
Department of Electronics
University of Pavia
Via Ferrata 1
27100 Pavia, Italy

Vittorio Degiorgio is Full Professor of quantum electronics at the University of Pavia, since 1980. His scientific activity has been devoted to laser physics, laser-light scattering as applied to the study of phase transitions and aggregation phenomena in complex fluids, and nonlinear optical materials. Recent work is focused on the Raman fiber laser, on wavelength conversion in nonlinear waveguides and its application to optical communications, on nonlinear optical interactions in microstructured fibers. He is a Fellow of the Optical Society of America and a member of the Italian Physical Society.
e-mail: vittorio.degiorgio@unipv.it
Department of Electronics
University of Pavia
Via Ferrata 1
27100 Pavia, Italy

Rim Cherif received her engineering degree in telecommunications from the National Institute of Applied Sciences and Technology (INSAT), Tunisia, in 2004, and her M.Sc. degree from the Engineering School of Communication of Tunis (Sup'Com), Tunisia, in 2005. Presently, she is pursuing her Ph.D. in Sup'Com. Her current research focuses on numerical and experimental characterization of photonic crystal fiber properties.
e-mail: rim.cherif@isetcom.rnu.tn
Cirta'Com Laboratory
Engineering School of Communication of Tunis (Sup'Com)
Ghazala Technopark
2083 Ariana, Tunisia

Mourad Zghal received his engineering degree in telecommunications from the Engineering School of Communication of Tunis (Sup'Com), Tunisia, in 1995, his M.Sc. degree in 1996, and his Ph.D. degree in electrical engineering in 2000. He worked as an instructor in telecommunication from 1995 to 2001. In 2001, he joined the Electronics Department of the National Institute of Engineers of Tunis, where he started to investigate characterization of new generation optical fiber such as photonic crystal fibers and Bragg fibers. He joined in 2003 the Electronics Department of Sup'Com. Dr. Zghal is involved in numerous international collaborations involving laboratories in Canada, France, Italy, and South Africa. He is a founding member of the African Laser Centre and the Optical Society of Tunisia.
e-mail: mourad.zghal@supcom.rnu.tn
Cirta'Com Laboratory
Engineering School of Communication of Tunis (Sup'Com)
Ghazala Technopark
2083 Ariana, Tunisia

Invited paper

RoFnet – Reconfigurable Radio over Fiber Network Architecture Overview

Maria C. R. Medeiros, Ricardo Avó, Paula Laurêncio, Noélia S. Correia, Alvaro Barradas, Henrique J. A. da Silva, Izzat Darwazeh, John E. Mitchell, and Paulo M. N. Monteiro

Abstract—This paper introduces the basic operational concepts of the RoFnet – reconfigurable radio over fiber network, which is a project supported by the Portuguese Foundation for Science and Technology. This project proposes an innovative radio over fiber optical access network architecture, which combines a low cost base station (BS) design, incorporating reflective semiconductor optical amplifiers, with fiber dispersion mitigation provided by optical single sideband modulation techniques. Optical wavelength division multiplexing (WDM) techniques are used to simplify the access network architecture allowing for different BSs to be fed by a common fiber. Different wavelength channels can be allocated to different BSs depending on user requirements. Additionally, in order to improve radio coverage within a cell, it is considered a sectorized antenna interface. The combination of subcarrier multiplexing with WDM, further simplifies the network architecture, by using a specific wavelength channel to feed an individual BS and different subcarriers to drive the individual antenna sectors within the BS.

Keywords*— *optical access networks, optical single sideband, radio over fiber, reflective semiconductor optical amplifiers, wavelength division multiplexing.

1. Introduction

Internet technologies are now considered as the universal communication platform. Broadband access communication is rapidly becoming widely available, e.g., asymmetric digital subscriber line (ADSL) is now available in almost all parts of Europe. In parallel to the growth of the Internet, wireless and mobile network technologies have witnessed a great development. Mobile phone penetration exceeds that of fixed phones in most developed countries.

Wireless communications are entering a new phase where the focus is shifting from voice to multimedia services. Present mobile network users want to be able to use their mobile terminals and enjoy the same user experience as they do while connected to their fixed network either at work or at home. Wireless local area network (WLAN) hotspots based on IEEE 802.11 are a reality, and many consumer devices (Laptop PCs, mobile telephones, PDAs, etc.) have Bluetooth enabling them to establish a wireless personal area network. In this context, third generation (3G) of wireless networks have already adopted IP as the core network protocol in their data subsystems, as well as promising guaranteed quality for multimedia service, in both access and core networks. However, the services offered by wired local area network (LAN) connections require a broadband network with capacity even higher than 7 Mbit/s per radio channel. Unfortunately, the actual wireless telecommunication network only provides narrowband communications when compared to wired LAN connections and thus a radio interface capable of supporting very high data rates, has to be developed. Over the last decade the millimeter-wave frequency band (26 to 100 GHz) has been pointed out as the best spectral region to provide broadband access to wireless networks [1]. However, the limited propagation characteristics of these high frequencies lead to small cell sizes. As a consequence, a large number of remote antenna base stations (BSs) is necessary to cover an operational geographical area. The multiple BSs providing wireless connectivity to users via millimeter-wave radio links are connected with a central office (CO) via an optical fiber access network. The CO performs the switching and routing functionalities.

The RoFnet – reconfigurable radio over fiber network project, introduced here, uses optical wavelength division multiplexing (WDM) techniques to simplify the network architecture allowing different BSs to be fed by a common fiber, with different WDM channels feeding different BSs. Additionally, in order to improve radio coverage within a cell, utilization of sectorized antenna interfaces is considered. Each antenna sector should be driven by an individual signal. The combination of subcarrier multiplexing (SCM) with WDM, simplifies the network architecture, since a specific WDM channel is fed to an individual BS and different SCM channels carried on the WDM wavelength channel are used to drive the individual antenna sectors within the BS.

For the downlink the millimeter-wave signals are transmitted directly over the fiber. This approach has the advantage of a simplified BS design but is susceptible to fiber chromatic dispersion that severely limits the transmission distance [2]. The RoFnet will employ optical single sideband (OSSB) modulation techniques to overcome fiber dispersion effects.

For the realization of the uplink of a radio over fiber (RoF) system using WDM, the BSs must incorporate an optical source, which is modulated by the millimeter-wave uplink radio signals. This approach suffers from several disadvantages. Namely, each BSs requires a WDM optical sources and a high-speed external modulator, resulting in a high cost BS. The RoFnet proposes a novel low cost uplink configuration, which eliminates the need for an expensive WDM source and the optical external modulator at the BS. This is accomplished by using a reflective semiconductor optical amplifier (RSOA) in the BS which replaces the high cost WDM source and the high-speed external modulator. This approach offers several advantages. First, it avoids the need of stabilized a laser at each BS. Second, the RSOA can be used as a modulator which accomplishes both modulation and amplification functions. Moreover, this amplification function gives additional gain enabling the possibility of avoiding the use of an erbium-doped fiber amplifier (EDFA) in the system. For the first time, this uplink configuration exploits the capabilities of using RSOAs in RoF systems and this alternative may be applied to other wireless networks such as 3G mobile communication systems.

The reminder of this paper is organized as follows. Section 2, the network architecture is presented, emphasizing both the uplink and downlink operation. Section 3 discusses the fiber transmission limitations due to the fiber chromatic dispersion and how they can be minimized by the use of optical single sideband. The advantages of using WDM technology in radio over fiber systems are considered in Section 4 and finally Section 5 concludes the paper.

2. Network Description

Figure 1 shows the schematic of the RoFnet architecture concept, where N base stations provide the wireless connectivity to users via millimeter-wave radio links. The BSs are connected with a central office via an optical fiber access network employing WDM technology. Each BS is connected to the fiber access network by two fibers, one for uplink transmission and another for downlink transmission.

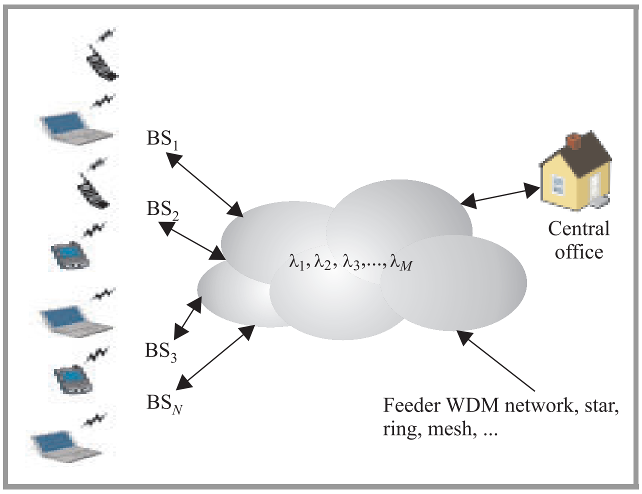

Fig. 1. Overall RoFnet architecture.

Each BS incorporates an antenna with L sectors. Each antenna sector is fed by an SCM channel. The use of WDM provides a simple topology, leading to easier network management and increases the capacity by allocating different wavelengths to individual remote nodes [3]. This solution is widely accepted and the necessary WDM technology is available. However, if this approach is to be implemented a cost effective implementation needs to be found.

A dynamic wavelength allocation scheme for WDM RoF systems using a novel add-drop multiplexer was demonstrated in [4]. An important feature of this scheme is the possibility of dynamic network reconfiguration when needed, namely through the wavelength reassignment to different base stations. Flexible wavelength allocation is an elegant strategy for dealing with traffic fluctuations since it allows efficient allocation of network resources by adaptively adjusting to the offered load. However, the implementation presented in [4] requires a new expensive device. The RoFnet architecture, by using a RSOA in the BS, eliminates the need of expensive devices. RSOAs are presently considered key devices for the future high-speed passive access optical networks (PONs) [5]. A RSOA can be used with both modulation and amplification functions. Moreover, a RSOA operated in the gain saturation region can reduce the intensity noise of the optical signal. The 3 dB electrical bandwidth of commercially available devices is up to 1.5 GHz in the long wavelength bands in the range of 50 to 100 nm. The wavelength range mainly depends on the RSOA manufacturing process.

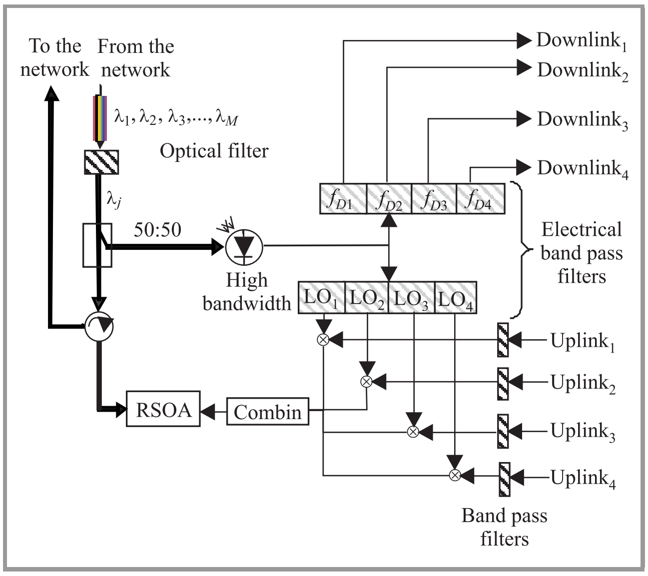

Fig. 2. Schematic diagram of a base station.

In the RoFnet architecture, the CO, as well as performing all the switching, routing and frequency management, also generates the M optical WDM carriers required for uplink operation of the N BSs of the RoF network.

Each BS, as represented in Fig. 2, is equipped with a fixed optical filter, and thus operates only with a unique specific wavelength λ_j.

2.1. Downlink Operation

Base station j receives the downlink millimeter-wave signal on wavelength channel λ_j. The downlink millimeter-wave signal is composed by L multiplexed subcarriers combined with a set of unmodulated RF carriers, as shown in Fig. 3.

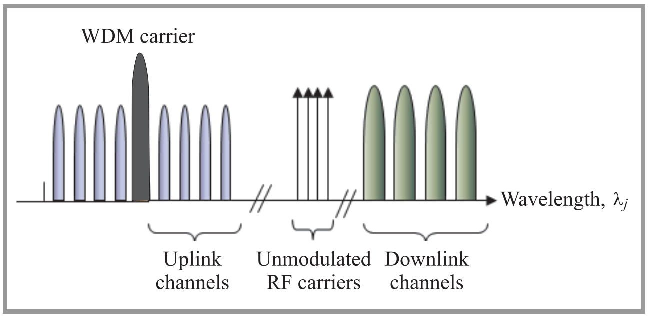

Fig. 3. Optical spectrum around wavelength carrier.

The L SCM channels feed the L antenna sectors, and the set of unmodulated RF carriers are used in the uplink operation. The unmodulated RF carriers and the downlink signals are generated at the CO and modulate an optical carrier using optical single sideband modulation. The OSSB modulation is used in order to minimize the fiber dispersion effects and to improve spectral efficiency.

We note that OSSB modulation is required only at the CO, and thus it does not increase the cost of the BS. At the BS, the downlink optical signal in wavelength channel λ_j is split by a fiber coupler. One part is directed to the RSOA, and the other part is detected by a high bandwidth receiver. The detected signal consists of the downlink millimeter-wave signal and the unmodulated RF carriers.

2.2. Uplink Operation

The downlink optical carrier travels through the RSOA, where it is amplified and modulated by the uplink data, which has been down converted to an intermediate frequency (IF). The unmodulated RF carriers act as local oscillators (LO) and are used to down-convert the uplink data to an IF, within the electrical bandwidth of the RSOA (1.2 GHz). The RSOA is directly modulated by the SCM uplink signals, and thus the optical carrier is double sideband modulated, as represented in Fig. 3.

Using this technique, the uplink optical signal is generated by recovering a portion of the optical carrier used in the downlink transmission. Although optical frequency reuse techniques previously used eliminate the need for a WDM optical source at each BS, they require a high-speed external modulator at the BS. However, the necessary bandwidth of the external optical modulator can be reduced if the uplink signal is down converted by mixing it with a local oscillator. The generation of a LO at the BS increases its complexity and therefore should be avoided. The solution adopted in RoFnet is the remote delivery of the LO, as implemented in [6].

3. Transmission Limitation in Radio over Fiber Networks

The performance of RoF systems may be severely impaired by fiber chromatic dispersion [2]. This effect can be overcome by using optical single sideband modulation. The benefits of OSSB modulation have been demonstrated both for radio frequency carriers modulated onto optical carriers and baseband systems. The OSSB improves immunity to chromatic dispersion relative to transmission using conventional optical double sideband (ODSB) modulation, as well as enhancing spectral efficiency.

The importance of OSSB has driven the development of multiple techniques for its implementation. They can be classified into optical heterodyning technique, filtering methods and OSSB modulators. In this project we will focus on OSSB modulators. The simplest design is based on a dual-electrode Mach-Zehnder electrooptic modulator driven by electrical signals with a 90° phase-shift (Hilbert transformed). Other designs also use Hilbert transformed electrical signals applied to either a series combination of intensity and phase modulator or other configurations [7], [8]. Recently, an optoelectrical filter for 40 GHz OSSB generation has been demonstrated [9].

Although, it has been demonstrated that optical single sideband when combined with subcarrier multiplexing techniques (named OSSB/SCM) can significantly improve the system immunity to chromatic dispersion, as well as being more spectrally efficient, increasing and understanding OSSB/SCM system performance continues deserving great interest [10]. As in conventional SCM systems, two important transmission limitations exist in OSSB/SCM systems: the relative intensity noise (RIN) and the intermodulation distortion. Optical carrier suppression has been shown experimentally to be a key issue affecting the performance of OSSB/SCM systems [8]. Chen and Way [10] have developed a powerful analysis which is able to quantify the composite second-order (CSO) and composite tripe beat (CTB) of an OSSB/SCM system, however their analysis is restricted to the case where the optical carrier is not suppressed. The analysis presented in [11] removes this restriction and shows how the suppression of the optical carrier affects the intermodulation distortion in terms of CTB and CSO. Other important feature of OSSB/SCM is its combination with wavelength division multiplexing.

4. Dynamic Wavelength Allocation

Traffic in wireless networks is highly dynamic. Therefore the access network should be reconfigurable depending on the traffic scenario. The network architecture defined in the previous section is reconfigurable and therefore can dynamically change its state according to the traffic needs. The RoFnet network is operated with M optical WDM sources and N BSs. Each BS is equipped with a fixed optical filter and therefore operates only with a unique specific wavelength λ_j. We consider $M < N$, i.e., the number of optical carriers present in the network is less than the number of served BSs. Such assumption means that rather than providing fixed capacity tailored to the "busy-hour" across the network, the optical carriers are allocated to BSs depending on their needs. The optical carriers are generated by fixed lasers as well as by tunable lasers. The fixed optical carriers are allocated to BSs which should be always on use and the tunable carriers are allocated to BSs that might be out of use during some time. Therefore, besides demonstrating the feasibility of the RoFnet architecture another objective is to exploit its capabilities namely by developing wavelength allocation algorithms able to allocate network resources depending on varying user demand and quality of service (QoS).

5. Conclusion

This paper introduces a novel network architectures suited for radio over fiber networks, combining low complexity with flexibility and cost effectiveness. Its two main characteristics are: low cost BS based on RSOAs and use of optical single sideband modulation to improve the system immunity to chromatic dispersion, as well as the spectral efficiency. Additionally, an important advantage of RoFnet is the generation and management of the optical carriers at the CO. As well as facilitating wavelength monitoring and control this approach provides flexible wavelength allocation for the BSs depending on user requirements.

Acknowledgments

This work was supported by the Foundation for Science and Technology within the project PTDC/EEA-TEL/71678/2006.

References

[1] J. J. O'Reilly, P. M. Lane, J. Attard, and R. Griffin, "Broadband wireless systems and networks: an enabling role for radio-over-fibre", *Phil. Trans. Royal Soc.*, vol. 358, no. 1773, pp. 2297–2308, 2000.

[2] H. Schmuck, "Comparison of optical millimeter-wave system concepts with regard to chromatic dispersion", *Electron. Lett.*, vol. 31, pp. 1848–1849, 1995.

[3] H. Bolcskei, A. J. Paulraj, K. V. S. Hari, and R. U. Nabar, "Fixed broadband wireless access: state of the art, challenges, and future directions", *IEEE Commun. Mag.*, vol. 39, no. 1, pp. 100–108, 2001.

[4] W.-P. Lin, "A robust fiber-radio architecture fow wavelength-division-multiplexing ring-access network", *J. Lightw. Technol.*, vol. 23, no. 9, pp. 2610–2620, 2005.

[5] A. Borghesani, "Optoelectronic components for WDM-PON", in *Proc. ICTON 2007*, Rome, Italy, 2007, pp. 305–308.

[6] C. Lim, A. Nirmalathas, D. Novak, and R. Waterhouse, "Millimeter-wave broad-band fiber-wireless system incorporating baseband data transmission over fiber remote LO delivery", *J. Lightw. Technol.*, vol. 18, no. 10, pp. 1355–1363, 2004.

[7] G. H. Smith, D. Novak, and Z. Ahmed, "Technique for optical SSB generation to overcome dispersion penalties in fiber-radio systems", *Electron. Lett.*, vol. 33, no. 1, pp. 74–75, 1997.

[8] A. Loayssa, R. Hernandez, and B. Benito, "Optical single sideband modulators and their applications", *Fib. Integr. Opt.*, vol. 23, pp. 171–188, 2004.

[9] D. Fonseca, A. V. T. Cartaxo, and P. Monteiro, "Opto-electrical filter for 40 Gb/s optical single sideband signal generation", in *Proc. OFC Conf.*, Anaheim, USA, 2006, Paper JThB14.

[10] W. H. Chen and W. I. Way, "Multichannel single-sideband SCM/DWDM transmission systems", *J. Lightw. Technol.*, vol. 22, no. 7, pp. 1679–1693, 2004.

[11] P. Laurencio, S. O. Simões, and M. C. R. Medeiros, "Impact of the combined effect of RIN and intermodulation distortion on OSSB/SCM systems", *J. Lightw. Technol.*, vol. 24, no. 11, pp. 4250–4260, 2006.

Maria C. R. Medeiros obtained the B.Sc. in electronics engineering from the University of Aveiro, Portugal, and the M.Sc. and Ph.D., both in electronic engineering, from the University of Wales, UK. Presently she is an Auxiliary Professor in telecommunications for the Faculty of Science and Technology at the University of Algarve, Portugal. She previously worked as a researcher at the University of Wales. Her research interests include modeling and optimization of optical WDM networks and radio over fiber techniques for access networks. She acted as the leader of several research projects namely the RoFnet project. Prof. Medeiros is the leader of the Center of Electronics, Optoelectronics and Telecommunications (CEOT).

e-mail: cmedeiro@ualg.pt
Center for Electronics, Optoelectronics
and Telecommunications (CEOT)
University of Algarve
8000 Faro, Portugal

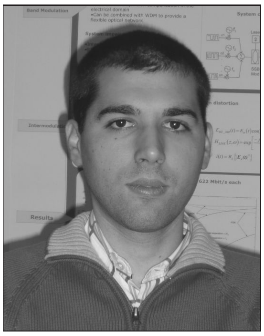

Ricardo Avó received the Licenciatura degree from the University of Algarve, Portugal, in 2006. Currently, he is a researcher at the Center of Electronics, Optoelectronics and Telecommunications conducting research towards his Ph.D. His research interests include optical networks and radio over fiber access networks.

e-mail: ricardoavo@ualg.pt
Center for Electronics, Optoelectronics
and Telecommunications (CEOT)
University of Algarve
8000 Faro, Portugal

Paula Laurêncio received the Licenciatura degree in electrical engineering and the M.Sc. degree in telecommunications and computers from the Lisbon Technical University, Portugal. She obtained a Ph.D. degree in computing and electronics engineering in the University of Algarve, Faro, Portugal, in 2006. Her main current research interests include characterization and modeling of single sideband fiber optic communications systems and subcarrier and radio over fiber techniques.
e-mail: plaurenc@ualg.pt
Center for Electronics, Optoelectronics
and Telecommunications (CEOT)
University of Algarve
8000 Faro, Portugal

Noélia S. Correia works as Professor at the Faculty of Science and Technology of the University of Algarve, Portugal. She received her B.Sc. and M.Sc. in computer science from the University of Algarve. The Ph.D. in survivable WDM networks, obtained at the University of Algarve, was done in collaboration with the University College London, UK. Her research interests include throughout and network cost optimization, survivability, and other related optical network issues.
e-mail: ncorreia@ualg.pt
Center for Electronics, Optoelectronics
and Telecommunications (CEOT)
University of Algarve
8000 Faro, Portugal

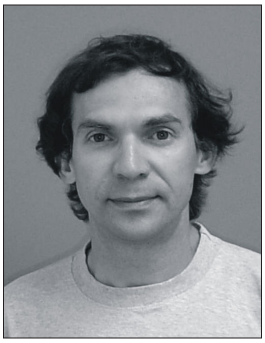

Alvaro Barradas received his M.Sc. in computer science from the University of Algarve, Portugal, in 2004. Currently he is an assistant lecturer at the Faculty of Science and Technology and a Ph.D. student in the Center for Electronics, Optoelectronics and Telecommunications at the University of Algarve. His research area focuses on provisioning of quality of service improvement mechanisms for optical burst switching networks based on contention avoidance schemes. His present research interests also include other optical network switching paradigms, their related communication protocols, and the object oriented approach to the simulation of communications systems. His previous professional experience includes 2 years of work as a programmer/analyst for a large computer science and telecommunications consulting company, doing system test at the telecommunications branch. He is also a CCNA instructor at the local Cisco Academy.
e-mail: abarra@ualg.pt
Center for Electronics, Optoelectronics
and Telecommunications (CEOT)
University of Algarve
8000 Faro, Portugal

Henrique J. A. da Silva received his Ph.D. degree in communication systems engineering from the University of Wales, UK, in 1988. Since then he has been with the Department of Electrical and Computer Engineering at the University of Coimbra, Portugal, where he is now an Associate Professor. He is the leader of the Optical Communications Group of the Institute of Telecommunications at the University of Coimbra, since 1992. His research interests include optical and mobile communication systems, with emphasis on enabling technologies and transmission techniques.
e-mail: hjas@ci.uc.pt
Institute of Telecommunications
Department of Electrical and Computer Engineering
University of Coimbra
Pólo II, Pinhal de Marrocos
P-3030-290 Coimbra, Portugal

Izzat Darwazeh holds the University of London Chair of Communications Engineering in the Department of Electronic and Electrical at the University College London (UCL), UK. Born in 1963, he obtained his first degree in electrical engineering from the University of Jordan in 1984 and the M.Sc. and Ph.D. degrees, from the University of Manchester Institute of Science and Technology (UMIST), in 1986 and 1991, respectively. He worked in the Universities of Wales and Manchester before joining UCL in Oct. 2001, where he is currently the Head of the 80 strong Communications and Information System (CIS) Group and the Director of UCL Telecommunications for Industry Programme. He is a Fellow of the IET and a senior member of the IEEE. His research interests are mainly in the areas of wireless communication system design, modeling and implementation, high-speed optical communication systems and networks, microwave circuits and MMICs for optical fibre applications and in mobile and wireless

communication circuits and systems. He has authored/co-authored more than 130 research papers.

e-mail: I.darwazeh@ee.ucl.ac.uk
Telecommunications Research Group
Department of Electronic and Electrical Engineering
University College London (UCL)
Torrington Place, London, WC1E 7JE, UK

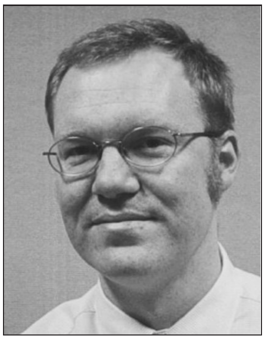

John E. Mitchell received the Ph.D. degree in electronic engineering from the University College London (UCL), UK, in 2000. In 1999 he became a research fellow in the Department of Electronic and Electrical Engineering at UCL, becoming a lecturer and senior lecturer in 2000 and 2006, respectively. He has published over 40 papers in the area of optical communications. His research interests include optical access technologies and the transport of millimeter-wave radio signals over optical fibre for communications, and noise relating to crosstalk in optical networks. He is a member of the Institute of Engineering and Technology (IET) and the IEEE Lasers and Electro-Optics Society (IEEE-LEOS).

e-mail: J.mitchell@ee.ucl.ac.uk
Telecommunications Research Group
Department of Electronic and Electrical Engineering
University College London (UCL)
Torrington Place, London, WC1E 7JE, UK

Paulo Monteiro was born in Coimbra, Portugal, in 1964. He received the diploma and doctoral (Ph.D.) degrees in electronics and telecommunications from the University of Aveiro, Portugal, and the M.Sc. degree from the University of Wales, UK. He is Optical Networks Technology Manager at the Transport, Aggregation and Fixed Access Department of Nokia Siemens Networks. He is also Associate Professor at the University of Aveiro and researcher at the Institute of Telecommunications. His main research interests include high speed communications for access and core optical networks, fixed-mobile convergence. He has acted as a reviewer of the IEEE Journal of Lightwave Technology, IEE Electronics Letters, ETRI Journal and OSA Journal of Optical Networking (JON), SPIE Optical Engineering. He has participated in several national and European projects and his currently the project coordinator of the large-scale integrating project FUTON. He has authored/co-authored more than 18 patent applications and over 200 refereed papers and conference contributions.

e-mail: Paulo.1.monteiro@nsn.com
Nokia Siemens Networks Portugal S.A.
R. Irmãos Siemens st 1
2720-093 Amadora, Portugal

Institute of Telecommunications
University of Aveiro
3810-193 Aveiro, Portugal

Invited paper

Methods of Step-Size Distribution Optimization Used in S-SSFM Simulations of WDM Systems

Marek Jaworski

Abstract—Brief review of methods used for simulation of signal propagation in wavelength division multiplexed (WDM) links is presented. We propose two novel methods of step-size distribution optimization used to improve symmetrized split step Fourier method (S-SSFM) numerical efficiency: pre-simulated local error S-SSFM (PsLE S-SSFM) and modified logarithmic (ML S-SSFM). The PsLE S-SSFM contains two stages: in the initial stage step-size distribution optimization is carried out by combining local error method and pre-simulation with signal spectrum averaging; in the second stage conventional SSFM is used by applying optimal step-size distribution obtained in the initial stage. The ML S-SSFM is generalization of logarithmic method proposed to suppress spurious FWM tones, in which a slope of logarithmic step-size distribution is optimized. Overall time savings exceed 50%, depending of a simulated system scenario.

Keywords— ***local error method, logarithmic step, simulation, split step Fourier method, WDM systems.***

1. Introduction

Split step Fourier method (SSFM) is commonly used for simulating of light propagation in an optical fibre, described by the nonlinear Schrödinger equation (NLSE) [1], due to its high numerical efficiency. Optimization of simulation time and accuracy is considered in many publications [2]–[12]. Higher order numerical methods (i.e., explicit Adams-Bashforth and implicit Adams-Moulton, etc.) or predictor-corrector methods [2] are used when the highest accuracy is needed. In this case the numerical effectiveness is better than for conventional symmetrized SSFM (S-SSFM). These methods are especially useful for simulations of soliton propagation, where linear (L) and nonlinear (N) operators in SSFM are self-balanced.

Typically, there are higher dispersion and lower nonlinearity in wavelength division multiplexed (WDM) transmission, when comparing to soliton transmission. As a consequence, special tailored methods should be applied for simulation of signal propagation in WDM links. In this case, S-SSFM is especially effective. It is a method of order $O(h^2)$, which is adequate for relatively low accuracy required (of the order of $10^{-2} - 10^{-3}$). Besides common used S-SSFM, another methods are used in special cases, e.g., split step wavelet collocation is faster then S-SSFM in very wideband simulations [3], but is applicable only for zero dispersion slope ($\beta_3 = 0$).

Modern WDM systems contain large number of channels and occupy very wide bandwidth, which cause difficulties in simulations due to spurious four wave mixing (FWM) and walk-off effect. Two class of methods are distinguished: single-band [1]–[7], [12] – in which full-bandwidth of WDM transmission is simulated, and multi-band [8]–[11] – in which separate channels are simulated by taking into consideration an influence of adjacent channels (Fig. 1). The single-band methods give an exact solution of the nonlinear Schrödinger equation, including the impact of nonlinear phenomena, like: self-phase modulation (SPM), cross-phase modulation (XPM) and FWM, but on the other hand, these methods are used mainly in narrow bandwidth cases due to its high simulation time. The multi-band methods are faster and more flexible, but give only limited information of nonlinear phenomena (i.e., SPM, XPM but not FWM) derived from other channels.

An optimal step-size in S-SSFM is of uttermost importance to improve the numerical efficiency. Local error method (LEM) is especially useful for step-size optimization, because it automatically adjusts simulation step for required accuracy [5]. In this method step-size is selected by calculating the relative local error δ_L of each single step, taking into account the error estimation and linear extrapolation. LEM provides higher accuracy than S-SSFM method, because it is of order $O(h^3)$. Simulations are conducted simultaneously with coarse ($2h$) and fine (h) steps, which needs additional 50% operations comparing with S-SSFM. Different multi-band methods have been evaluated in [11] and application of LEM method to XPM simulation in place of fixed-step was proposed, which improves simulation accuracy and efficiency up to 30%.

Lately, methods known in quantum mechanics was used for step-size calculation [4]. The optimal step-size $h_{optimal}$ can be estimated analytically for required global error δ_G. This procedure is fast in the case of lossless fiber. In a more realistic case with lossy fiber, the optimal step-size can be estimated as well, but with an additional computational effort [4].

In pre-simulation method the step-size is selected by calculating the global error δ_G in a series of fixed-step S-SSFM pre-simulations with signal spectrum averaging [6]:

$$\left|U_n^{red}\right| = \sqrt{\sum_{i=n\cdot N_{red}}^{n\cdot N_{red}+N_{red}-1} \left|U_i\right|^2},$$

$$\arg(U_n^{red}) = \arg\left[\sum_{i=n\cdot N_{red}}^{n\cdot N_{red}+N_{red}-1} \left(\left|U_i\right| \cdot U_i\right)\right], \qquad (1)$$

where: $U = \Im(u)$ is the Fourier transform of the original discrete signal with N samples, N_{red} is the reduction ratio,

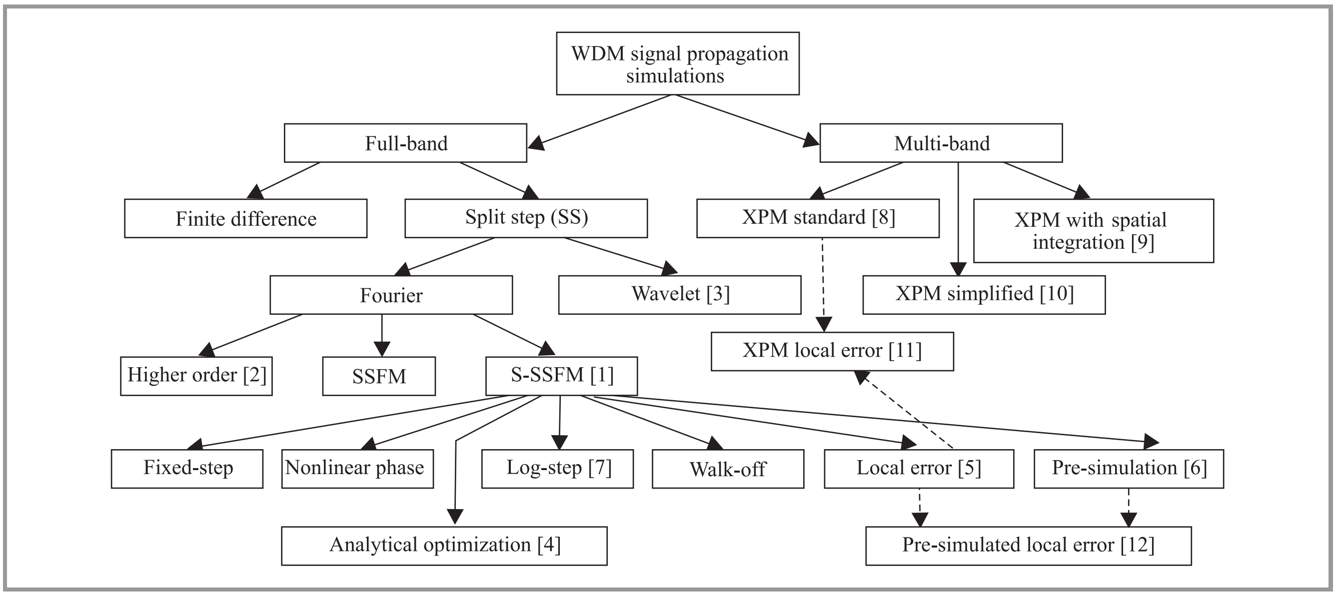

Fig. 1. Review of WDM signal propagation simulation methods.

and $n = -N/(2N_{red}),\ -N/(2N_{red})+1,\dots,N/(2N_{red})-1$. For a given N_{red}, split step pre-simulation of the test signal can be much faster ($> N_{red}$) than the corresponding simulation of the original signal. Several pre-simulations must be carried-out iteratively to calculate optimal step-size $h_{optimal}$, required to achieve desired global accuracy. Pre-simulations typically takes 30% of full spectrum simulation time [6].

2. Pre-simulated Local Error S-SSFM

We proposed novel simulation method which comprises two stages: step-size optimization is carried out in the initial stage, combining local error and pre-simulation methods and in the second stage conventional S-SSFM is used by applying optimal step-size distribution $h_{optimal}(z)$, obtained in the initial stage. Overall time savings up to 50% are realistic, depending of simulated system scenario. We called this novel procedure pre-simulated local error S-SSFM (PsLE S-SSFM).

Modified LEM algorithm with averaged signal spectrum Eq. (1) is used in PsLE S-SSFM. Method of order $O(h^3)$ is utilized in [5] by combining a fractions of coarse u_c and fine u_f solutions to calculate the next step. In our method only fine solution u_f is used in pre-simulation and u_c is utilized only to calculate local error, which gives better stability and does not degrade accuracy considerably in the case of WDM simulations, where the global error δ_G is low – of the order of 10^{-3}. Contrary to original pre-simulation method [6], the duration of the initial stage is only a small percentage (2%) of the second stage, in which the full-band simulation is carried out.

Results. We have explored the applicability of PsLE S-SSFM method to WDM systems with different number of channels. The method was used for simulation of WDM link with the following parameters: RZ modulation format, bit rate of 40 Gbit/s, channel spacing of 100 GHz, channel power of 1 mW, simulated bandwidth of 320 GHz/channel and bit sequence length of 2^9, and various number of channels. Transmission line comprises two types of fiber, with parameters given in Table 1.

Table 1
Fiber parameters used in the simulations

Parameter [unit]	SSMF1	SSMF2
Length [km]	100	100
Attenuation [dB/km]	0.22	0.22
Dispersion [ps/(nm·km)]	16.00	5.00
Dispersion slope [ps/(nm·km)^2]	0.08	0.00
Nonlinear coefficient [1/(W·km)]	1.32	1.32

Results shown in Fig. 2 indicate that the PsLE S-SSFM is up to 50% faster than the walk-off method in all simulated

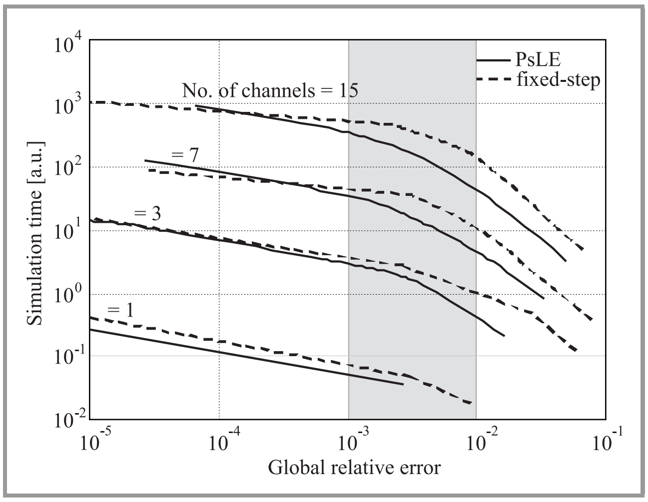

Fig. 2. Simulation time versus global relative error for fixed-step (dashed line) and PsLE (solid line) methods.

cases, in critical global error range of $10^{-2}-10^{-3}$. Relation between the method parameter and the global error was considered for fixed-step and PsLE methods (Fig. 3). The parameter of method is a parameter in a split step method that should be varied to obtain required accuracy. For required global error $\delta_G = 10^{-3}$ the local error (i.e., the parameter of PsLE method) varies from $2 \cdot 10^{-5}$ to $3 \cdot 10^{-4}$ for different number of simulated channels, in the same conditions the step-size (i.e., the parameter of fixed-step method) varies in a much wider range – from 8 m to 5000 m. As a rule of thumb, the global relative error equals $\delta_G = \sqrt{N} \cdot \delta_L$, where N is the number of steps and δ_L is the local relative error. It is clear that the local relative error δ_L in PsLE method is better criterion to assess global error than the step-size in fixed-step method. The same is true for walk-off method, which in fact, is fixed-step method with automatically adjusted the step-size.

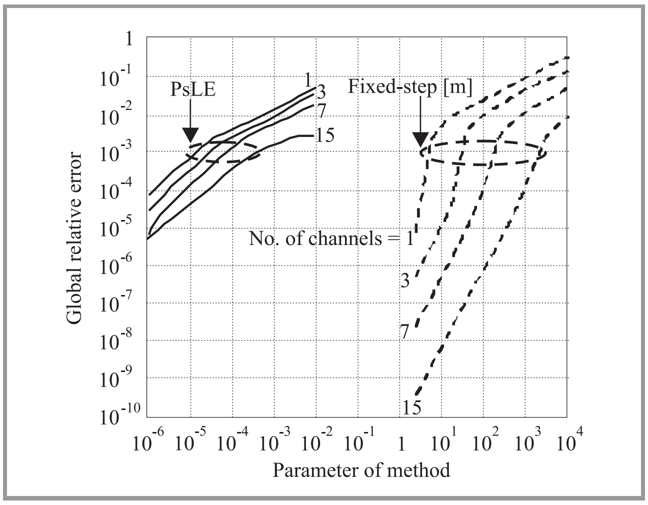

Fig. 3. Global relative error versus parameter of the method: local error for PsLE and step-size for fixed-step.

The PsLE method has two basic advantages: shorter simulation time of up to 50% in comparison with walk-off method, which is known as the most efficient in WDM simulations [5] and offers simply accuracy criterion, i.e., the local error, which is a good indicator of the global accuracy.

3. Role of FWM Spurious Tones on Accuracy of S-SSFM Simulations

Four wave mixing fictitious tones generated during S-SSFM simulations are one of the main sources of errors. Detailed knowledge of their properties is the key factor to improve S-SSFM simulations speed and accuracy.

Actual FWM efficiency η decreases versus the channel separation Δf [1]. Fixed-step S-SSFM with uniform distribution of step-size leads to fictitious FWM efficiency η', presenting several peaks at frequencies f_{p_i}, which was analyzed analytically in [7].

Figure 4 shows the FWM efficiency versus the channel separation Δf after the propagation through a fiber span. The first peak ($\Delta f = f_{p_1}$) on η' curve was shown around 270 GHz. Whatever (signal or noise) is at that spectral distance from a carrier acts like an unrealistic pump for spurious tones. In the walk-off method, uniform step-size distribution is used, in the same way as in the fixed-step method, but the step-size h is adjusted to maintain frequency f_{p_1} of the first fictitious peak at spurious FWM efficiency curve $\eta'(\Delta f)$ outside simulated bandwidth $\Delta f_{\max}$, which is fulfill for $h \ll 1/(2\pi|\beta_2|\Delta f_{\max}^2)$.

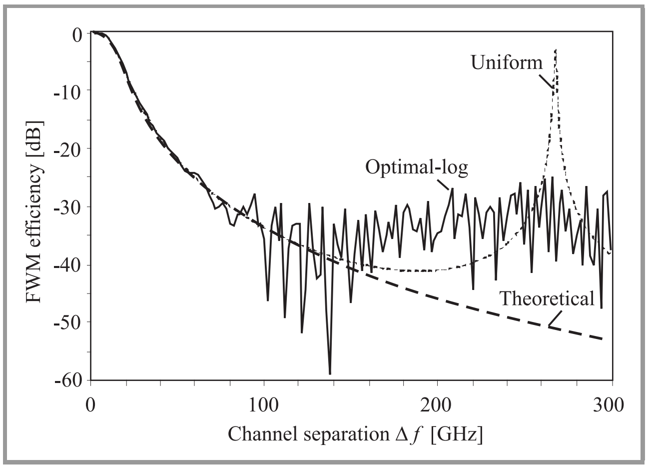

Fig. 4. FWM efficiency as a function of channel separation Δf. True – theoretical, and spurious: for optimal-log and uniform distributions, respectively.

In case of the logarithmic step-size distribution, the FWM spurious distortions η'' follows proper value of η, up to the critical step-size h_{p_1} and then, for higher number of steps K, the η'' behaves like a white noise, with root mean square value inverse-proportional to K. In [7] an analysis was carried out for a simplified case with comb of CW carriers, leading to the following logarithmic step-size distribution:

$$h_n = z_{n+1} - z_n = \frac{1}{2\alpha} \ln \left(\frac{1 - nd}{1 - (n-1)d} \right), \; n \in \langle 1, K \rangle, \quad (2)$$

where: $d = \frac{1-e^{-2\alpha z}}{K}$, α is the fiber attenuation coefficient and K is the number of steps.

If $\Delta f_{\max} \ll f_{p_1}$, spurious FWM efficiency η' for uniform distribution is only slightly higher than for logarithmic distribution η''. However, step-size h_{p_1} is typically very low (e.g., of the order of 1 m for 15×40 Gbit/s system with 1 nm distance between channels) and larger step-size could be used to obtain global relative error level of 10^{-3}, which is typically sufficient for analysis of WDM system properties [6]. On the other hand, uniform step-size distribution spurious efficiency η' grows sharply for step-size higher than h_{p_1} .

The accuracy gain $\delta_{fix/log}^{\max}$ obtained in S-SSFM simulations with logarithmic step-size distribution compared with uniform one, increases as square root of the number of simulation steps K:

$$\delta_{fix/log} = \sqrt{K} \quad (3)$$

and reaches maximum $\delta^{\max}_{fix/log}$ for the step-size h_{p_1}, corresponding to the resonant frequency f_{p_1}, which is shown in Fig. 5. Additionally, optimal value of parameter A is shown in Fig. 5, which is a slope of logarithmic step-size distribution. The maximum ratio $\delta^{\max}_{fix/log}$ at critical step-size h_{p_1} may exceed 30 dB, which means that the uniform step-size

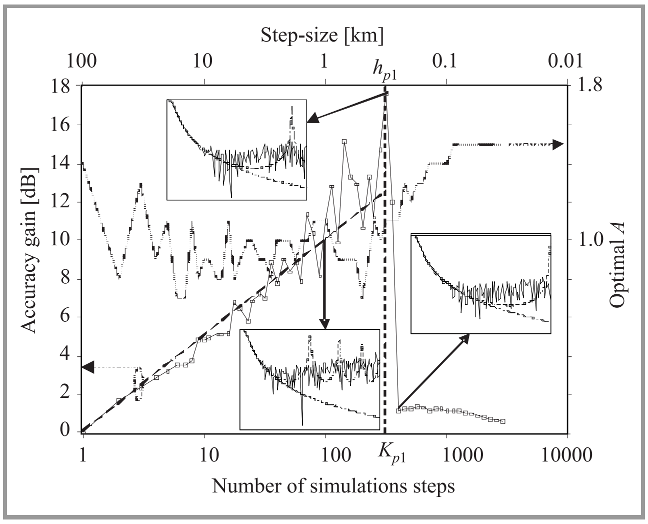

Fig. 5. Accuracy gain of logarithmic distribution over uniform one as a function of number of simulation steps K (or alternatively step-size). Simulation – solid line and theoretical approximation Eq. (3) – dashed line. Insets – FWM efficiencies for a given K.

distribution is not applicable for this step-size, contrary to logarithmic one. Moreover, for step-size far from critical step-size h_{p_1}, e.g., for $5h_{p_1}$, logarithmic distribution is still more accurate than uniform one, for the same number of steps K, and accuracy gain is always consistent with the following limit:

$$\delta^{\max}_{fix/log} \geq \frac{L}{L_{eff}} = \frac{\alpha L}{1 - \mathrm{e}^{-\alpha L}}, \tag{4}$$

where L_{eff} is the fiber effective length.

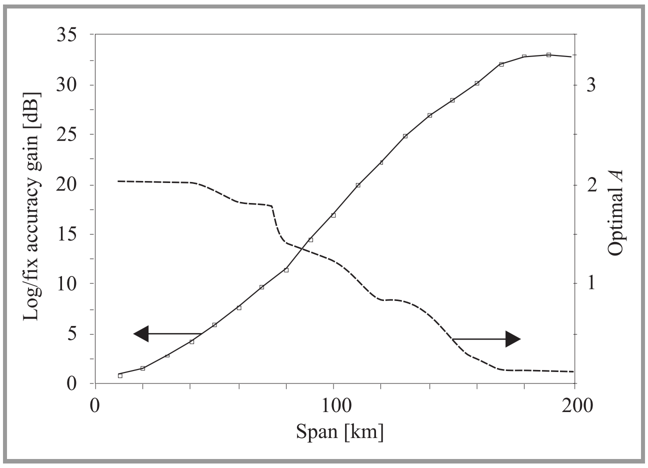

Fig. 6. Accuracy gain of logarithmic distribution over uniform one and optimal value of parameter A as a function of fiber span.

The step-size h is a compromise between the global error δ_G and the simulation time in a real WDM system. In such a system, additional effects, not only FWM, are the source of errors, i.e., SPM and XPM. Moreover, an inter-channel effects (IFWM, IXPM) are generated even in a single channel system.

As can be seen in Fig. 6, optimal value of parameter A, which is a slope of logarithmic step-size distribution, tends to 2 for short simulated fiber spans, and this value has been chosen in [5], which was the source of worsen results of logarithmic distribution, because $A = 2$ is far from optimal value in S-SSFM simulation of actual WDM systems, which is shown in the next section.

4. Modified Logarithmic Step-Size Distribution

Step-size distribution Eq. (2) is used as reference in [5], with conclusion that logarithmic step-size method is somewhat poorer than that of the nonlinear phase and walk-off methods in a single-channel simulations and even further deteriorates in a multi-channel simulations, because the step-size choice is only based on limiting spurious FWM, which is only one of the potential sources of error.

On the other hand, LEM method [5] provides near constant relative local error, which is good strategy to minimize the relative global error, but is slower than the walk-off method (with uniform step-size distribution) due to required parallel calculation of coarse and fine solutions.

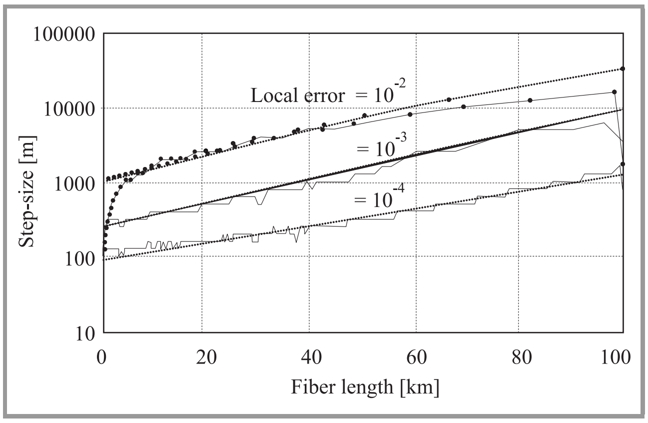

Fig. 7. Step-size distributions obtained in LEM method and its logarithmic approximations for various levels of relative local error (fiber SSMF1, 7 channels, system parameters – see Section 2).

We have found out that the step-size distribution obtained in LEM method is very close to logarithmic, with exception of local fluctuations caused by an algorithm used to maintain the optimal step (see Fig. 7). We have performed several simulations, and each time logarithmic step-size distribution was better than the uniform one, under the assumption that its slope was optimized. Our conclusion is contradiction of that obtained in [5], but in that case not optimal slope of logarithmic step-size distribution was used.

Table 2
Results of S-SSFM simulation for various WDM system scenarios, with the following step-size distributions: uniform, logarithmic obtained by PsLE and optimal logarithmic, for $\delta_G = 2\cdot 10^{-3}$

Number of channels	Dispersion [ps/(nm·km)]	Span [km]	Number of steps			
			optimal-log (A)	PsLE-log	fixed-step	fixed/log
1	5	100	8 (0.5)	8	16	2.00
3	5	100	122 (0.5)	126	225	1.84
7	5	100	725 (0.6)	740	1400	1.93
15	5	100	3420 (0.5)	3480	6400	1.87
31	5	100	14600 (0.6)	14700	27300	1.87
63	5	100	60000 (0.5)	61000	110600	1.84
1	16	100	17 (0.7)	17	36	2.12
3	16	100	280 (0.7)	300	517	1.85
7	16	100	1600 (0.7)	1780	3150	1.96
15	16	100	7600 (0.7)	7900	14200	1.87
31	16	100	32500 (0.7)	34000	60800	1.87
1	5	50	6 (0.5)	6	8	1.33
3	5	50	92 (0.5)	93	111	1.21
7	5	50	550 (0.5)	560	720	1.31
15	5	50	2570 (0.4)	2590	3150	1.23

It can be shown that when the local signal power is $P(z) = P_0 e^{-\alpha z}$, and the relative local error $\delta(z)$ is proportional to $P(z)^{A\alpha}$, where A is some constant, then the relative local error is uniform in each simulation step, if the following relations:

$$\int_0^{z_1}\delta(z)\mathrm{d}z = \int_{z_1}^{z_2}\delta(z)\mathrm{d}z = \cdots = \int_{z_{K-1}}^{z_K}\delta(z)dz = \frac{1}{K}\int_0^{z_K}\delta(z)dz$$
$$= \frac{1-e^{-A\alpha z}}{A\alpha K} = \frac{d}{A\alpha}, \quad \text{for} \quad d = \frac{1-e^{-A\alpha z}}{K}, \qquad (5)$$

are satisfied, which, in turn, occurs when

$$h_n = z_{n+1} - z_n = \frac{1}{A\alpha}\ln\left(\frac{1-nd}{1-(n-1)d}\right), \; n \in \langle 1, K\rangle. \quad (6)$$

As can be seen, Eq. (6) is general form of Eq. (2), with additional parameter A, which represents a slope of logarithmic step-size distribution.

Results. The global relative error was calculated for S-SSFM simulation with the following step-size distributions: uniform, logarithmic obtained by PsLE and optimal logarithmic, taking into account various WDM system scenarios. Results are summarized in Table 2.

The optimal value of parameter A for typical simulated WDM systems lays between 0.4 and 0.7 for $\delta_G = 2\cdot 10^{-3}$, depending of the influence of spurious FWM on the global error. Optimal value of parameter A should be calculated for each simulation and it is time consuming task. PsLE S-SSFM method can be helpful here. In this case, modified logarithmic step-size distribution is a smoothed version of distribution obtained in PsLE S-SSFM pre-simulation. Up to 2 times less steps are needed when optimal logarithmic step-size distribution is used, comparing with walk-off method – known as the most efficient to date.

The optimal logarithmic step-size distribution gives always better results than the uniform one, which is shown in Fig. 8. Logarithmic step-size distribution obtained by pre-simulation local error method is very close to the optimal

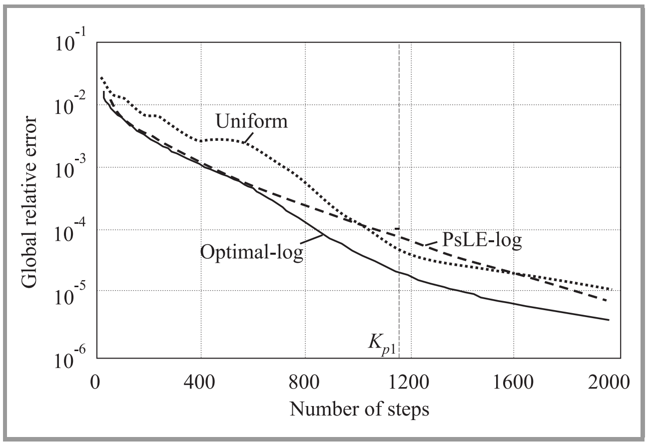

Fig. 8. Global relative error as a function of the number of steps in S-SSFM for various step-size distributions (fiber SSMF1, 3 channels, system parameters – see Section 2).

one in an important global error range of $10^{-2} - 10^{-3}$, but for lower levels of global error the results is even slightly worse than for the uniform distributions, due to the bigger than optimal value of the parameter A, which occurs for global relative error lower than $5 \cdot 10^{-4}$ (see Fig. 9).

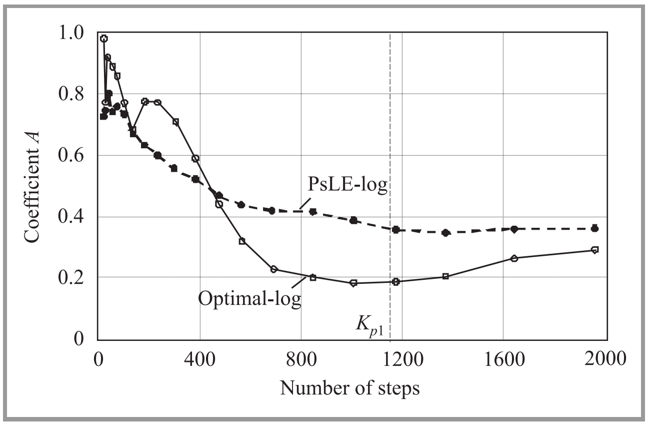

Fig. 9. Optimal and obtained by PsLE method, coefficient A of logarithmic step-size distributions as a function of the number of steps in S-SSFM (fiber SSMF1, 3 channels, system parameters – see Section 2).

Dependence between the relative global error and the coefficient A is presented in Fig. 10.

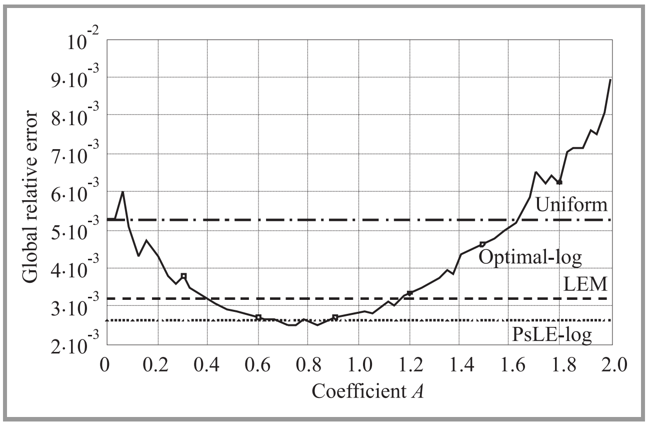

Fig. 10. Relative global error as a function of coefficient A for S-SSFM simulation. Results of fixed-step (uniform) and LEM methods are presented for comparison (fiber SSMF1, 7 channels, system parameters – see Section 2).

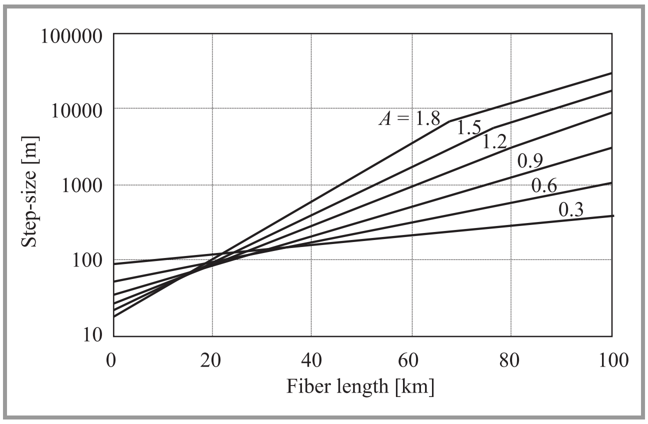

Fig. 11. Step-size distributions as a function of fiber length for various values of parameter A (100 km of fiber with $\alpha = 0.22$).

As can be seen in Fig. 10 optimal value of parameter A lays between 0.5–1.0 and for $A = 2$ used in [5], error is two times higher than obtained for uniform step-size distribution. The step-size distributions corresponding to various values of parameter A, for 100 km of fiber with $\alpha = 0.22$, are shown in Fig. 11.

As a rule of thumb, logarithmic step-size distribution improves global relative accuracy by

$$\Delta\delta_G = \frac{L}{L_{eff}} = \frac{\alpha L}{1 - \mathrm{e}^{-\alpha L}}$$

as compared to uniform step-size distribution, which is illustrated in Fig. 12.

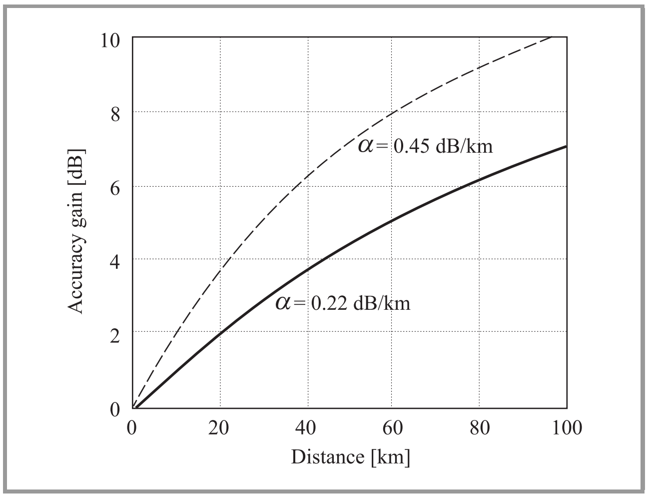

Fig. 12. Accuracy gain as a function of the distance for uniform step-size distribution.

Our future work is concentrated on finding more accurate and faster methods to chose optimal values of the parameter A and the number of steps K, needed for a given relative global error δ_G.

5. Conclusions

Pre-simulated local error S-SSFM typically halves simulation time of WDM links, comparing to conventional fixed-step S-SSFM. Moreover, local error used in pre-simulation seems to be a good indicator of the global accuracy. Even more effective step-size distribution can be achieved using modified logarithmic method, although in this case, methods to found the optimal value of slope for logarithmic step-size distribution and the number of steps, for a given global accuracy, should be further studied. To the best of our knowledge proposed two novel methods are faster than other methods for simulations of light propagation in WDM links. Up to 2 times less steps are needed when optimal logarithmic step-size distribution is used, comparing with walk-off method – known as the most efficient until now.

References

[1] G. P. Agrawal, *Nonlinear Fiber Optics*, 3rd ed. San Diego: Academic Press, 2001.

[2] X. Liu and B. Lee, "A fast method for nonlinear Schrödinger equation", *IEEE Photon. Technol. Lett.*, vol. 15, no. 11, pp. 1549–1551, 2003.

[3] T. Kremp, "Split-step wavelet collocation methods for linear and nonlinear optical wave propagation". Ph.D. thesis, High-Frequency and Quantum Electronics Laboratory, University of Karlsruhe. Cuvillier Verlag Göttingen, 2002.

[4] A. A. Rieznik, T. Tolisano, F. A. Callegari, D. F. Grosz, and H. L. Fragnito, "Uncertainty relation for the optimization of optical-fiber transmission systems simulations", *Opt. Expr.*, vol. 13, no. 10, pp. 3822–3834, 2005.

[5] O. V. Sinkin, R. Holzlöhner, J. Zweck, and C. R. Menyuk, "Optimization of the split-step Fourier method in modeling optical-fiber communications systems", *J. Lightw. Technol.*, vol. 21, no. 1, pp. 61–68, 2003.

[6] C. J. Rasmussen, "Simple and fast method for step size determination in computations of signal propagation through nonlinear fibres", in *Proc. OFC 2001 Conf.*, Anaheim, USA, 2001, paper WDD29-1.

[7] G. Bosco, A. Carena, V. Curri, R. Gaudino, P. Poggiolini, and S. Benedetto, "Suppression of spurious tones induced by the split-step method in fiber systems simulation", *IEEE Photon. Technol. Lett.*, vol. 12, no. 5, pp. 489–491, 2000.

[8] T. Yu, W. M. Reimer, V. S. Grigoryan, and C. R. Menyuk, "A mean field approach for simulating wavelength-division multiplexed systems", *IEEE Photon. Technol. Lett.*, vol. 12, no. 4, pp. 443–445, 2000.

[9] J. Leibrich and W. Rosenkranz, "Efficient numerical simulation of multichannel WDM transmission systems limited by XPM", *IEEE Photon. Technol. Lett.*, vol. 15, no. 3, pp. 395–397, 2003.

[10] G. J. Pendock and W. Shieh, "Fast simulation of WDM transmission in fiber", *IEEE Photon. Technol. Lett.*, vol. 18, no. 15, pp. 1639–1641, 2006.

[11] M. Jaworski and M. Chochol, "Split-step-Fourier-method in modeling wavelength-division-multiplexed links", in *Proc. ICTON 2007 Conf.*, Rome, Italy, July 2007, vol. 4, paper Mo.P.13, pp. 47–50.

[12] M. Jaworski and M. Marciniak, "Pre-simulated local-error-method for modelling of light propagation in wavelength-division-multiplexed links", in *Proc. ICTON-MW 2007 Conf.*, Sousse, Tunisia, Dec. 2007, paper Fr4B.4, pp. 1–4.

Marek Jaworski was born in Warsaw, Poland, in 1958. He received the M.Sc. degree in electronic engineering from the Warsaw University of Technology in 1982 and a Ph.D. degree in communications engineering from the National Institute of Telecommunications (NIT) in Warsaw, in 2001. He has been with NIT since 1982, working on modeling and design of optical fiber transmission systems, measurement methods and test equipment for optical networks. He has been engaged in several European research projects since 2003, including COST Actions 270, 291 and 293. This included research of polarization mode dispersion in optical fiber, numerical simulations of telecommunication systems, advanced modulation formats and nonlinear photonics. Dr. Jaworski is an author of 3 Polish patents and 25 scientific papers in the field of optical fiber communications and measurements in optical networks, as well as one of the "Journal of Telecommunications and Information Technology" associate editors.

e-mail: M.Jaworski@itl.waw.pl
National Institute of Telecommunications
Szachowa st 1
04-894 Warsaw, Poland

Invited paper

Spectroscopic Ellipsometry Analysis of Rapid Thermal Annealing Effect on MBE Grown $GaAs_{1-x}N_x$

Nebiha Ben Sedrine, Jaouher Rihani, Jean-Christophe Harmand, and Radhouane Chtourou

Abstract—We report on the effect of rapid thermal annealing (RTA) on $GaAs_{1-x}N_x$ layers, grown by molecular beam epitaxy (MBE), using room temperature spectroscopic ellipsometry (SE). A comparative study was carried out on a set of $GaAs_{1-x}N_x$ as-grown and the RTA samples with small nitrogen content (x = 0.1%, 0.5% and 1.5%). Thanks to the standard critical point model parameterization of the $GaAs_{1-x}N_x$ extracted dielectric functions, we have determined the RTA effect, and its nitrogen dependence. We have found that RTA affects more samples with high nitrogen content. In addition, RTA is found to decrease the E_1 energy nitrogen blueshift and increase the broadening parameters of E_1, $E_1+\Delta_1$, E'_0 and E_2 critical points.

Keywords— ***$GaAs_{1-x}N_x$, optical constants, optoelectronic device, rapid thermal annealing, semiconductors, spectroscopic ellipsometry.***

1. Introduction

Recently, the nitrogen containing GaAs alloys are intensively studied since these semiconductors have a promising potential for optoelectronic device applications due to their unique electronic and optical properties especially in the telecommunication wavelength range [1]–[3]. However, an increase in nitrogen incorporation needed to achieve the desired bandgap energy, has been found to cause a degradation in the material quality [4]–[6]. Post-growth treatments, such as rapid thermal annealing (RTA), on $GaAs_{1-x}N_x$ materials were largely studied using either photoluminescence (PL) [7], [8] or high-resolution X-ray diffraction (HRXRD) [9] in order to improve the material quality.

However, an undesirable effect is often induced: a shift toward the blue of the emission peak is observable as RTA proceeds. In previous works, spectroscopic ellipsometry (SE) was used for the GaAsN material to investigate the nitrogen effect on GaAs host matrix [10], [11]. Very recently, Pulzara-Mora *et al.* [12] studied the growth temperature (from 420 to 600°C) effect of GaAsN on GaAs substrate by photoreflectance (PR) spectroscopy and phase modulated ellipsometry (PME), and established the corresponding growth mode. In a previous work [12], we have reported results relative to RTA effect on the $GaAs_{1-x}N_x$: the accurate optical constants, and the decrease of the E_1 transition energy nitrogen dependence.

In this work, we study the rapid thermal annealing effect using room temperature spectroscopic ellipsometry technique on $GaAs_{1-x}N_x$ (x = 0.1%, 0.5% and 1.5%) layers grown by molecular beam epitaxy (MBE) on GaAs substrate. The study will lead us to accurately determine the RTA effect on the samples, using the fitting analytic line shapes to the dielectric function imaginary part second derivatives, by the way of the critical points parameters (broadenings Γ_1, $\Gamma_{\Delta 1}$, Γ'_0, Γ_2 and amplitudes A_1, $A_{\Delta 1}$, A'_0, A_2) nitrogen dependence.

2. Experiment

The study is based on $GaAs_{1-x}N_x$ (x = 0.1%, 0.5% and 1.5%) samples grown on (001) GaAs substrate by MBE equipped with a radio-frequency (RF) plasma as nitrogen source. The samples consist of a GaAs buffer layer and a 0.1–0.2 μm $GaAs_{1-x}N_x$ layers grown at 450°C. Rapid thermal annealing was performed for 90 s under N_2 flow ambient at 680°C. The crystal quality and the nitrogen content of the samples were determined from HRXRD measurements.

Spectroscopic ellipsometry measurements were performed at room temperature using an automatic ellipsometer SOPRA GES5. The system uses a 75 W xenon lamp, a rotating polarizer, an autotracking analyzer, a double monochromator, and a photomultiplier tube as detector. Data were collected in the 1.6–5.5 eV energy range with a step of 5 meV, at incidence angle of 75°. Spectroscopic ellipsometry determines the complex reflectance ratio ρ defined in terms of the standard ellipsometric parameters ψ and Δ as

$$\rho = \frac{r_p}{r_s} = (\tan\psi)e^{i\Delta}, \tag{1}$$

where r_p and r_s are the reflection coefficients for light polarized parallel (p) and perpendicular (s) to the sample's plane of incidence, respectively.

3. Results and Discussion

The imaginary part ε_2 of the pseudo-dielectric function spectra covering the photon energies range of 1.6–5.5 eV for rapid thermal annealed $GaAs_{1-x}N_x$ (x = 0.1%, 0.5% and 1.5%) samples compared to the reference sample GaAs (x = 0.0%) and shifted for clarity, are plotted in Fig. 1. The pseudo-dielectric function is obtained by assuming the samples as bulk, and can be obtained by using an analytical relation to the experimentally measured data. This can be used as a rough estimation of the nitrogen incorporation effect in $GaAs_{1-x}N_x$. However, the nitrogen induced effect on our samples has already been studied [11] which was in good agreement with previous reports [10]. In Fig. 1, four peaks are clearly observed at 2.9, 3.1, 4.5 and 4.8 eV, which correspond, respectively, to the E_1, $E_1+\Delta_1$, E_2 and E_0' transitions.

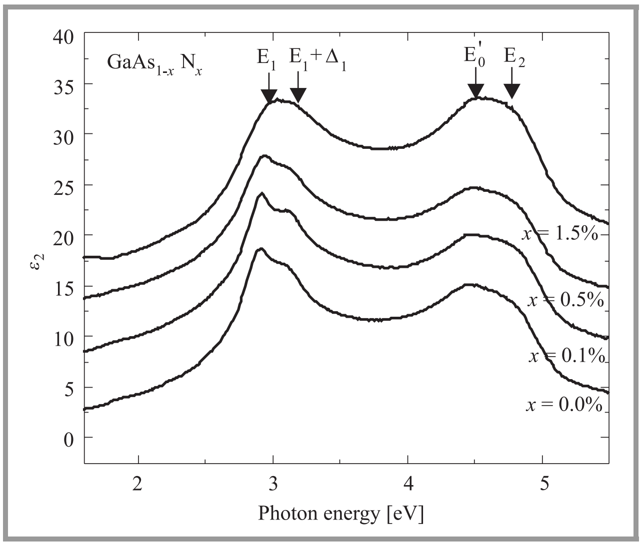

Fig. 1. Pseudo-dielectric function imaginary parts of the RTA $GaAs_{1-x}N_x$ layers compared to GaAs. The spectra of the samples with $x = 0.1\%$, 0.5% and 1.5% are shifted for clarity by 5, each.

We have reported in a previous work [13] on the $GaAs_{1-x}N_x$ optical constants, that we accurately extracted using the Newton-Raphson method applied to the four-phase model (ambient –oxide – $GaAs_{1-x}N_x$ layer – GaAs substrate), together with a conventional SE analysis. The oxide in the model used there was assumed to be the GaAs native oxide. The procedure was performed for both as-grown and RTA samples with (x = 0.1%, 0.5% and 1.5%). We presented the refractive indices (n) and absorption coefficients (k) of the as-grown and RTA $GaAs_{1-x}N_x$ (x = 0.1%, 0.5% and 1.5%) layers resulting from the best-fit model analysis. We have found that, in the visible energy range, it appears that a small decrease of the refractive index (n) of about 0.4 and 0.15, respectively, for samples with x = 0.1% and 0.5% is noted by annealing.

However, an opposite largest effect (increase of the refractive index of about 0.7) is observed for the sample with the highest nitrogen content ($x = 1.5\%$). For the absorption coefficients (k), the same behavior is observed in the high energy side; an improvement of the absorption coefficient by the annealing treatment is clear for the 1.5% nitrogen sample. These behaviors versus annealing can allow us to conclude that RTA seems to affect more the highest nitrogen containing $GaAs_{1-x}N_x$ material, leading to an improvement of the complex refractive index reaching the values of diluted $GaAs_{1-x}N_x$ alloys (under 1% of nitrogen).

We have analyzed the RTA effect on the dielectric function $\varepsilon(E) = \varepsilon_1(E) + i\varepsilon_2(E)$ which is closely related to the material band-structure. An accurate determination of the interband transition energies (or critical points – CP's) was

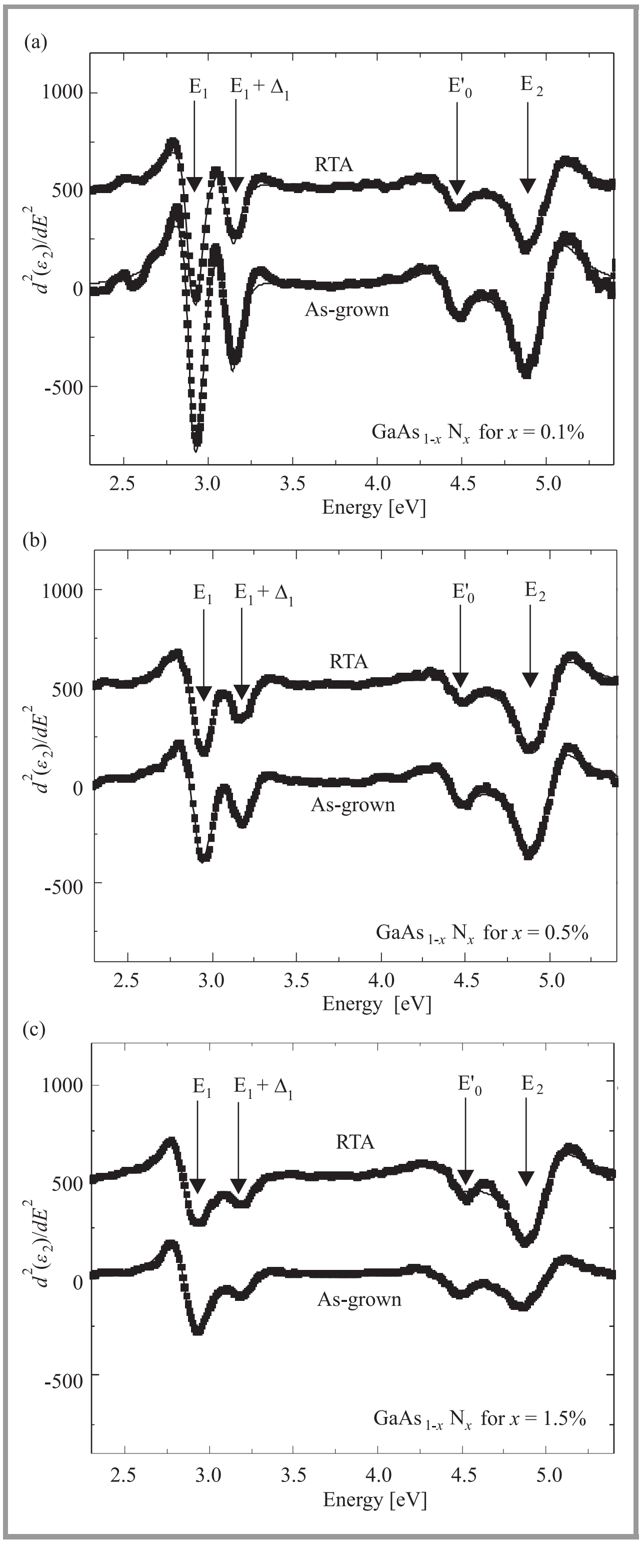

Fig. 2. Second derivative of the dielectric function imaginary parts for as-grown and after RTA $GaAs_{1-x}N_x$ samples: (a) $x = 0.1\%$; (b) 0.5%; (c) 1.5%. Scatters (solid lines) refer to experimental (best-fit calculated) spectra.

performed by fitting analytic line shapes to the numerically calculated dielectric function imaginary part second derivatives. For small nitrogen content, like in GaAs at room temperature [14], the derivative spectra in the vicinity of the critical points (E_1, $E_1+\Delta_1$, E_2 and E_0') can be assumed as two-dimensional line-shapes:

$$\frac{d^2\varepsilon}{dE^2} = \sum_{j=1}^{N}\left[A_j e^{i\phi_j}(E-E_{cj}+i\Gamma_j)^{-2}\right], \qquad (2)$$

where: A_j is the amplitude of the critical point, E_{cj} its energy, Γ_j is a broadening parameter, and ϕ_j a phase angle. In Fig. 2 [13], the best-fit calculated $d^2\varepsilon_2(E)/dE^2$ spectra (solid lines) from Eq. (2) are compared to the numerically second-derivatives extracted results (scatters) using the Levenberg-Marquardt regression algorithm. In order to improve the quality of the fit, peaks (j) were fitted simultaneously by taking A_j, E_{cj}, Γ_j and ϕ_j as free parameters.

We have found [13] that the best-fit critical point energies show a very small dependence of $E_1+\Delta_1$, E_2 and E_0' upon annealing, however, a notable effect on the E_1 interband transition is observed: RTA decreases the E_1 nitrogen dependence. From the fit curvatures that match well with the extracted experimental results, we can also deduce the RTA effect on the critical points amplitudes A_j and broadening parameters Γ_j. Tables 1 and 2 show the best-fit broadening parameters (Γ_1, $\Gamma_{\Delta1}$, Γ_0' and Γ_2) for the E_1, $E_1+\Delta_1$, E_0' and E_2 critical points, for as-grown and RTA $GaAs_{1-x}N_x$ ($x = 0.1\%$, 0.5% and 1.5%) samples. A clear increase of the broadening parameters upon annealing is noted for each nitrogen composition, reaching about 10 meV for the $\Gamma_{\Delta1}$ corresponding to the 1.5% sample. Lautenschlager *et al.* in [14] studied the effect of temperature on the broadening parameters of GaAs; they have noted a linear increase for temperatures above 300K.

Table 1
The broadening parameters for the E_1, $E_1+\Delta_1$, E_0' and E_2 critical points, for as-grown samples $GaAs_{1-x}N_x$: $x = 0.1$, 0.5 and 1.5% (errors obtained from the fitting procedure are given in parentheses)

Energy [eV]	$x = 0.1\%$	$x = 0.5\%$	$x = 1.5\%$
Γ_1	0.088 (0.002)	0.109 (0.002)	0.120 (0.002)
$\Gamma_{\Delta1}$	0.087 (0.003)	0.097 (0.005)	0.136 (0.007)
Γ_0'	0.122 (0.008)	0.134 (0.007)	0.182 (0.008)
Γ_2	0.164 (0.003)	0.165 (0.003)	0.187 (0.004)

Table 2
The broadening parameters for the E_1, $E_1+\Delta_1$, E_0' and E_2 critical points, for RTA samples $GaAs_{1-x}N_x$: $x = 0.1$, 0.5 and 1.5% (errors obtained from the fitting procedure are given in parentheses)

Energy [eV]	$x = 0.1\%$	$x = 0.5\%$	$x = 1.5\%$
Γ_1	0.095 (0.001))	0.113 (0.002)	0.129 (0.003)
$\Gamma_{\Delta1}$	0.089 (0.003)	0.102 (0.005)	0.149 (0.009)
Γ_0'	0.129 (0.009)	0.150 (0.009)	0.192 (0.009)
Γ_2	0.165 (0.003)	0.170 (0.003)	0.190 (0.003)

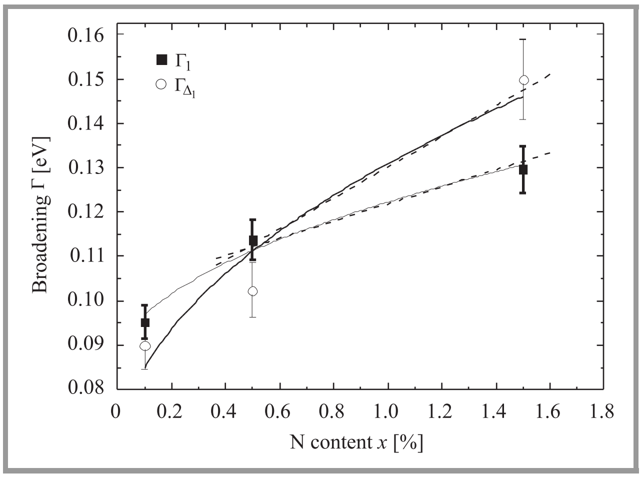

Fig. 3. The broadening parameters Γ_1 and $\Gamma_{\Delta1}$ for the E_1, $E_1+\Delta_1$ critical points, respectively, versus N molar fraction x (x = 0.1, 0.5 and 1.5%) for RTA samples. The symbols represent the results of fitting Eq. (2) to the second derivative of the experimental spectra. The full line represents the square-root-like dependence of Γ. The additional dashed line represents the nearly linear increase of Γ above 0.4% N molar fraction x.

Figure 3 represents the increase of the broadening parameters Γ_1, $\Gamma_{\Delta1}$ for the RTA samples versus nitrogen content x. Both Γ_1 and $\Gamma_{\Delta1}$ show a root-square-like dependence on x, following $y = a + b\sqrt{x}$ and the corresponding constant prefactors a and b, obtained using the Levenberg-Marquardt regression algorithm, are given in Table 3. We found that our results are in good agreements with the work of Tish *et al.* [15] for $GaAs_{1-x}N_x$ samples grown by metal organic vapor phase epitaxy (MOVPE). For N content below 0.4%, we note a strong increase of the broadening parameters Γ_1, $\Gamma_{\Delta1}$ of about 10 meV per 0.1% nitrogen. However, for higher nitrogen content, the broadening linearly increases ($y = cx + d$), and the corresponding constant prefactors c and d, obtained using the Levenberg-Marquardt regression algorithm, are given in Table 3. For our MBE-grown $GaAs_{1-x}N_x$ samples, the same trend of

Table 3
Values for the constant prefactors (a and b) for the square-root-like dependence of Γ_1 and $\Gamma_{\Delta1}$ ($y = a + b\sqrt{x}$) and (c and d) for the linear fit ($y = cx + d$) corresponding to the E_1, $E_1+\Delta_1$ critical points (errors obtained from the fitting procedure are given in parentheses)

Parameter	a [eV]	b [eV]	c [eV]	d [eV]
Γ_1	0.085 (0.004)	0.373 (0.046)	1.9 (0.2)	0.103 (0.002)
$\Gamma_{\Delta1}$	0.064 (0.008)	0.672 (0.076)	3.5 (0.2)	0.095 (0.002)

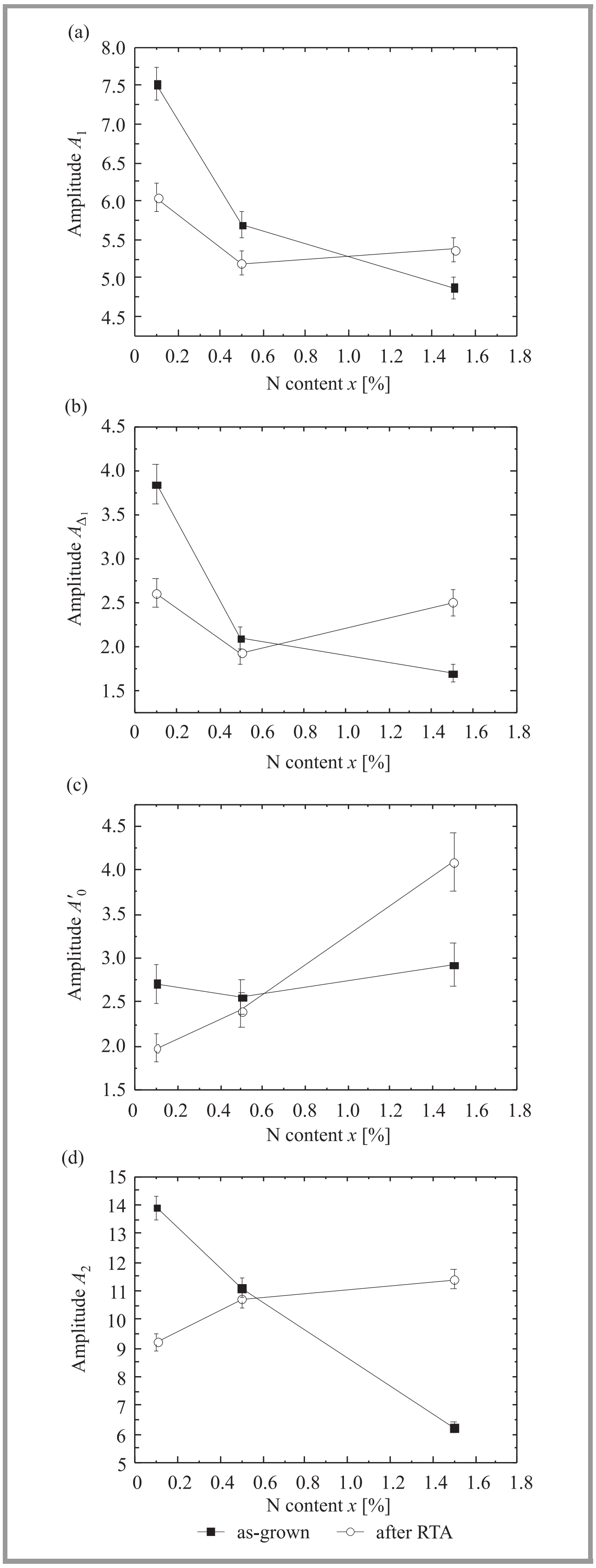

Fig. 4. $GaAs_{1-x}N_x$ critical points amplitudes (a) A_1, (b) $A_{\Delta 1}$, (c) A'_0, and (d) A_2 versus nitrogen content x ($x = 0.1\%$, 0.5% and 1.5%) results of fitting Eq. (2) to the second derivative of the experimental spectra for as-grown and RTA samples, lines are guides for eyes.

the Γ_1, $\Gamma_{\Delta 1}$ dependence versus nitrogen content x is observed. We note that the linearly increase of the $\Gamma_{\Delta 1}$ ($c = 3.5$ eV) is more than that of Γ_1 ($c = 1.9$ eV). This effect was interpreted as the consequence of an assembly of several closely spaced critical points of the $E_1 + \Delta_1$ [15].

In Fig. 4 the critical points amplitudes ($A_1, A_{\Delta 1}, A'_0$, and A_2) versus nitrogen content x, resulting from fitting Eq. (2) to the second derivative of the experimental spectra for as-grown and RTA samples, are shown. The most notable effect in these representations is the increase of the amplitude of all the critical points (A_1, $A_{\Delta 1}$, A'_0, and A_2) after annealing for the highest nitrogen containing sample ($x = 1.5\%$). We remind that the used dielectric function $\varepsilon(E)$ in the standard critical point model is given by:

$$\varepsilon(E) = \sum_{j=1}^{N} \left[C_j - A_j e^{i\phi_j} \ln\left(E - E_{cj} + i\Gamma_j\right) \right], \qquad (3)$$

where the amplitude A_j is proportional to $\varepsilon(E)$.

These behaviors versus annealing can allow us to conclude, like for the complex refractive index [13], that RTA seems to affect more the highest nitrogen containing $GaAs_{1-x}N_x$ material. Consequently, the material degradation due to high nitrogen content can be improved by RTA.

4. Conclusion

We have presented an analysis of the RTA effect on $GaAs_{1-x}N_x$ layers using room temperature SE. The study was performed on a set of as-grown and RTA (680°C for 90 s) $GaAs_{1-x}N_x$ ($x = 0.1\%$, 0.5% and 1.5%) samples. We have found that RTA post-growth treatment affects more the high containing nitrogen samples, leading to optical parameters close to those of GaAs in terms of the standard critical point model applied to the complex dielectric function: a decrease of the E_1 transition energy nitrogen dependence, an increase of the critical points amplitude. This behavior is interpreted as a better alloy uniformity and nitrogen reorganization in the $GaAs_{1-x}N_x$ layers.

References

[1] M. Weyers, M. Sato, and H. Ando, "Red shift of photoluminescence and absorption in dilute GaAsN alloy layers", *Jpn. J. Appl. Phys.*, part 2, vol. 31, pp. L853–L855, 1992.

[2] R. Chtourou *et al.*, "Effect of nitrogen and temperature on the electronic band structure of $GaAs_{1-x}N_x$ alloys", *Appl. Phys. Lett.*, vol. 80, pp. 2075–2077, 2002.

[3] M. Kondow *et al.*, "GaInNAs: a novel material for long-wavelength-range laser diodes with excellent high-temperature performance", *Jpn. J. Appl. Phys.*, part I, vol. 35, pp. 1273–1275, 1996.

[4] H. P. Xin and C. W. Tu, "GaInNAs/GaAs multiple quantum wells grown by gas-source molecular beam epitaxy", *Appl. Phys. Lett.*, vol. 72, pp. 2442–2444, 1998.

[5] S. Francoeur *et al.*, "Luminescence of as-grown and thermally annealed GaAsN/GaAs", *Appl. Phys. Lett.*, vol. 72, pp. 1857–1859, 1998.

[6] I. A. Buyanova *et al.*, "Mechanism for low-temperature photoluminescence in GaNAs/GaAs structures grown by molecular beam epitaxy", *Appl. Phys. Lett.*, vol. 75, pp. 501–503, 1999.

[7] L. H. Li *et al.*, "Effect of rapid thermal annealing on the optical properties of $GaAs_{1-x}N_x$/GaAs single quantum well structure grown by molecular beam epitaxy", *J. Appl. Phys.*, vol. 87, pp. 245–247, 2000.

[8] F. Bousbih *et al.*, "Effect of rapid thermal annealing observed by photoluminescence measurement in $GaAs_{1-x}N_x$ layers", *Mat. Sci. Eng. B*, vol. 123, pp. 211–214, 2005.

[9] E. Tournié, M.-A. Pinault, and A. Guzmán, "Mechanisms affecting the photoluminescence spectra of GaInNAs after post-growth annealing", *Appl. Phys. Lett.*, vol. 80, pp. 4148–4150, 2002.

[10] G. Leibiger *et al.*, "Nitrogen dependence of the GaAsN interband critical points E_1 and $E_1 + \Delta_1$ determined by spectroscopic ellipsometry", *Appl. Phys. Lett.*, vol. 77, pp. 1650–1652, 2000.

[11] N. Ben Sedrine *et al.*, "Spectrscopic ellipsometry analysis of $GaAs_{1-x}N_x$ layers grown by molecular beam epitaxy", *Mat. Sci. Eng. C*, vol. 28, pp. 640–644, 2008.

[12] A. Pulzara-Mora *et al.*, "Study of optical properties of GaAsN layers prepared by molecular beam epitaxy", *J. Cryst. Growth*, vol. 301–302, pp. 565–569, 2007.

[13] N. Ben Sedrine *et al.*, "Optical constants of As-grown and RTA $GaAs_{1-x}N_x$ layers analysed by spectroscopic ellipsometry", in *Proc. ICTON-MW'07 Conf.*, Rome, Italy, 2007.

[14] P. Lautenschlager *et al.*, "Interband critical points of GaAs and their temperature dependence", *Phys. Rev. B*, vol. 35, pp. 9174–9189, 1987.

[15] U. Tish, E. Finkman, and J. Salzman, "Fine structure of the $E_1 + \Delta_1$ critical point in GaAsN", *Phys. Rev. B*, vol. 65, pp. 153204–153207, 2002.

Nebiha Ben Sedrine was born in Tunis, Tunisia, in 1978. She received the M.Sc. degree in quantum physics from the Tunis University of Sciences in 2006. She is actually a Ph.D. student-researcher in the Laboratory of Photovoltaïc, Semiconductors and Nanostructures (LPVSN) at the Research and Technology Energy Center (CRTEn), Tunisia. She is an author and co-author of 14 scientific papers in the field of material science, optical and structural studies (ellipsometry, photoluminescence, reflectivity, microscopy), and more than 16 national and international communications. She is a member of the Société Tunisienne de Physique and the Optical Society of America.

e-mail: bsnebiha@yahoo.fr
e-mail: nebiha.bensedrine@crten.rnrt.tn
Laboratory of Photovoltaïc, Semiconductors
and Nanostructures (LPVSN)
Research and Technology Energy Center (CRTEn)
BP. 95, Hammam-Lif 2050, Tunisia

Jaouher Rihani was born in Beja, Tunisia, in 1978. He received the M.Sc. degree in quantum physics from the Tunis University of Sciences in 2004. He is actually a Ph.D. student-researcher in the Laboratory of Photovoltaïc, Semiconductors and Nanostructures (LPVSN) at the Research and Technology Energy Center (CRTEn), Tunisia. He is an author or co-author of 7 scientific papers in the field of material science, optical and structural studies (ellipsometry, photoluminescence, reflectivity, microscopy). He works as an Assistant at the Gafsa University of Sciences, Tunisia, since 2007.

e-mail: rihani_jaouher@yahoo.fr
e-mail: jawher.rihani@crten.rnrt.tn
Laboratory of Photovoltaïc, Semiconductors
and Nanostructures (LPVSN)
Research and Technology Energy Center (CRTEn)
BP. 95, Hammam-Lif 2050, Tunisia

Jean-Christophe Harmand obtained his Ph.D. in physics at the University of Paris 7, France, in 1988 for his work on GaAlAs/GaAs HBTs. From 1988 to 1990, he was at the Optoelectronic Research Laboratory of Matsushita (Osaka, Japan), where he was involved in studies on metamorphic AlGaInAs/GaAs HEMTs. He obtained state-of-the-art transport properties in these lattice-mismatched heterostructures. His expertise in molecular beam epitaxy being recognized, he was recruited at CNET/France Telecom to study the growth of III-V materials for micro- and optoelectronics, from 1990 to 1999. In 2000, he joined a new laboratory created by the CNRS: the Laboratory for Photonics and Nanostructures (LPN), where he conducts epitaxial growth research. Following pioneering works, he also initiated in France the catalyzed growth of III-V nanowires. At the national level, he is actually leading a GdR (group of research) on Semiconductor Nanowires and Nanotubes bringing together researchers from about 30 laboratories. He is an author and co-author of about 170 scientific papers and 60 communications in the fields of III-Vs materials and devices (index H = 23). He holds 8 patents.

e-mail: jean-christophe.harmand@lpn.cnrs.fr
Laboratory for Photonics and Nanostructures (LPN)
CNRS Route de Nozay
91 460, Marcoussis, France

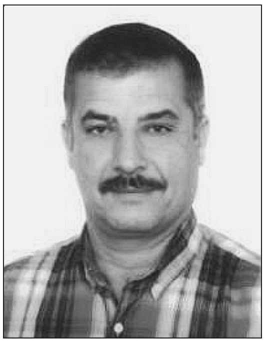

Radhouane Chtourou received his Master's degree in physics at the Faculty of Sciences of Tunis in 1983, his M.Sc. degree in solid-state physics in 1985. During the period 1986–1988, he was a physics teacher at the Nefta High School in the south of Tunisia. During 1988–1998, he joined the Raman Spectroscopic Laboratory of the Faculty of Sciences of Tunis. He was physic sciences Assistant between 1988–2003 at the Medjez-Elbab Engineering Institute. He obtained his Ph.D. in physics at the University of Tunis Elmanar in 1997. He obtained his University Habilitation degree in 2003 for his work of optical properties of semiconductors photonic crystals, electronic and optical properties of GaAsN alloys. During the period 1998–2003, he set up the Laboratory of the Semiconductor Physics at the Preparatory Institute of Scientific and Technical Studies of La Marsa in Tunis. Since 2003, he joined the Laboratory of Photovoltaïc, Semiconductors and Nanostructures (LPVSN). Prof. Chtourou is the Head of the Semiconductor Nanostructures Group. His research is currently focused on studies of electronic and optical properties of photonic crystals based on silicon and porous silicon, on gas bi-dimensional electrons in the III-V hetero-structures, and III-V semiconductors alloys for optoelectronic applications. He is the author of more than 40 scientific papers and 100 international communications. He is an active member of the Société Tunisienne de Physique.

e-mail: radhouane.chtourou@inrst.rnrt.tn
Laboratory of Photovoltaïc, Semiconductors
and Nanostructures (LPVSN)
Research and Technology Energy Center (CRTEn)
BP. 95, Hammam-Lif 2050, Tunisia

Invited paper

Control Mechanism for All-Optical Components

Ridha Rejeb and Mark S. Leeson

Abstract—In this article, we give a brief overview of security and management issues that arise in all-optical networks (AONs). Then we present an outline of the multiple attack localization and identification (MALI) algorithm that can participate in some of the tasks for fault management in AONs. Consequently, we discuss a hardware-based control unit that can be embedded in AON nodes to accelerate the performance of the MALI algorithm. We conclude the article with a discussion concerning the applicability and implementation of this device in AON management systems.

Keywords— ***all-optical networks, fault and performance management, securing optical networks.***

1. Introduction

Network management is an indispensable constituent of communication systems since it is responsible for ensuring the secure and proper operation of any network. Specifically, a network management implementation should be capable of handling the configuration, fault, performance, security, accounting, and safety in the network. However, network management for all-optical networks (AONs) faces additional challenges such as performance monitoring and ensuring adequate quality of service (QoS) guarantees in the network. Performance management is germane to successful AON operation since it provides signal quality measurements at very low bit error rates and fault diagnostic support. In particular, signal quality monitoring is difficult in AONs as the analogue nature of optical signals means that miscellaneous transmission impairments aggregate and can impact the signal quality enough to reduce the QoS without precluding all network services. This results in the continuous monitoring and identification of the impairments becoming challenging in the event of transmission failures.

The presence of a network management system (NMS) is essential to ensure efficient, secure, and continuous operation of any network. Specifically it handles the management of configuration, fault, performance, accounting, and security aspects, which are usually interlinked to one other. A key component in this system is performance management as it provides signal quality measurements at very low bit error rates and fault diagnostic support for fault management. Performance management is still a major complication for AONs, particularly, because signal quality monitoring in them is too difficult as the analogue nature of optical signals means that miscellaneous transmission impairments aggregate and can impact the signal quality enough to reduce the QoS without precluding all network services. This results in the continuous monitoring and identification of the impairments becoming challenging in the event of transmission failures. However, a simple and reliable signal quality monitoring method does not exist at present. Despite new methods for detection and localization of transmission failures having been proposed, no robust standards or techniques exist to date for guaranteeing the QoS in AONs. Therefore, the need for expert diagnostic techniques and more sophisticated management mechanisms that assist managing the proper function of AONs is highly desirable [1]–[7].

In this article, Sections 2 and 3 give a brief overview on the security and management issues that may arise in AONs. Section 4 introduces the control plane architectures taking into consideration still open and unsolved development issues. Section 5 presents an outline of the multiple attack localization and identification (MALI) algorithm [8] that can participate in some of the tasks for fault management in AONs. Section 6 discusses the efficiency of this algorithm focusing on its cost and complexity. Section 7 presents a hardware-based control unit [9] that can be embedded in AON nodes, in order to process the MALI's localization procedures in a real time fashion. Finally, in Section 8, we conclude the article with a discussion concerning the applicability and implementation of this device in AON management systems.

2. Security Issues in AONs

AONs are emerging as a promising technology for very high data rates, flexible switching and broadband application support. Specifically, they provide transparency capabilities and new features allowing routing and switching of traffic without any regression or modification of signals within the network. Although AONs offer many advantages for high data rate communications, they have unique features and requirements in terms of security and management that distinguish them from traditional communication networks. In particular, the unique characteristics of AON components and network architectures bring forth a set of new challenges for network security. By their nature, AON components are particularly vulnerable to various forms of denial of service, QoS degradation, and eavesdropping attacks. Since even short (in terms of duration) faults and attacks can cause large amounts of data to be lost, the need for securing and protecting optical networks has become increasingly significant [1], [2].

In the context of this work, a security *attack* is defined as an intentional action against the proper and secure functioning of the network, whereas a *fault* is defined as an unintentional action against the ideal and secure functioning of the network. *Failures* are referred to as the faults and attacks that can interrupt the ideal functioning of the network. Security attacks upon AONs may range from a simple physical access to more complex attacks exploiting:

– the peculiar behaviors of optical fibers;

– the unique characteristics of AON components;

– the shortcomings of available supervisory techniques and monitoring methods.

Attacks can be classified as eavesdropping or service disruption [1]. In this scenario, they are different in nature ranging from malicious users (i.e., users inserting higher signal power) to eavesdroppers. Thus, attacks differ from conventional faults and should be therefore be treated differently. This is because they appear and disappear sporadically and can be launched elsewhere in the network. In particular, the attacker may thwart simple detection methods, which are in general not sensitive enough to detect small and sporadic performance degradations. Furthermore, a disruptive attack, which is erroneously identified as a component failure, can spread rapidly through the network causing additional failures and triggering multiple erroneous alarms. Security attacks therefore must be detected and identified at any node in the network where they may occur [2]. Moreover, the speed of attack detection and localization must be commensurate with the data transmission rate. Furthermore, transparency in AONs may introduce significant miscellaneous transmission impairments such as optical crosstalk, amplified spontaneous emission noise, and power divergence [3]. In AONs, those impairments accumulate as they propagate and can impact the signal quality so that the received bit error rate at the destination node might become unacceptable high.

3. Management Issues in AONs

Following from the previous sections, it is clear that network management for AONs faces additional challenges and still unsolved problems. One of the main premises of AONs is the establishment of a robust and flexible control plane for managing network resources, provisioning lightpaths, and maintaining them across multiple control domains. Such a control plane must have the ability to select lightpaths for requested *end-to-end* connections, assign wavelengths to these lightpaths, and configure the appropriate resources in the network. Furthermore, it should be able to provide updates for link state information to reflect which wavelengths are currently being used on which fiber links so that routers and switches may make updated routing decisions. An important issue that arises in this regard is how to address the *trade-off* between service quality and resource utilization. Addressing this issue requires different scheduling and sharing mechanisms to maximize resource utilization while ensuring adequate QoS guarantees. One possible solution is the aggregation of traffic flows to maximize the optical throughput and to reduce operational and capital costs, taking into account qualities of optical transmission in addition to protection and restoration schemes to ensure adequate service differentiation and QoS assurance. A control plane should therefore offer dynamic provisioning and accurate performance monitoring, plus efficient restoration in the network and most of these functions need to move to the optical domain. Connection provisioning, for example, should enable a fast automatic setup and teardown of lightpaths across the network thereby allowing dynamic reconfiguration of traffic patterns without conversion to the electrical domain [5]–[7].

Another related issue arises from the fact that the implementation of a control plane requires information exchange between the control and management entities involved in the control process. To achieve this, fast signaling channels need to be in place between switching nodes. These channels might be used to exchange *up-to-date* control information that is needed for managing all supported connections and performing other control functions. In general, control channels can be realized in different ways; one might be implemented *in-band* while another may be implemented *out-of-band*. There are, however, compelling reasons for decoupling control channels from their associated data links. An important reason for this is that data traffic carried in the optical domain is transparently switched to increase the efficiency of the network and there is thus no need for switching nodes to have any understanding of the protocol stacks used for handling the control information. Another reason is that there may not be any active channels available while the data links are still in use, for example, when bringing one or more control channels down gracefully for maintenance purposes. From a management point of view, it is unacceptable to teardown a data traffic link, simply because the control channel is no longer available. Moreover, between a pair of switching nodes there may be multiple data links and it is therefore more efficient to manage these as a bundle using a single separated out-of-band control channel [6].

4. Control Plane Architectures

The design of an optical network is an important and very practical issue. As stated above, a desirable architecture should feature, *inter alia*, flexible management, automatic lightpath protection and restoration, and the ability to compile an inventory. Moreover, network architectures should support the gradual introduction of new technologies into the network without time consuming and costly changes to embedded technologies. However, the network architectures currently used may be categorized in two main models, namely the *overlay model* and the *peer model*. Although both models consist essentially of an optical core that provides wavelength services to client interfaces, which reside at the edges of the network, they are intrinsi-

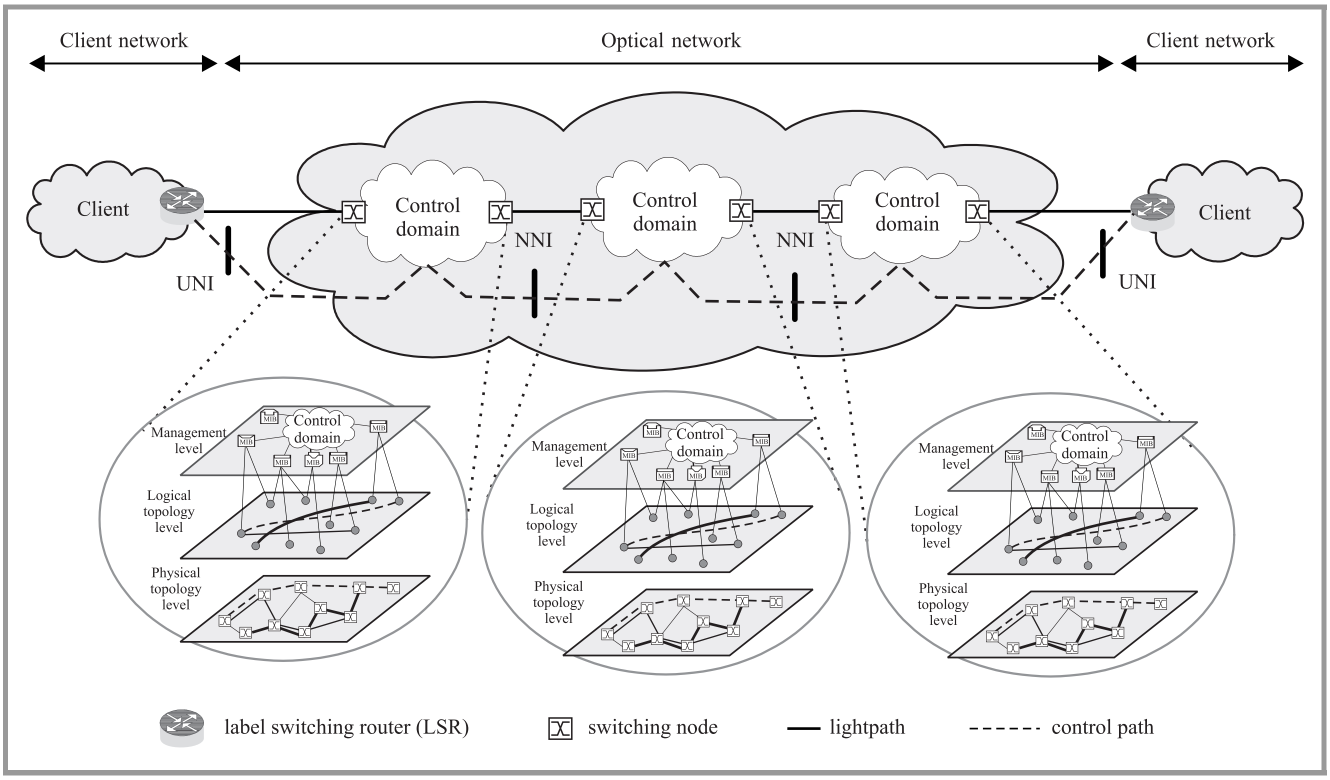

Fig. 1. Control plane management architecture.

cally different and offer up two key concepts for managing traffic flows in the network [10].

The overlay model hides the internal elements of the optical network and thus requires two separate, yet interoperable, control mechanisms for provisioning and managing optical services in the network. One mechanism operates within the core optical network and the other acts as the interface between the core components and the edge components which support lightpaths that are either dynamically signaled across the core optical network or statically provisioned without seeing inside the topology of the core. The overlay model therefore imposes additionally control boundaries between the core and edge by effectively hiding the contents of the core network.

The peer model considers the network as a single domain, opening the internal entities of the core optical network to the edge components making the internal topology visible and able to participate in provisioning and routing decisions. Whilst this has the advantage of providing a unified control plane, there are some significant considerations:

- The availability of topological information to all components in the network makes this model less secure.
- New standard control mechanisms are required since available proprietary ones cannot be employed.
- Additionally approaches for traffic protection and restoration are required.

Another model, known as the hybrid model, combines both the overlay and peer approaches, taking advantages from both models and providing more flexibility. In this model, some edge components serve as peers to the core network and share the same instance of a common control mechanism with the core network through the network-network interface (NNI). Other edge components could have their own control plane (or a separate instance of the control plane used by the core network), and interface with the core network through the user-network interface (UNI).

From a control plane point of view, the notion of the control domain is very useful. The control plane management architecture is presented in Fig. 1. The UNI is the interface between a node in the client network and a node in the core optical network. The NNI is the interface between two nodes in different control domains. The management information base is distributed among control domains, each of which has a partial knowledge of the global control information. A large optical network, as shown in Fig. 1, may be portioned into moderate control domains mainly for the following reasons [10]:

- To enforce administrative, management and protocol boundaries making them sufficiently reliable.
- To ensure rapid and accurate actions to be taken in response to failed conditions. For example, performing failure localizing processes in commensurate time.
- To increase the scalability of management functions and control planes.

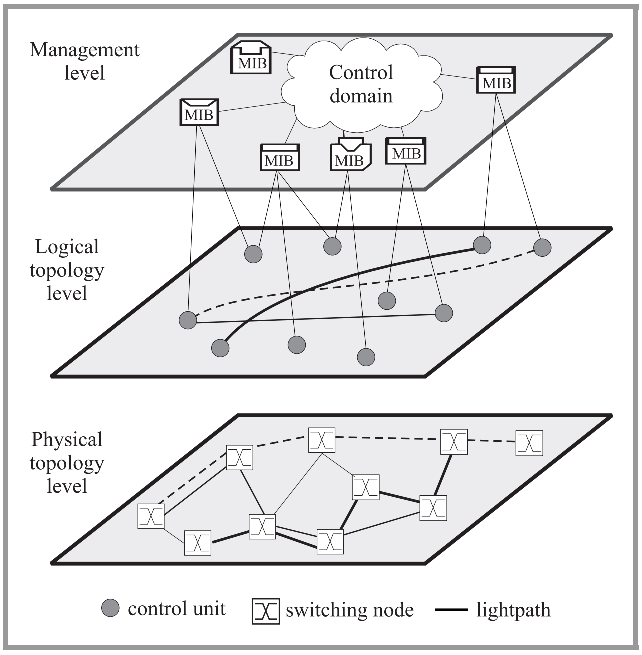

Fig. 2. The MIB distributed among element management systems.

The management information base (MIB) in a typical domain, as shown in Fig. 2, is distributed among its element management systems where each one has only a partial knowledge of the whole domain control and management information. However, there are still open and unsolved problems in the development of secure AONs that should be carefully addressed. One particular security issue is related to the UNI and NNI within the control plane employed. Consequently, the analysis of protocol stacks from a security perspective is an important prerequisite. Another issue related to network protection is a comparative study of the trade-off between network complexity and traffic restoration time.

5. The MALI Algorithm

This section presents an outline of the MALI algorithm that can participate in some of the tasks for fault management in AONs. The main task of the algorithm is to correlate multiple security failures and attacks locally at any AON node and to discover their tracks through the network. The MALI algorithm is distributed and relies on a reliable management system such as the link management protocol [11], since its overall success depends upon correct message passing and processing at the local nodes.

The key concepts of the MALI algorithm are based on the optical cross-connect (OXC) node model proposed in [8]. This model defines an OXC node as a 7-tuple $OXC = (F, W, D, S, M, \chi, \mu)$, where F, W, D, S, and M are nonempty component sets of fiber ports, supported wavelengths, wavelength demultiplexers, optical switches, and wavelength multiplexers, respectively. The main key functions of the OXC node model are represented by χ and μ. These are responsible for updating the connection and monitoring information of all established lightpaths that copropagate through the OXC node simultaneously. The model denotes the numbers of fiber ports and supported wavelengths by n and m, respectively. To identify the source and nature of detected performance degradation, the algorithm makes particular use of *up-to-date* connection and monitoring information of any established lightpath, on the input and output side of each node in the network. The required monitoring information can be correlated at local nodes or acquired from remote monitoring nodes [12].

The majority of the MALI algorithm comprises a generic localization procedure, which will be initiated at the downstream node that first detects serious performance degradation at an arbitrary lightpath on its output side.

A downstream node, which first notices serious performance degradation at a disturbed lightpath, raises an alarm, indicating that a failure has been detected on its output side. It then determines the set of lightpaths that share the same output fiber with the disturbed lightpath. For each of these, it determines the set of lightpaths that pass through the same optical switch at the same time. Hence, it delegates the localization process to the next upstream node when the status of a lightpath channel is nonzero on the input side of the node. Otherwise, it terminates the localization process for this lightpath and notifies the NMS that the disturbed channel is most likely to be affected in the current node.

An upstream node that receives the localization process with a disturbed lightpath starts the localization procedure from scratch and repeats all the steps when the channel status of the disturbed lightpath is nonzero on the output side of the node. Otherwise, it terminates the localization process and notifies the NMS indicating that the failure is most likely to be at the optical fiber link interconnecting both upstream and downstream nodes.

The localization procedure provides the NMS with state information about locations of possible disruption failures and attacks through the network. This information can be included as part of the failure notification. Once the origins of the detected failures have been localized, the NMS can then make accurate decisions (for example, which offender lightpaths should be disconnected or rerouted) to achieve finer grained recovery switching actions.

6. Cost and Complexity Analysis

Analyzing the cost and complexity of an algorithm has come to mean predicting the resources that the algorithm requires. Occasionally, resources such as memory, communication bandwidth, or hardware equipment are of prime concern, but most often it is ***computational time*** that we want to measure. The running time of the MALI's localization procedure is the sum of running times for each statement executed. For the worst-case, in which it is assumed that an OXC node is fully loaded and that any lightpath can affect any other co-propagating lightpath of one form or another, it can be seen that the local running time of the localization procedure is of the order $O(m \cdot n)$. The major concern, however, is estimating the overall running time of the required recursive calls of the localization procedure when delegating the localization process to the next upstream nodes backwards through the network [9].

As stated in the previous section, the MALI's localization process is triggered immediately in the downstream node after detecting a failure. Then, it is delegated to certain upstream nodes involved in the localization process. As shown in Fig. 3, these nodes can be modeled as a rooted tree. The downstream node, which first notices the performance degradation on its output side, is referred to as the root node. The number of children of a node is called its degree. Thus, the maximal degree of any node is equal to the number of its input ports. The length of a localization path from the root node to an arbitrary node is called its depth in the tree. The height of a node in the tree is the number of links on the longest path from the node to a leaf. The height of the tree is the height of its root node and is equal to the largest depth in the tree.

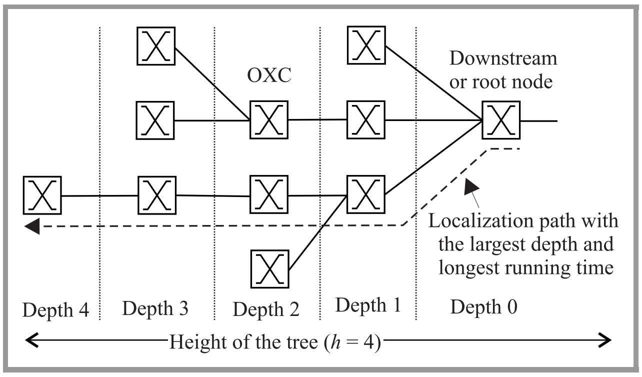

Fig. 3. Localization path tree.

Due to the distributed nature of the localization process it is expected that the localization procedure will be performed synchronously in all nodes of the same depth stage in the localization tree. Thus, the expected overall worst-case running time of the localization process is of the order $h \cdot O(m \cdot n)$, where h denotes the height of the localization tree. The height h is random since it depends on the distribution of upstream nodes involved in the localization process. Thus, it might impact the overall performance of the localization process particularly when it is becomes large [9].

7. Hardware Based Control Unit

In the previous section we saw that the local running time of the MALI's localization procedure is nonlinear, of the order $O(m \cdot n)$. However, to reduce the computational time required for running this procedure, it is reasonable to process some of computing steps in a parallel way. One of the significant conditions for running the localization procedure is that the computing steps required can be performed independently from each other. Since the localization procedure merely uses the current connection and channel state information at the input and/or output sides of the current node [8], it is not necessary to process it in a sequential way.

An optimal solution to solve this issue is to use a hardware-based control unit that can be embedded in AON nodes to process the localization procedure in a real time fashion. The device determines in *one-step* the set of established lightpaths that share the same output fiber with the disturbed lightpath at the same time. For each of these lightpaths, it checks the state of lightpaths that copropagate through the optical switch simultaneously. Hence, the computational time required is proportional to the *number of wavelengths* supported in the node.

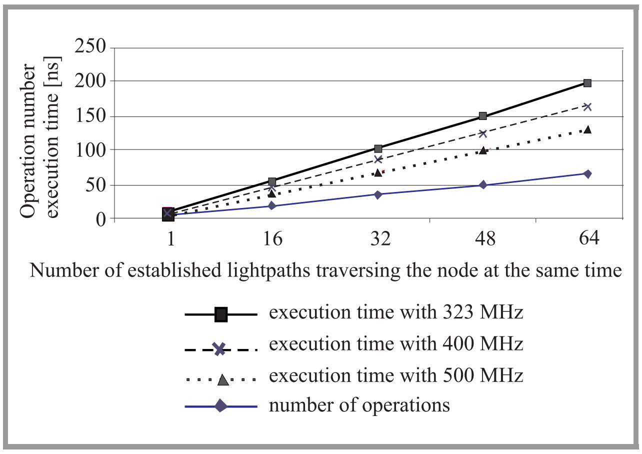

Fig. 4. Number of operation and execution time as a function of established lightpaths in 64×64-OXC node.

The performance evaluation of this approach is shown in Fig. 4. The internal design and simulation of this device was performed by a hardware simulation tool with a frequency of 323 MHz. The lower line shows the number of operations as a function of established lightpaths that share the same output fiber with the disturbed lightpath, whilst the upper plots the running time required for processing these steps. Both dotted lines are plotted with estimated values which are computed using higher frequences of 400 MHz and 500 MHz, respectively. The values are given by *time* $\sim$ *number of operation/frequency*. Both curves show unambiguously that the running time is decreasing as the frequency is increasing. Compared to the sequential approach, it is apparent that this method is more advantageous offering the benefit of reducing the running time required for processing the MALI's localization procedure. The resulting computational time is linear of the order $O(n)$, where n is the number of wavelengths supported in the node. Thus, it may ensure relaxation of the high cost and complexity of signal quality monitoring in AONs.

8. Conclusion

In this paper, we have presented a brief overview of the security and management issues that may arise in AONs. Then we have introduced the MALI algorithm that can be used for localizing the origins of multiple failures and security attacks upon AONs in a distributed manner. Consequently, we discussed a hardware-based control unit that can be embedded in AON nodes to process the MALI's localization procedures in a real time fashion. As a direct consequence, this device can participate in some tasks for fault management of AONs offering the benefit of relaxing the high cost and complexity of signal quality monitoring.

Although this approach may offer several benefits, there are several related issues that require further consideration. First, design concepts for the functional relationship between the hardware-based control unit and available management systems should be questioned. In particular, the development of efficient schemes for performance degradation resistant network control and management algorithms should be taken into consideration. Second, available and proposed control and management protocols that provision lightpaths within the network may be investigated and where necessary tailored to the control unit.

References

[1] M. Medard, S. R. Chinn, and P. Saengudomlert, "Node wrappers for QoS monitoring in transparent optical nodes", *J. High Speed Netw.*, vol. 10, no. 4, pp. 247–268, 2001.

[2] R. Bergman, M. Médard, and S. Chan, "Distributed algorithms for attack localization in all-optical networks", in *Proc. Netw. Distrib. Syst. Secur. Symp.*, San Diego, USA, 1998.

[3] B. Ramamurthy *et al.*, "Impact of transmission impairments on the teletraffic performance of wavelength-routed optical networks", *J. Lightw. Technol.*, vol. 17, no. 10, pp. 759–764, 1999.

[4] C. Larsen and P. Andersson, "Signal quality monitoring in optical networks", *Opt. Netw. Mag.*, vol. 1, no. 4, pp. 17–23, 2000.

[5] C. Mas Machuca, I. Tomkos, and O. K. Tonguz, "Optical networks security: a failure management framework", in *Proc. Conf. ITCom. Opt. Commun. Multimed. Netw.*, Orlando, USA, 2003.

[6] R. Rejeb, M. S. Leeson, and R. J. Green, "Fault and attack management in all-optical networks", *IEEE Commun. Mag.*, vol. 44, no. 11, pp. 79–86, 2006.

[7] J. K. Patel, S. U. Kim, and D. Su, "A framework for managing faults and attacks in WDM optical networks," in *Proc. DARPA Inform. Survivab. Conf. Expos. DISCEX 2001*, Anaheim, USA, 2001, vol. II, pp. 137–145.

[8] R. Rejeb, M. S. Leeson, and R. J. Green, "Multiple attack localization and identification in all-optical networks", *Opt. Switch. Netw.*, vol. 3, no. 1, pp. 41–49, 2006.

[9] R. Rejeb, M. S. Leeson, and R. J. Green, "Hardware-based control unit for all-optical components", in *Proc. 10th IEEE Int. Conf. Transp. Opt. Netw. ICTON'08*, Athens, Greece, 2008, vol. 3, pp. 6–9.

[10] D. Saha, B. Rajagopalan, and G. Berstein, "The optical network control plane: state of the standards and deployment", *IEEE Commun. Mag.*, vol. 41, no. 8, pp. S29–S34, 2003.

[11] J. Lang, "Link management protocol (LMP)", RFC 4204, Oct. 2005.

[12] T. Wu and A. K. Somani, "Necessary and sufficient condition for *k* crosstalk attacks localization in all-optical networks", in *Proc. IEEE Globecom 2003 Conf.*, San Francisco, USA, 2003.

Ridha Rejeb is the Managing Director of the IAER Ltd. and an Assistant Professor at the Physics Institute, Faculty of Basic Sciences at the Esslingen University of Applied Sciences in Germany. He has more than 18 years of industrial experience in network and computer operating systems. He graduated in mathematics at the Stuttgart University of Applied Sciences in Germany. He received his M.Sc. degree in data communications systems from the Brunel University and his Ph.D. in engineering from the University of Warwick, UK. His major research interests include security in communication systems, resilience in transparent optical networks and information theory. He is an Associate Fellow in the School of Engineering, University of Warwick, UK. He is the Technical Program Chair of the ICTON-MW, member of the IEEE, editorial member of the Meditation Journal of Computers and Networks, and member of the CSNDSP technical committee.

e-mail: ridha.rejeb@iaer.eu

Institute for Advanced Engineering and Research

Felix-Wankel-Str. 4/1

73760 Ostfildern, Germany

Mark S. Leeson received a Ph.D. for work on planar optical modulators from the University of Cambridge, UK, in 1990 and then worked as a network analyst for a UK bank until 1992. Subsequently, he held academic appointments in London and Manchester before joining the University of Warwick, UK, in March 2000. He is an Associate Professor in the School of Engineering at the University of Warwick. His major research interests are optical receivers, optical communication systems, communication protocols, coding and modulation, ad hoc networking and evolutionary optimization. To date he has over 140 publications in these fields. He is a chartered member of the UK Institute of Physics, a senior member of the IEEE and a member of the UK EPSRC grants Peer Review College.

e-mail: mark.leeson@warwick.ac.uk

School of Engineering

University of Warwick

Gibbet Hill Road

Coventry, CV4 7AL, United Kingdom

Invited paper

Fault Tolerant Dense Wavelength Division Multiplexing Optical Transport Networks

Yousef S. Kavian, Wei Ren, Majid Naderi, Mark S. Leeson, and Evor L. Hines

Abstract—Design of fault tolerant dense wavelength division multiplexing (DWDM) backbones is a major issue for service provision in the presence of failures. The problem is an NP-hard problem. This paper presents a genetic algorithm based approach for designing fault tolerant DWDM optical networks in the presence of a single link failure. The working and spare lightpaths are encoded into variable length chromosomes. Then the best lightpaths are found by use of a fitness function and these are assigned the minimum number of wavelengths according to the problem constraints using first-fit (FF) algorithm. The proposed approach has been evaluated for dedicated path protection architecture. The results, obtained from the ARPA2 test bench network, show that the method is well suited to tackling this complex and multi-constraint problem.

Keywords— *dedicated path protection architecture, and genetic algorithm, DWDM, fault tolerant networks, optical networks.*

1. Introduction

Dense wavelength division multiplexing (DWDM) optical transport networks provide bulk carriage for client networks such as Internet protocol (IP) networks or synchronous optical networking (SONET) and synchronous hierarchy (SDH) networks [1]. Such networks, based on optical cross-connects (OXCs) and optical add-drop-multiplexers (OADMs), have recently received much attention as backbones to design high speed next generation telecommunication networks [2]. The large capacity expansion resulting from DWDM enables satisfaction of the dramatically increasing bandwidth demanded by applications. It also delivers reduced cost core networks and simplified bandwidth management by virtue of the integration of IP over DWDM via generalized multiprotocol label switching (GMPLS) technology [3].

DWDM optical networks are prone to network component failures that may dramatically impact the network quality of service (QoS) delivered to applications. Therefore maintaining a high level of resiliency is a crucial issue in the design of fault tolerant DWDM optical networks [4]. A resilient network can operate at an acceptable performance level in the event of failure by utilizing redundant resources. The concepts, architectures, models and mechanisms of resilient optical network for fault management have been well addressed in the literature [5].

The design of resilient DWDM optical networks is known as an NP-hard problem [6]. The main object of the work to date has been to develop mathematical models for routing wavelength assignment (RWA) and capacity allocation (CA) problems. These are then solved by the application of integer linear programming (ILP) [6], [7] or heuristic approaches [8]–[11] to get feasible and near optimal solutions, where the objective is to design cost optimal backbone networks by efficient usage of network resources.

Evolutionary algorithms have increasingly been exploited to solve optimization problems in many diverse fields in science and engineering. Genetic algorithms (GAs) [12] comprise a subset of evolutionary algorithms based on natural biological evolution. Many different GA schemes have been developed for communication network design. For example, they have been used in capacitated network design [13], in the design of ring based SDH optical core networks [14] and for routing [15].

This paper presents an application of a GA to design fault tolerant DWDM optical transport networks by establishing a pair of working and spare lightpaths for each connection request in a demand matrix using the dedicated path protection (DPP) architecture. The DPP architecture is an offline survivability approach where the working and spare lightpaths are established before network operation. The backup resources along the spare lightpaths are specifically dedicated to a particular lightpath and can not be utilized by other spare ligthpaths.

The rest of the paper is as follows: Section 2 presents the genetic algorithm model of dedicated path protection. Section 3 describes the results obtained for a predefined demand matrix based on ARPA2 test bench network, while overall conclusions are presented in Section 4.

2. Genetic Algorithm Based Fault Tolerance Approach

This section describes the GA model for failure covering in DWDM optical transport networks. The network topology is represented as a directed graph $G\,(N,L,W)$, where $N = \{n_1, n_2, \dots, n_N\}$ is the set of nodes, $L = \{l_1, l_2, \dots, l_L\}$ is the set of connecting links in the network and $W = \{w_1, w_2, \dots, w_W\}$ is the set of wavelengths per links. The demand matrix $D\,[d_{(o,d)}]_{N\times N}$ aggregates demand between origin and destination node pairs (o,d) in terms of requested wavelengths. The sets of eligible working paths $K^{w}_{(o,d)}$, and spare paths $K^{s}_{(o,d)}$, between each node pair before and after of the event of failure, are precomputed using the *K-shortest* paths algorithm.

2.1. Chromosomes

One of the most important steps of providing a GA model is mapping the problem decision variables into chromosomes that affect the accuracy of the GA based solution. The chromosome is defined by assigning integers to each link with corresponding wavelength sets containing $\hat{W}$ wavelengths. Then, each path of the K-shortest paths between each origin-destination node pair is assigned a binary code and is encoded as a string. The least significant value code is assigned to the shortest path and the most significant value code is assigned to the longest path. The chromosome is then formed by concatenation of the assigned codes for connection requests in the demand matrix.

2.2. The Next Generation

In its progress towards an acceptable solution, a GA utilizes methods to evolve its population to contain a better selection of individuals (as defined by the fitness function).

Crossover. This operation produces new, fitter chromosomes having some parts of their genetic material from both parents. In the context of optical networks, path crossover involves the exchange of two of the permitted lightpaths that are used to handle traffic between an origin and destination node pairs.

Mutation. Mutation is the random adjustment of one part of the chromosome and often enables the recovery of good genetic material that may be lost through the generations. In this case, a binary mutation operates on a gene (bit) of an element (binary path code) of a chromosome and complements it.

Selection. This process emphasizes the fitter solutions. In this work, a virtual roulette wheel is employed to select fitter parent chromosomes. Each chromosome in the population is associated with a sector in this wheel and the area of each sector is proportional to the fitness value of its chromosome, increasing the probability that the fitter chromosomes are selected.

2.3. The Initial Population

The initial path between origin and destination can be generated by randomly choosing any path between each (o,d) from the K-shortest paths available. Here, testing revealed that a better approach was to adapt a heuristic method in which the initial paths were chosen to be the shortest paths from the K-shortest paths for all requests, in the demand matrix.

2.4. Termination

The stochastic nature of GA searching means that it can be difficult to specify convergence criteria to terminate the evolution cycle. Here, the GA is terminated when one of three conditions are met. Firstly, the algorithm may determine that the rate of change, $\varepsilon = 10\exp(-3)$, of the fitness function means that it has reached a minimum; secondly, the error in the fitness function falls below the error threshold; thirdly, the number of generations exceeds a predetermined maximum.

2.5. Fitness Function and Constraints

The amount of working capacity (number of wavelengths required) allocated to working (spare) lightpaths is denoted by f_l^w (f_l^s) for link l. The minimization of the wavelengths utilized by working and spare lightpaths to service a given demand matrix may be written as

$$f_{itness} = \text{minimize}\left\{\sum_{l=1}^{L}(f_l^w + f_l^s)\right\}, \tag{1}$$

$$f_l^w = \sum_{(o,d)}\sum_{p_l^{w,k}}\sum_{w} w_w^{k,od}\,,\ \forall D, \tag{2}$$

$$f_l^s = \sum_{(o,d)}\sum_{p_l^{s,k}}\sum_{w} s_w^{k,od}\,,\ \forall D. \tag{3}$$

Link l is traversed by a set of kth working (spare) paths $P_l^{w,k}$ $(P_l^{s,k})$. The decision variable $w_w^{k,od}$ $(s_w^{k,od})$ is set to 1 if the kth working (spare) path between node pair (o,d) uses wavelength w, and to 0 otherwise.

2.6. Constraints

The link-capacity constraint. The total number of occupied wavelengths, working and spare, on each link is bounded by the number of wavelengths per link $\hat{W}$:

$$f_l^w + f_l^s \leq \hat{W},\ \forall l \in L. \tag{4}$$

The satisfaction constraint. Each link of the working and spare paths that is assigned for a connection request between each node pair (o,d) must satisfy the demand between that node pair:

$$\sum_{w=1}^{\hat{W}} w_w^{od} = d_{(o,d)},\ \forall(o,d) \in D, \tag{5a}$$

$$\sum_{w=1}^{\hat{W}} s_w^{od} = d_{(o,d)},\ \forall(o,d) \in D. \tag{5b}$$

The wavelength utilization constraint. Each wavelength can be utilized only by working paths or by spare paths:

$$w_w + s_w \leq 1,\ \forall w \in W. \tag{6}$$

The w_w (s_w) is set to 1 if wth wavelength assigned to working (spare) path, and to 0 otherwise.

The disjoint constraint. The working path and the spare path, $(P^w_{(o,d)}, P^s_{(o,d)})$, between each node pair (o,d) must be link disjoint (so will not fail together) to accommodate single link failure:

$$P^w_{(o,d)} \cap P^s_{(o,d)} = \phi,\ \forall (o,d) \in D. \tag{7}$$

This constraint is satisfied if and only if $K^w_{(o,d)} \cap K^s_{(o,d)} = \phi$, $\forall (o,d) \in D$.

3. Simulation Results

This section describes the results of application of the GA approach for establishing spare and working lightpaths in fault tolerant DWDM optical networks. To illustrate the method, the ARPA2 network (21 nodes, 25 links) is considered here, shown in Fig. 1. The solu-

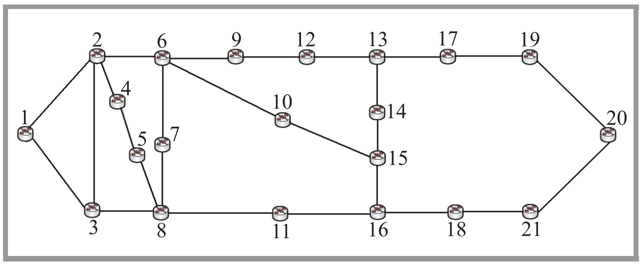

Fig. 1. The ARPA2 network topology.

tions have been achieved by considering 40 wavelengths per link. All links in the physical layer were bidirectional and all nodes were capable of full wavelength conversion. The number of shortest paths considered during each iteration was four and therefore each path was assigned a two bit binary code. For the GA, the population size was maintained at 100, running for 150 generations with a crossover probability of 0.9 and a mutation probability of 0.01. The demand matrix employed was $\mathbf{D} = \big[(1,11,10); (2,7,6); (3,4,7); (6,4,5); (5,17,8); (6,11,9); (17,10,6); (11,4,11); (13,8,13)\big]$, where each element of this matrix is treated as (origin node, destination node, volume of demand).

3.1. Working Lightpaths

The RWA simulation results for the ARPA2 network with demand matrix **D** are shown in Table 1. Working wavelengths were assigned to paths using the simple but effective first-fit strategy, which chooses the available wavelength with the smallest index. The ARPA2 network requires 271 wavelengths with an average of 30.1 wavelengths per request. In the ARPA2 network, there are a few routes that may be employed, e.g., 13-14-15-16-11-8 between nod pair 13-8 and this result in extremely high usage of bandwidth

Table 1
RWA solutions for working paths for ARPA2 network

Node pair	Demand	Working path	Working wavelength
(1,11)	10	1-3-8-11	$(\lambda_1 \ldots \lambda_{10})$/all links in the path
(2,7)	6	2-6-7	$(\lambda_1 \ldots \lambda_6)$/all links in the path
(3,4)	7	3-2-4	$(\lambda_1 \ldots \lambda_7)$/all links in the path
(6,4)	5	6-2-4	$(\lambda_1 \ldots \lambda_5)$/(6-2), and $(\lambda_8 \ldots \lambda_{12})$/(2-4)
(5,17)	8	5-8-7-6-9-12-13-17	$(\lambda_1 \ldots \lambda_8)$/all links in the path
(6,11)	9	6-7-8-11	$(\lambda_1 \ldots \lambda_9)$/all links in the path
(17,10)	6	17-13-14-15-10	$(\lambda_1 \ldots \lambda_6)$/all links in the path
(11,4)	11	11-8-5-4	$(\lambda_1 \ldots \lambda_{11})$/all links in the path
(13,8)	13	13-14-15-16-11-8	$(\lambda_7 \ldots \lambda_{19})$/{(13-14)-(14-15)}, $(\lambda_1 \ldots \lambda_{13})$/{(15-16)-(16-11)}, and $(\lambda_{12} \ldots \lambda_{24})$/(11-8)

(more than double the average in the case of the example route).

3.2. Spare Lightpaths: Dedicated Path Protection

The dedicated path protection RWA solutions for the spare lightpaths are shown in Table 2. The working and spare lightpaths of all requests are link disjoint, the scheme thus protects against any single link failure because at most

Table 2
RWA solutions for spare paths by DPP for ARPA2 network

Node pair	Demand	Spare path	Spare wavelength
(1,11)	10	1-2-6-10-15-16-11	$(\lambda_1 \ldots \lambda_{10})$/{(1-2)-(6-10)-(10-15)}, $(\lambda_7 \ldots \lambda_{16})$/(2-6), and $(\lambda_{14} \ldots \lambda_{23})$/{(15-16)-(16–11)}
(2,7)	6	2-3-8-7	$(\lambda_1 \ldots \lambda_6)$/(2-3), $(\lambda_{11} \ldots \lambda_{16})$/(3-8), and $(\lambda_9 \ldots \lambda_{14})$/(8-7)
(3,4)	7	3-8-5-4	$(\lambda_{17} \ldots \lambda_{23})$/(3-8), and $(\lambda_{12} \ldots \lambda_{18})$/{(8-5)-(5-4)}
(6,4)	5	6-7-8-5-4	$(\lambda_{10} \ldots \lambda_{14})$/{(6-7)-(7-8)}, and $(\lambda_{19} \ldots \lambda_{23})$/{(8-5)-(5-4)}
(5,17)	8	5-4-2-6-10-15-16-18-21-20-19-17	$(\lambda_{24} \ldots \lambda_{31})$/{(5-4)-(15-16)}, $(\lambda_{17} \ldots \lambda_{24})$/(2-6), $(\lambda_{11} \ldots \lambda_{18})$/{(6-10)-(10-15)}, and $(\lambda_1 \ldots \lambda_8)$/{(16-18)-(18-21)-(21-20)-(20-19)-(19-17)}
(6,11)	9	6-10-15-16-11	$(\lambda_{19} \ldots \lambda_{27})$/{(6-10)-(10-15)}, $(\lambda_{32} \ldots \lambda_{40})$/(15-16), and $(\lambda_{24} \ldots \lambda_{32})$/(16-11)
(17,10)	6	17-19-20-21-18-16-11-8-7-6-10	$(\lambda_1 \ldots \lambda_6)$/{(17-19)-(19-20)-(20-21)-(21-18)}, $(\lambda_8 \ldots \lambda_{13})$/(18-16), $(\lambda_{33} \ldots \lambda_{38})$/(16-11), $(\lambda_{25} \ldots \lambda_{30})$/(11-8), $(\lambda_{15} \ldots \lambda_{20})$/(8-7), $(\lambda_9 \ldots \lambda_{14})$/(7-6), $(\lambda_{28} \ldots \lambda_{33})$/(6-10)
(11,4)	11	11-16-15-10-6-2-4	$(\lambda_1 \ldots \lambda_{11})$/{(11-16)-(10-6)}, $(\lambda_{12} \ldots \lambda_{19})$/(16-15), $(\lambda_7 \ldots \lambda_{17})$/(15-10), $(\lambda_6 \ldots \lambda_{16})$/(6-2), $(\lambda_{13} \ldots \lambda_{23})$/(2-4)
(13,8)	13	13-12-9-6-7-8	$(\lambda_8 \ldots \lambda_{20})$/(13-12), $(\lambda_1 \ldots \lambda_{13})$/{(12-9)-(9-6)}, and $(\lambda_{15} \ldots \lambda_{27})$/{(6-7)-(7-8)}

one of the two working and spare lightpaths will fail. The number of assigned wavelengths to spare lightpaths is 434 meaning an average of 48.2 wavelengths per request have been additionally assigned to provide protection.

4. Conclusion

This paper has addressed the design of fault tolerant DWDM optical networks using a GA model based on variable length chromosomes. This has been employed to solve the static RWA problem based on dedicated path protection architecture for ARPA2 network in the context of a single link failure. The optimum number of shortest paths was four, with a greater number producing greatly diminished returns. The results demonstrated that the GA is able to design fault tolerant DWDM optical transport networks.

References

[1] *WDM Optical Networks: Concepts, Design, and Algorithms*, C. S. R. Murthy and M. Gurusamy, Eds. New York: Prentice Hall, 2004.

[2] B. Mukherjee, "WDM optical communication networks: progress and challenges", *IEEE J. Select. Areas Commun.*, vol. 18, no. 10, pp. 1810–1824, 2000.

[3] N. Ghani, S. Dixit, and T. S. Wang," On IP-WDM integration: a retrospective", *IEEE Commun. Mag.*, vol. 41, no. 9, pp. 42–45, 2003.

[4] D. Zhou and S. Subramaniam, "Survivability in optical networks", *IEEE Network*, vol. 14, pp. 16–23, 2000.

[5] J. Zhang and B. Mukherjee, "Review of fault management in WDM mesh networks: basic concepts and research challenges", *IEEE Network*, vol. 18, no. 2, pp. 41–48, 2004.

[6] S. Ramamurthy, L. Sahasrabuddhe, and B. Mukherjee, "Survivable WDM mesh networks", *J. Lightw. Technol.*, vol. 21, no. 4, pp. 870–883, 2003.

[7] J. L. Kennington, E. V. Olinicka, and G. Spiride, "Basic mathematical programming models for capacity allocation in mesh-based survivable networks", *Int. J. Manage. Sci.*, vol. 35, pp. 1–16, 2006.

[8] R. Shenai and K. Sivalingam, "Hybrid survivability approaches for optical WDM mesh networks", *J. Lightw. Technol.*, vol. 23, no. 10, pp. 3046–3055, 2005.

[9] P. H. Ho and H. T. Mouftah, "A novel survivable routing algorithm for shared segment protection in mesh WDM networks with partial wavelength conversion", *IEEE J. Select. Areas Commun.*, vol. 22, no. 8, pp. 1548–1560, 2004.

[10] C. Ou, J. Zhang, H. Zang, H. L. Sahasrabuddhe, and B. Mukherjee, "New and improved approaches for shared-path protection in WDM mesh networks", *J. Lightw. Technol.*, vol. 22, no. 3, pp. 1223–1232, 2004.

[11] G. Lei, C. Jin, Y. Hongfang, and L. Lemin, "Path-based routing provisioning with mixed shared protection in WDM mesh networks", *J. Lightw. Technol.*, vol. 24, no. 3, pp. 1129–1141, 2006.

[12] D. E. Goldberg, *Genetic Algorithms in Search, Optimization, and Machine Learning.* Harlow: Addison-Wesley, 1989.

[13] C. C. Lo and W. H. Chang, "A multiobjective hybrid genetic algorithm for the capacitated multipoint network design problem", *IEEE Trans. Syst., Man Cybern. B*, vol. 30, no. 3, pp. 461–470, 2000.

[14] L. He, C. P. Botham, and C. D. O'Shea, "An evolutionary design algorithm for ring-based SDH optical core networks", *BT Technol. J.*, vol. 22, no. 1, pp. 135–144, 2004.

[15] C. W. Ahn and R. S. Ramakrishna, "A genetic algorithm for shortest path routing problem and the sizing of populations", *IEEE Trans. Evolut. Comput.*, vol. 6, no. 6, pp. 566–579, 2002.

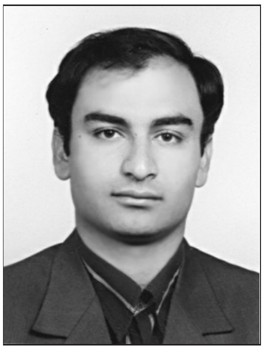

Yousef S. Kavian received his B.Sc. (Hons) degree in electronic engineering from the University of Shahid Beheshti, Tehran, Iran, in 2001, M.Sc. degree in control engineering from the Amkabir University, Tehran, in 2003 and the Ph.D. degree in electronic engineering from the Iran University of Science and Technology (IUST), Tehran, 2007. He joined the Shahid Chamran University as an Assistant Professor in 2008. His research interests include fault tolerant circuits and systems, optical networks, intelligent computing and ad hoc networks. He is the author of more than 25 conference and journal papers in these fields.

e-mail: y.s.kavian@scu.ac.ir
Faculty of Engineering
Shahid Chamran University
Golestan Blvd
61936 Ahvaz, Iran

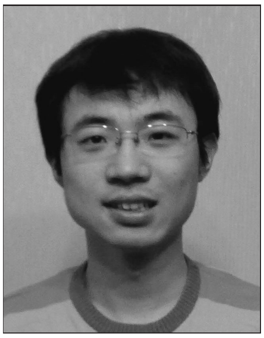

Wei Ren received his B.Sc. in computer science from the University of Warwick, UK, in 2005. He is currently a Ph.D. student at the University of Warwick in the field of electronic engineering. His research interests lie in intelligent systems and network routing optimization.

e-mail: w.ren@warwick.ac.uk
School of Engineering
University of Warwick
Gibbet Hill Road
Coventry, CV4 7AL, United Kingdom

Majid Naderi received his Ph.D. from the Kent University, UK, in 1977. Since 1978 he has been at the Iran University of Science and Technology (IUST), where he is currently a Professor in the Electrical Engineering Department, involved in teaching and research.

e-mail: m_naderi@iust.ac.ir
Electrical Engineering Department
Iran University of Science and Technology (IUST)
Narmak, 16846, Teheran, Iran

Evor L. Hines joined the School of Engineering at the University of Warwick, UK, in 1984. He was promoted a readership in 2005 and obtained his D.Sc. (Warwick) in 2007. He is FHEA, CEng, and FIET. His main research interest is concerned with intelligent systems (also known by other names such as computational intelligence) and their applications. Most of the work has focused on artificial neural networks, genetic algorithms, fuzzy logic, neuro-fuzzy systems and genetic programming. Typical application areas include intelligent sensors (e.g., electronic nose); medicine; non-destructive testing of, for example, composite materials; computer vision; telecommunications; amongst others. Dr. Hines has co-authored more than 200 articles and he currently leads the School's Intelligent Systems Engineering Laboratory and Information and Communication Technologies Research Group.

e-mail: e.l.Hines@warwick.ac.uk
School of Engineering
University of Warwick
Gibbet Hill Road
Coventry, CV4 7AL, United Kingdom

Mark S. Leeson – for biography, see this issue, p. 62.

Invited paper

Network Topology Effect on QoS Delivering in Survivable DWDM Optical Networks

Yousef S. Kavian, Habib F. Rashvand, Mark S. Leeson, Wei Ren, Evor L. Hines, and Majid Naderi

Abstract—The quality of service (QoS) is an important and considerable issue in designing survivable dense wavelength division multiplexing (DWDM) backbones for IP networks. This paper investigates the effect of network topology on QoS delivering in survivable DWDM optical transport networks using bandwidth/load ratio and design flexibility metrics. The dedicated path protection architecture is employed to establish diverse working and spare lightpaths between each node pair in demand matrix for covering a single link failure model. The simulation results, obtained for the Pan-European and ARPA2 test bench networks, demonstrate that the network topology has a great influence on QoS delivering by network at optical layer for different applications. The Pan-European network, a more connected network, displays better performance than ARPA2 network for both bandwidth/load ratio and design flexibility metrics.

Keywords— *dedicated path protection, DWDM, network topology, optical networks, QoS, survivability.*

1. Introduction

The provision of acceptable service in the presence of failures and attacks is a major issue in the design of next generation dense wavelength division multiplexing (DWDM) networks as backbones for future Internet protocol (IP) networks with enhanced quality of service (QoS) [1]. In DWDM technology a fibre can potentially provide multiple terabits per second (Tbit/s) transmission rate by multiplexing different wavelength channels [2], so a fibre cut can lead to tremendous traffic and venue loss which dramatically affect the network QoS delivering to applications [3]. Therefore maintaining a high level of resiliency is an important and crucial issue to design fault tolerant DWDM optical networks against component failures [4]. A survivable network can operate at an acceptable level of performance in the event of failure by failure covering through anticipated redundant resources [5]. This problem is known to be NP-hard [6]. The integer linear programming (ILP) [6], [7] and heuristics approaches [8]–[12] are employed by network researches and engineers to design optimal survivable backbones for different applications such as data, voice and videos.

In survivable networks the working and spare lightpaths established between each node pair must be link disjoint to guarantee that upon any single link failure both paths will not fail simultaneously. Therefore the spare path is able to protect the working path in the event of any single link failure. The dedicated path protection architecture is an offline survivability approach where the working and spare lightpaths are established before network operation. The backup resources along the spare lightpaths are specifically dedicated to a particular lightpath and can not be utilized by other spare lightpaths.

The resource reservation algorithms provide working and spare paths which minimize the bandwidth utilization and they may not be suitable to accommodate the QoS requirements, while QoS requirements will extend network resource utilization [13]. The quality of service refers to the ability of a network to enforce preferential treatment to an application, through a series of classification. Although QoS is not directly responsible for ensuring that the network is up and running all the time, it has a direct impact on the survivability of the network [14]. In general QoS requirements extend network resource utilization, assured through bandwidth trading. The primary contribution of this paper is the investigation of the effect of network topology on delivering QoS in survivable DWDM optical transport networks for bandwidth and delay sensitive applications.

The rest of the paper is as follows: Section 2 presents mathematical formulation for bandwidth management and QoS propagation delay requirement. Section 3 describes the results obtained for a heavy load demand matrix and analyzes the effect of network topology, while overall conclusions are presented in Section 4.

2. Problem Statement

The network topology is represented as a directed graph $G(N,L)$, where $N = \{n_1, n_2, \ldots, n_{\hat{N}}\}$ is the set of nodes and $L = \{l_1, l_2, \ldots, l_{\hat{L}}$ is the set of connecting links in the network. The $W = \{\omega_1, \omega_2, \ldots, \omega_{\hat{W}}\}$ is the set of wavelengths per link. The demand matrix $T[d_{(o,d)}]_{\hat{N}\times\hat{N}}$ aggregates demand between origin and destination node pairs (o,d). The sets of eligible working paths, κ^{w}_{od}, and spare paths κ^{s}_{od}, between each node pair before and after of the event of failure are precomputed using the *K-shortest* paths algorithm [15].

2.1. Bandwidth Optimization

Delivering the required QoS requires a trade-off between network bandwidth and application requirements. The economic objective of the establishment of suitable resilient working, P, and spare, S, paths entails the discovery of routes with minimum bandwidth occupation to working, b^p_{od}, and spare, b^s_{od}, paths between node pair (o,d) may be written as

$$B = \text{minimize}\left\{ \sum_{(o,d)} (b^p_{od} + b^s_{od}) \right\}, \tag{1}$$

$$b^p_{od} = \sum_{l \in P} \sum_{\omega \in W} \omega^{k,od}_w, \quad \forall (o,d) \in T, \tag{2}$$

$$b^s_{od} = \sum_{l \in S} \sum_{\omega \in W} \omega^{k,od}_s, \quad \forall (o,d) \in T. \tag{3}$$

The decision variable $\omega^{k,od}_w$ $(\omega^{k,od}_s)$ is set to 1 if the kth working (spare) path between node pair (o,d) uses wavelength ω, and to 0 otherwise.

The link-capacity constraint. The total number of occupied wavelengths, working and spare, on each link is bounded by the number of wavelengths per link $\hat{W}$.

The satisfaction constraint. Each link of the working and spare paths that is assigned for a connection request between each node pair (o,d) must satisfy the demand between that node pair.

The wavelength utilization constraint. Each wavelength can be utilized only by working paths or by spare paths.

The disjoint constraint. The working path and the spare path, (P,S), between each node pair (o,d) must be link disjoint (so will not fail together) to accommodate single link failure.

2.2. Quality of Service Requirements

The QoS requirement for delay sensitive applications is to find resilient paths that minimize the propagation delay of working, d^p_{od}, and spare, d^s_{od}, paths between (o,d):

$$D = \text{minimize}\left\{ \sum_{(o,d)} (d^p_{od} + d^s_{od}) \right\}, \tag{4}$$

$$d^p_{od} = \sum_{l \in P} d_l, \quad \forall (o,d) \in T, \tag{5}$$

$$d^s_{od} = \sum_{l \in S} d_l, \quad \forall (o,d) \in T, \tag{6}$$

with d_l being the delay for link l, which is proportional to its length. Also, d^p_{od} (d^s_{od}) must be less than the maximum acceptable delay on the working and spare lightpaths for a request between node pair (o,d). The delay should also be less than $D^{\max}$, the maximum acceptable delay for the demand matrix (this condition will weed out very poor solutions from the population with minimal computation).

3. Simulation Results

This section describes some simulation results of designing survivable DWDM optical networks for both bandwidth and propagation optimization schemes. For this a programming code has been implemented using MATLAB. To illustrate the effect of network topology on QoS delivering, two contrasting networks are considered here, both are established benchmarks and are shown in Fig. 1. The Pan-European network is a highly connected example, comprising 18 nodes and 35 links. The ARPA2 network is a much less connected topology, containing 21 nodes with 25 links.

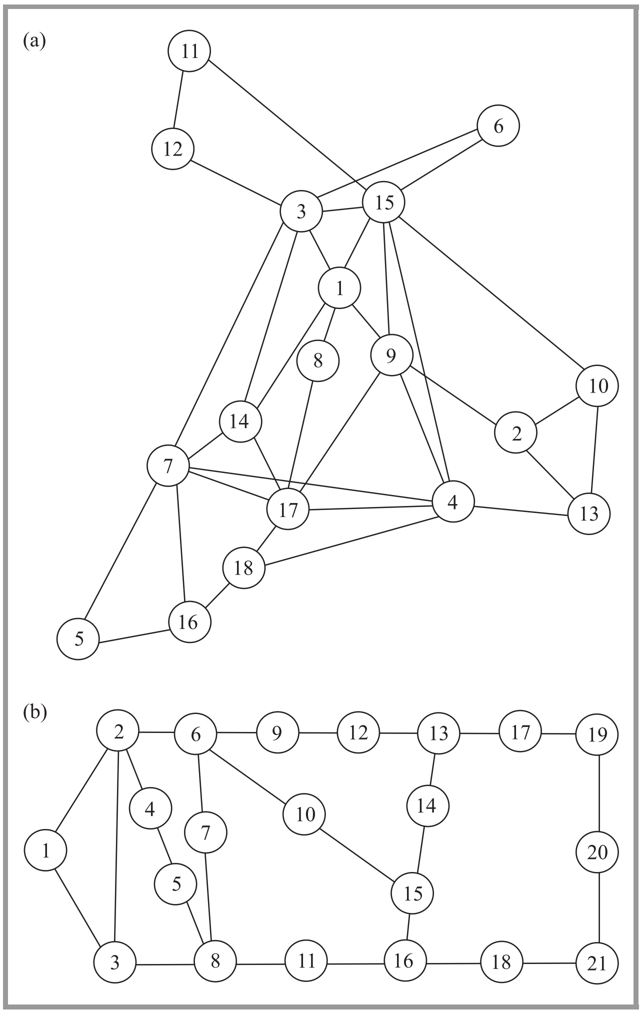

Fig. 1. The benchmark topologies: (a) the Pan-European and (b) the ARPA2 network topology.

These topologies are representative of popular mesh topologies employed in survivable optical mesh network design. All links in the physical layer were bidirectional and all nodes were capable of full wavelength conversion. The adjusted delay on each link is assumed to be 5 μs/km [16]. The number of shortest paths considered during each iteration were $\kappa^w_{od} = 4$ for working paths and $\kappa^s_{od} = 6$ for spare paths. The simple but efficient first-fit (FF) algorithm has been employed for wavelength assignment. It should be noted that the efficiency of the first-fit algorithm is not an issue here since the full wavelength conversion is considered for all nodes. In fact, in such scenario, where there is no wavelength continuity constraint, any wavelength assignment algorithm will achieve the same performance.

3.1. Evaluation the Bandwidth/Load Ratio

The effect of the bandwidth optimization scheme (BOS) and the propagation delay optimization scheme (DOS) on the routing wavelength assignment (RWA) problem was investigated via a heavy load traffic model. The arrival requests at all nodes are sent to all of the other nodes in the network. The wavelength requested per node was $\lambda = 5$. The results are compared for BOS and DOS in Tables 1 and 2, where the whole load of the network is $\hat{\lambda} = \lambda \hat{N}(\hat{N}-1)$ and $\hat{N}$ is a number of network nodes. For both optimization schemes, the working paths occupy less bandwidth than the spare paths and exhibit reduced latency time.

Table 1
Bandwidth and propagation delay for BOS

Network	$\hat{\lambda}$	Working bandwidth	Working propagation delay [s]	Spare bandwidth	Spare propagation delay [s]
Pan-European	1530	3570	30.75	4770	41.15
ARPA2	2100	7325	44.00	13475	81.45

Table 2
Bandwidth and propagation delay for DOS

Network	$\hat{\lambda}$	Working bandwidth	Working propagation delay [s]	Spare bandwidth	Spare propagation delay [s]
Pan-European	1530	4290	27.50	4835	40.45
ARPA2	2100	7400	43.75	13485	81.40

It may be seen that the type of optimization scheme has more influence on working bandwidth and propagation delay than spare bandwidth and delay. To examine this difference, it is useful to calculate the bandwidth/load ratio (BLR) given by the bandwidth allocated divided by the total network load $\hat{\lambda}$.

Figure 2 depicts the BLR for DOS against the BLR for BOS. In both cases, the BLR is substantially less for the working paths than for the spare paths. For the ARPA2 network, there is a negligible difference in BLR between BOS and DOS. However, although this is true for spare paths in the Pan-European network BOS delivers a lower BLR for working paths as would be hoped. The lack of enhanced performance in the ARPA2 network emphasizes the role of connectivity in performance since there are few choices to be made regarding alternative routes in this network.

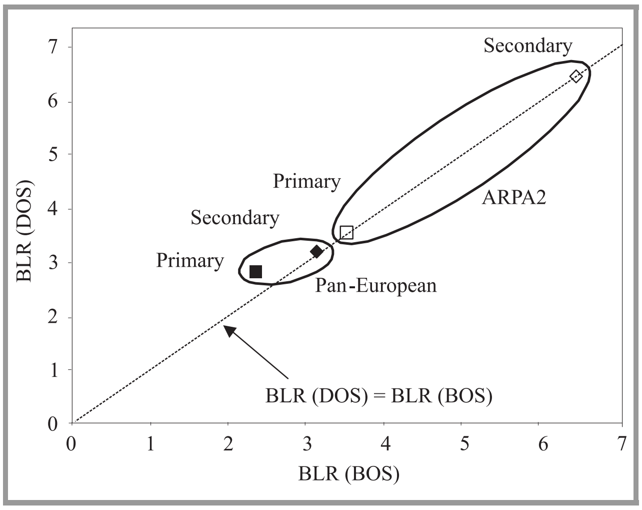

Fig. 2. Variation of BLR for DOS versus BOS.

3.2. Design Flexibility

The behavior of delay versus bandwidth is not a simple one, so it is interesting to investigate the flexibility of the benchmark networks. To this end, we define the percentage design flexibility (ζ) in terms of the ratio of the absolute difference between the BOS solution (χ^B) and the DOS solution (χ^D) over the BOS solution (χ^B). The quantities χ^B and so on may denote bandwidth or delay as appropriate:

$$\zeta = 100 \frac{|\chi^B - \chi^D|}{\chi^B}. \tag{7}$$

The delay flexibility versus the bandwidth flexibility is shown in Fig. 3, for both working and spare paths. A clear difference between the two networks is apparent. Although there is much less flexibility in both cases for the spare paths, the Pan-European network has the highest flexibility (10.5%, 20.2%). The network planner can find out how much it is possible to optimize a survivable network for bandwidth or delay. Again, the network topology has a large influence on design flexibility, resulting in the large difference arising from the greatly differing node degrees of the networks considered.

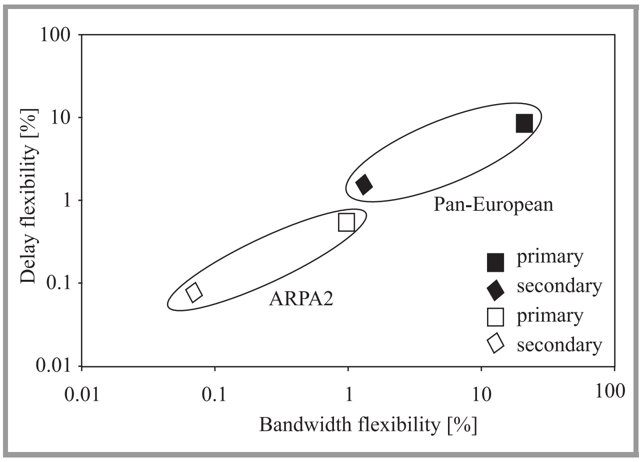

Fig. 3. Delay flexibility versus bandwidth flexibility.

4. Conclusion

Design of survivable DWDM optical networks for bandwidth and delay sensitive applications has been proposed. In the light of the importance of delay to QoS, the research also considered solutions based on DOS in addition to BOS. The BLR has been employed to illustrate performance when using BOS and DOS, showing that there is a significant difference for working paths for the Pan-European network. In the case of spare paths, and for all paths in the ARPA2 network, BOS and DOS perform equally in their loading of the network. Furthermore, a design flexibility factor has been defined to demonstrate the large influence of network topology, or more precisely node degree, on the QoS delivered. A more interconnected network, such as the Pan-European, displays an order of magnitude more flexibility than one of limited degree such as ARPA2.

References

[1] D. Zhou and S. Subramaniam, "Survivability in optical networks", *IEEE Network*, vol. 14, no. 6, pp. 16–23, 2000.

[2] B. Mukherjee, "WDM optical communication networks: progress and challenges", *IEEE J. Select. Areas Commun.*, vol. 18, no. 10, pp. 1810–1824, 2000.

[3] J. Zhang and B. Mukherjee, "Review of fault management in WDM mesh networks: basic concepts and research challenges", *IEEE Network*, vol. 18, no. 2, pp. 41–48, 2004.

[4] Y. S. Kavian, W. Ren, M. Naderi, M. S. Leeson, and E. L. Hines, "Survivable wavelength-routed optical network design using genetic algorithms", *Eur. Trans. Telecommun.*, vol. 19, no. 3, pp. 247–255, 2008.

[5] M. Medard and S. Lumetta, "Architectural issues for robust optical access", *IEEE Commun. Mag.*, vol. 39, no. 7, pp. 116–122, 2001.

[6] J. L. Kennington, E. V. Olinicka, and G. Spiride, "Basic mathematical programming models for capacity allocation in mesh-based survivable networks", *Int. J. Manage. Sci.*, vol. 35, pp. 1–16, 2006.

[7] S. Ramamurthy, L. Sahasrabuddhe, and B. Mukherjee, "Survivable WDM mesh networks", *J. Lightw. Technol.*, vol. 21, no. 4, pp. 870–883, 2003.

[8] R. Shenai and K. Sivalingam, "Hybrid survivability approaches for optical WDM mesh networks", *J. Lightw. Technol.*, vol. 23, no. 10, pp. 3046–3055, 2005.

[9] P. H. Ho and H. T. Mouftah, "A novel survivable routing algorithm for shared segment protection in mesh WDM networks with partial wavelength conversion", *IEEE J. Select. Areas Commun.*, vol. 22, no. 8, pp. 1548–1560, 2004.

[10] C. Ou, J. Zhang, H. Zang, H. L. Sahasrabuddhe, and B. Mukherjee, "New and improved approaches for shared-path protection in WDM mesh networks", *J. Lightw. Technol.*, vol. 22, no. 3, pp. 1223–1232, 2004.

[11] G. Lei, C. Jin, Y. Hongfang, and L. Lemin, "Path-based routing provisioning with mixed shared protection in WDM mesh networks", *J. Lightw. Technol.*, vol. 24, no. 3, pp. 1129–1141, 2006.

[12] K. Ratnam, Z. Luying, and M. Gurusamy, "Efficient multi-layer operational strategies for survivable IP-over-WDM networks", *IEEE J. Select. Areas Commun.*, vol. 24, no. 8, pp. 16–31, 2006.

[13] Y. Bejerano, Y. Breitbart, A. Orda, R. Rastogi, and A. Sprintson, "Algorithms for computing QoS paths with restoration", *IEEE/ACM Trans. Netw.*, vol. 13, no. 3, pp. 648–661, 2005.

[14] K. K. Lee, F. Lim, and B. H. Ong, *Building Resilient IP Networks*. Indianapolis: Cisco Press, 2006.

[15] S. Mittal and P. Mirchandani, "Implementation of *k*-shortest path Dijkstra algorithm used in all-optical data communication networks", SIE 546 Project Report, University of Arizona, Tucson, 2004.

[16] R. D. Larson, G. Nicholas, and J. Paulter, "A measurement of propagation delay", *Metrologia*, vol. 44, pp. 64–68, 2007.

Habib F. Rashvand received his B.Sc. in 1969 and postgraduate qualifications in 1970 from the University of Tehran. He was selected for a training mission as the head of division for development of a new Telecom Research Centre as under a new cooperation project between the Iranian PTT and Japanese Industries including the NTT, KTT following his Doctorate at the University of Kent in 1980. Since then he earned a rich blend of industrial research and development positions with industries in collaboration with many universities including University of Southampton, University of Reading, Portsmouth University, Warwick University and Coventry University. His academic positions compiles University of Tehran, University of Zambia, Coventry University, Magdeburg University and University of Warwick. His Professorship in Networks, Systems & Protocols applied in 1998 to the German Ministry of Education succeeded in 2001. Since 2004 he headed a Special Academic Quality Research Operation under Directorship of Advanced Communication Systems which involves ITU, CTO, WHO, IEEE/IEE/IET. He was the editor-in-chief, member of editorial board and invited speaker for many research journals and conferences.

e-mail: h.rashvand@warwick.ac.uk
School of Engineering
University of Warwick
Gibbet Hill Road
Coventry, CV4 7AL, United Kingdom

Mark S. Leeson – for biography, see this issue, p. 62.

Yousef S. Kavian, Wei Ren, and **Majid Naderi** – for biographies, see this issue, p. 66.

Evor L. Hines – for biography, see this issue, p. 67.

Paper

Fusion Splicing and Testing of Photonic Crystal Fibers

Krzysztof Borzycki

Abstract—Properties of two different photonic crystal fibers (PCF) were characterized, enabling comparisons. Properties investigated included spectral attenuation, polarization mode dispersion (PMD), optical time domain reflectometer characteristics, elastooptic factor describing transmission delay induced by axial strain plus effects of temperature cycling and fiber twist on PMD and loss. In particular, temperature and twist dependence of PMD was different for each fiber tested. For optical measurements, fibers were fusion spliced to pigtails with standard telecom single mode fibers. PCF splicing procedures and solutions adopted to minimize collapse of holes during arc fusion and splice loss are presented. It was found that fusion splicing procedure must be individually tailored to each combination of fibers.

Keywords— fusion splicing, measurements, mechanical testing, photonic crystal fiber, polarization mode dispersion, temperature cycling.

1. Introduction

Experiments presented in this paper have been carried out at the laboratories of National Institute of Telecommunications (NIT) in Warsaw as part of participation in the COST Action 299 "Optical Fibres for New Challenges Facing the Information Society" (FIDES)[1], dedicated to new applications of fiber optics. This includes research and characterization work on new fiber designs, in particular highly-doped and photonic crystal fibers.

Photonic crystal fibers with germanium-doped core, designated as 252b5 and 282b4 were provided by Institute of Photonic Technology (IPHT) Jena, Germany – another participant of COST-299.

Besides characterization of each photonic crystal fibers (PCF), another goal of work was to research fusion splicing of PCF to standard single mode fibers (SMF). Most fiber optic measuring instruments are designed specifically to test SMF and similar solid-glass fibers, so a convenient way to prepare sample of specialty fiber for measurements is to splice it to SMF pigtails with connectors of choice. As low splice loss and stability of loss and polarization orientation are highly desirable, a proven fusion splicing method is preferred. This is of particular importance during temperature cycling and mechanical experiments.

Earlier work at NIT within COST-299 on PCF characterization, including IPHT 252b5 has been reported in 2008 [1]. Some data from this paper are included here for comparisons.

[1]More information on this COST Action can be found at www.cost299.org

2. The Fibers

Both PCF were designed to be single mode at wavelengths above 1300 nm, made of silica, and had a small core doped with GeO_2, with a wider "base" and central "peak", surrounded by a multilayer array of holes. Fibers had thin, mechanically strippable, single-layer acrylate coating. Fiber data are listed in Table 1.

Table 1
Fiber data supplied by IPHT

Parameter	IPHT 252b5	IPHT 282b4
Cladding diameter [μm]	82.7	124.4
Number of holes	90	94
Hole diameter (d) [μm]	3.6	~0.7
Hole spacing (Λ) [μm]	4.2	4.2
Diameter of holey package [μm]	42.8	43.0
Cross-section occupied by holes [%]	17.1	0.3
Cladding diameter after collapse [μm]	75.3	124.2
Core diameter [μm]	0.5/2.0/4.1	1.2/3.9/7.3

Both fibers had relatively small cores and high doping levels in comparison to SMF used in communication networks, where typical core diameter is 7–9 μm [2], [3]. This applies in particular to IPHT 252b5, designed as highly nonlinear PCF for applications like optical signal processing. This property leads to considerable difficulties in making low-loss splices between PCF and SMF.

Hole diameters listed in Table 1 were measured with optical microscope; scanning electron microscope (SEM) observations at IPHT found that hole diameters in 282b4 vary considerably, down to about 0.5 μm.

3. Fusion Splicing

3.1. Connections to Test Instruments

For connection to test instruments each PCF was fusion spliced to pigtails with SMF fibers, most often Corning SMF-28 or OFS MC-SM, 2–3 m long and terminated with FC/PC connectors (Fig. 1). For optical time domain reflectometer (OTDR) measurements, SMF lengths must be increased to $\geq$ 100 m in order to eliminate the dead zone.

Splices were protected by standard 60 mm heat shrinkable sleeves reinforced with steel rods, being often subjected to thermal cycling or used to fix ends of PCF during mechan-

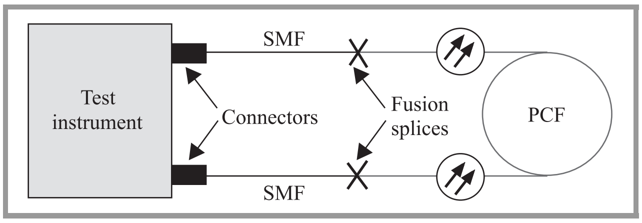

Fig. 1. Connection of PCF sample to measuring instrument.

ical tests. Because of differences between fibers, splicing procedure had to be adjusted individually.

In line with prior experience [1], no solvent was used in preparations for PCF cleaving; the coating was stripped mechanically and remains wiped away with dry tissue. A standard cleaver with tungsten carbide blade was used. Proportion of bad cleaves was significant for 252b5 fiber, while the 282b4 handled comparably to 125 μm telecom fibers. Fiber positioning before splicing was optimized using optical source and power meter. For most measurements an HP8153A optical multimeter with HP8153SM 1558 nm laser source and HP81532A power meter modules was used.

When splicing SMF to PCF, often of different diameter, three problems arise:

a) thinner fiber must receive less power to prevent overheating;

b) collapse of holes in the PCF tends to increase splice loss and shall be controlled;

c) sharp edges must be avoided to ensure splice strength.

A solution to problem (a) is to offset the fiber contact point from the axis of electrodes, so the smaller fiber is kept away from center of discharge zone and is heated less. This longitudinal offset shall not be greater than (1.5–2) $\times$ the diameter of thicker fiber; larger offset can lead to fiber deformation.

Collapse of holes in PCF is hard to avoid, but length affected is minimized by short fusion time, preferably 0.2–0.5 s, instead of 1–2 s common in splicing of conventional 125 μm single mode and multimode fibers. Careful control of arc power is essential. Unfortunately, too short fusion time and low arc power prevent proper rounding of edges when fiber diameters don't match, as molten glass does not have enough time to flow. This leads to fragile splices which break easily.

Loss of fusion splice between fibers of different core sizes and designs can be reduced by:

– insertion of a short piece of fiber with intermediate core parameters [4];

– individually optimized forming of fibers before fusion; examples include pulling hot fiber to reduce diameter before cleaving, thermal expansion of core by heat treatment and melting of PCF tip to close the holes over controlled length and expand light beam, or to create a ball lens [5].

The following sections describe experiences with splicing of PCF and SMF fibers.

3.2. Splicing IPHT 252b5 to SMF

Out of methods listed above, fusing of SMF and PCF tips into lenses [5] was of particular interest. It was applied at NIT to splice a sample of thin, small-core IPHT 252b5 fiber (Table 1) to Corning SMF-28 single mode fibers. Previous attempts [1], when SMF and PCF were butt-coupled with 150 μm offset during fusion produced splices with good strength, but loss of SMF-PCF-SMF assembly with 1 m of PCF was high: 16.8 dB at 1550 nm.

Splicing of IPHT 252b5 sample to SMF-28 pigtails is presented below, including photos taken through the microscope of fusion splicer and loss measurements at 1558 nm. The PCF sample was 16.08 m long; fiber attenuation and loss were 114 dB/km and 1.83 dB, respectively, at 1558 nm. Fusion splicer had 1 mm electrode gap, and the following settings (arc current – duration) were adopted:

– splicing (pre-fusion, fusion, annealing):
9 mA – 3.0 s / 18 mA – 0.5 s / 8.4 mA – 3.0 s;

– melting of fiber tip: 18 mA – 0.5 s.

Fiber feed during fusion was approx. 20 μm. Splicing standard SMF with the same machine requires 18–19 mA fusion current and 1.2 – 1.5 s fusion duration.

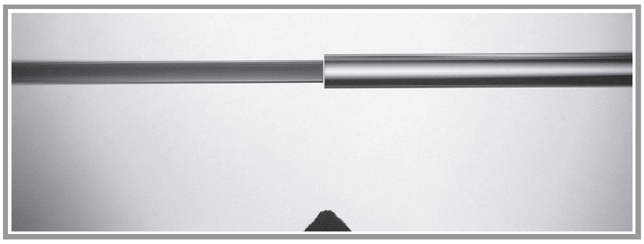

Fig. 2. Fibers cleaved and aligned with 10 μm gap (loss: 8.18 dB, electrode tip visible at the bottom).

Fig. 3. SMF tip melted into a ball: (a) phase 1; (b) phase 2.

Work began with connecting the first pigtail to a 1558 nm laser source. The opposite end of PCF was cleaved and connected to optical power meter. Figures 2–10 show making of the first splice, where light traveled from SMF to PCF. Field of view in all splicer photos is 0.88×2.35 mm. After cleaving and measuring reference loss (Fig. 2), fibers were melted to make ball lenses at their ends (Figs. 3–5). Melting of SMF tip had to be repeated for proper effect (Fig. 3).

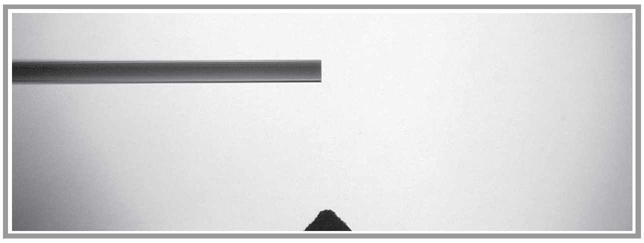

Fig. 4. PCF tip positioned for ball forming.

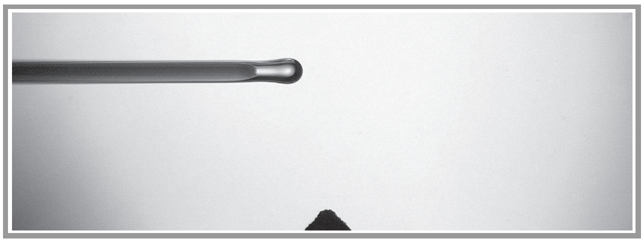

Fig. 5. PCF tip melted into a ball. Holes collapsed over 180–200 μm length.

Radii of ball lenses were 48 μm for PCF and 74 μm for SMF. Prepared fibers were positioned for best coupling, with longitudinal offset to reduce PCF heating during fusion (Fig. 6), than fused (Fig. 7).

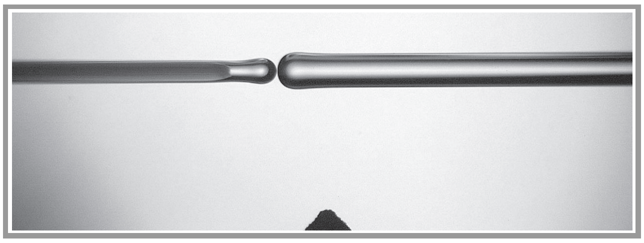

Fig. 6. Lens-tipped fibers positioned with ≈ 10 μm gap (offset: 200 μm, loss: 5.48 dB).

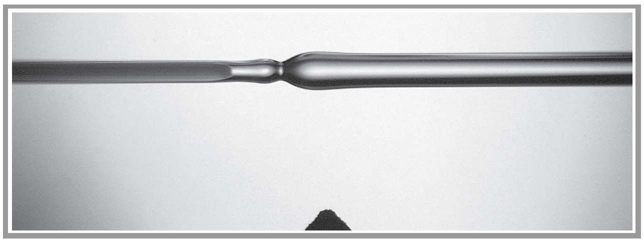

Fig. 7. PCF and SMF spliced (loss: 3.76 dB).

After fusion, attempts were made to reduce splice loss with additional heating, by repeating fusion program without moving fibers. It worked, but with diminishing effect (Figs. 8–10).

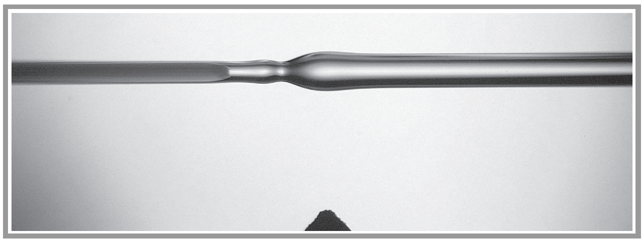

Fig. 8. PCF and SMF after additional heating no. 1 (loss: 3.43 dB).

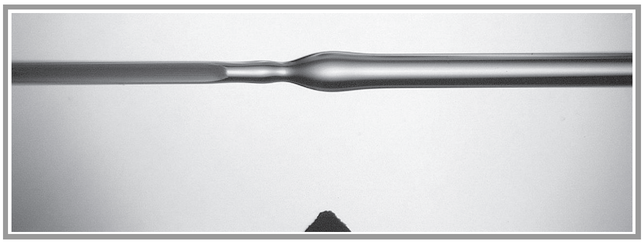

Fig. 9. PCF and SMF after additional heating no. 2 (loss: 3.24 dB).

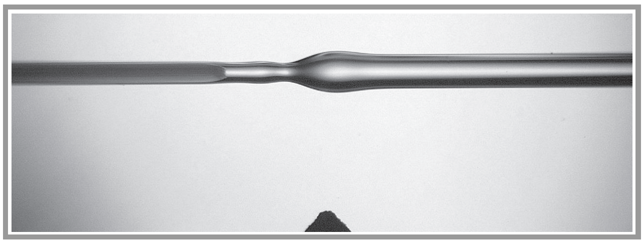

Fig. 10. PCF and SMF after additional heating no. 3 (loss: 3.19 dB).

Table 2
Loss of IPHT 252b5 sample during splicing to SMF pigtails

Conditions	Sample loss [dB]	Splice loss [dB]
SMF → PCF splice (first)		
Fibers cleaved and aligned	8.18	6.15
Lens-tipped fibers aligned	5.48	3.45
Fibers spliced	3.76	1.73
After heating no. 1	3.43	1.40
After heating no. 2	3.24	1.21
After heating no. 3	3.19	1.16
PCF → SMF splice (second)		
Fibers cleaved and aligned	8.98	5.79
Lens-tipped fibers aligned	5.37	2.18
Fibers spliced	4.61	1.42
After heating no. 1	4.38	1.19
After heating no. 2	4.28	1.09
After heating no. 3	4.17	0.98

The second splice transmitted light from PCF to SMF. For loss measurement, the second pigtail was connected to power meter. Loss values in various stages of splicing at both ends are listed in Table 2.
Subtracting 0.20 dB for connector loss and 1.83 dB for PCF loss, we get 2.14 dB for two splices. Transfer of light from SMF to PCF causes majority of loss: 1.16 dB, due to escape of radiation from the splice (Fig. 11).

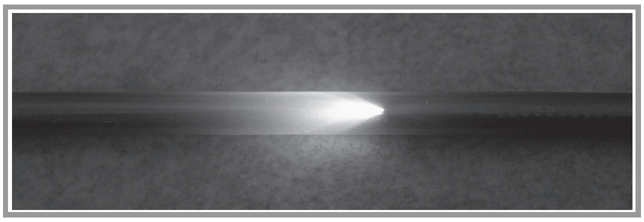

Fig. 11. Escape of visible light in transit from SMF (right) to IPHT 252b5 (left). Splice inside a heat-shrinkable sleeve filled with opaque hot melt glue. Illumination with supercontinuum (SC) source.

3.3. Splicing IPHT 282b4 to SMF

This PCF was spliced without longitudinal offset (Fig. 12), using 17 mA fusion current and other conditions as in Subsection 3.2. Fiber length, attenuation and loss at 1558 nm were 12.4 m, 62 dB/km and 0.77 dB, respectively. After fusion, holes collapsed over 280–300 μm (Fig. 13), but loss still fell in comparison to cleaved and aligned fibers, regardless of transmission direction.

Fig. 12. SMF (right) and IPHT 282b4 (left) cleaved and aligned with ≈ 10 μm gap.

Fig. 13. SMF and IPHT 282b4 fused.

Loss values at 1558 nm are listed in Table 3. Assuming 0.25 dB connector loss, the loss of two splices is 2.74 dB.

Table 3
Loss of IPHT 282b4 sample during splicing to SMF pigtails

Conditions	Sample loss [dB]	Splice loss [dB]
SMF → PCF splice (first)		
Fibers cleaved and aligned	3.73	2.71
Fibers spliced	2.50	1.48
Protective sleeve applied	2.52	1.50
PCF → SMF splice (second)		
Fibers cleaved and aligned	4.79	2.27
Fibers spliced	3.77	1.25
Protective sleeve applied	3.76	1.24

Loss in each direction of transmission is similar, as can be expected when core diameters of spliced fibers are comparable (Table 1). Part of splice loss is likely due to destruction of holey structure and escape of light. One can expect improvement when PCF heating is reduced by offset or lower arc current.

4. Spectral Loss

Loss spectra of two pigtailed IPHT 252b5 samples were acquired with supercontinuum light source Koheras SuperK Compact and optical spectrum analyzer Yokogawa AQ-6315B.

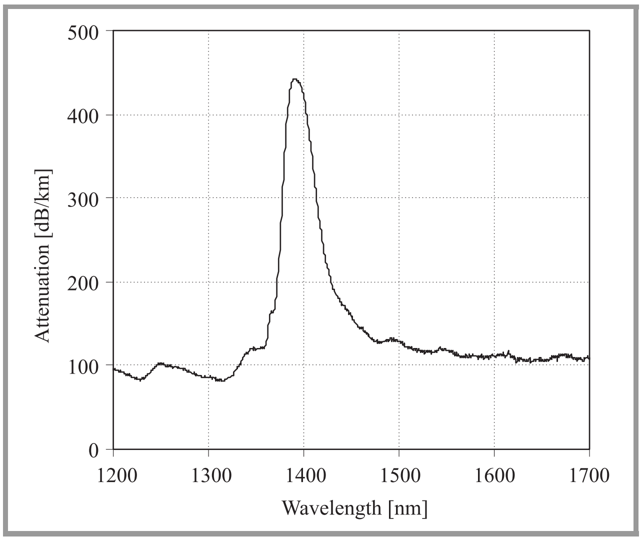

Fig. 14. Spectral attenuation of IPHT 252b5 fiber.

Characteristics of IPHT 252b5 fiber, shown in Fig. 14 and Table 4 was established by comparing loss spectra of two lengths: 0.50 m and 16.08 m, spliced in the same way to SMF pigtails. Attenuation can be attributed to waveguide imperfections (80–105 dB/km) and OH^- ion absorption (~ 355 dB/km at 1390 nm); the latter corresponds to water

Table 4
Attenuation of IPHT 252b5 fiber at selected wavelengths

Wavelength [nm]	Attenuation [dB/km]
1200	95
1248	103
1315	82
1390	443
1550	119
1700	110

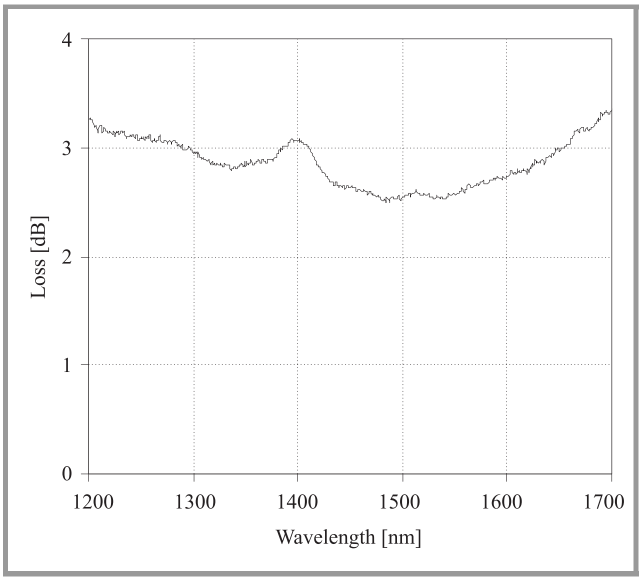

Fig. 15. Loss spectrum of 0.5 m sample of IPHT 252b5 with SMF pigtails.

content of about 7 ppm. Loss spectrum of the 0.50 m sample (Fig. 15) is pretty flat, with minimum splice loss at 1500 nm.

5. OTDR Measurements

Sample of 282b4 fiber was measured using Tektronix TFP2 OTDR fitted with FS 1315 optical module. The 252b5 sample available was too short for this purpose.

This PCF was characterized by very strong Rayleigh backscattering. Its OTDR trace (Fig. 16) was shifted upwards by approx. 9 dB with respect to trace of SMF (OFS MC-SM [3]) at wavelengths of 1310 nm and 1550 nm, when loss of splice and connector between SMF and PCF (0.5 dB) was corrected for. This means an 80-fold difference in backscatter power. Possibly, the photonic

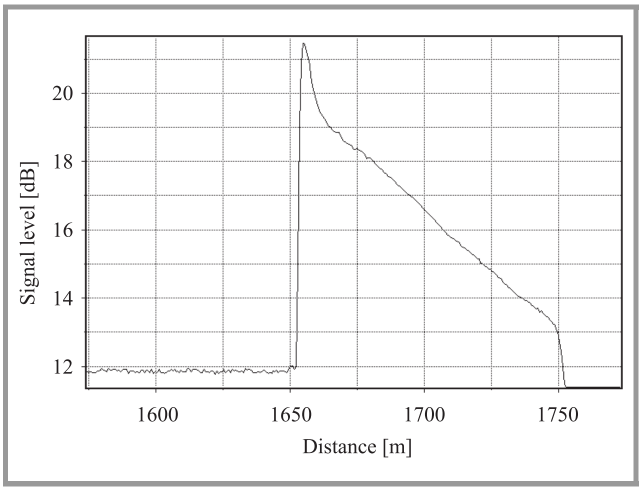

Fig. 16. OTDR trace of 104 m IPHT 282b4 preceded by 1645 m long SMF, $\lambda = 1310$ nm. Reflection spike is due to connector located between SMF and PCF.

structure around PCF core reflects scattered light back into the core. Backscattering coefficients are approx. –71 dB and –73 dB for a 1 m pulse at 1310 nm and 1550 nm, respectively.

Table 5
OTDR test results – IPHT 282b4

Parameter	Value
Fiber attenuation at 1310 nm [dB/km]	69.3
Fiber attenuation at 1550 nm [dB/km]	60.2
Trace shift versus MC-SM at 1310 nm [dB]	8.7
Trace shift versus MC-SM at 1550 nm [dB]	9.5

Optical time domain reflectometer traces were quite linear, with deviations within ± 0.2 dB. Loss values measured with OTDR were confirmed by measurement with laser source and optical power meter. Results are shown in Table 5.

6. Polarization Mode Dispersion

Measurements were made at room temperature with Adaptif Photonics A2000 PMD analyzer and Agilent HP8168F

Table 6
Results of PMD and polarization dependent loss (PDL) measurements

Fiber	Length [m]	PMD [ps]	PMD coefficient [ps/km]	PDL [dB]
IPHT 252b5	0.50	0.547	1094	0.23
IPHT 252b5	16.08	18.120	1127	0.15
IPHT 282b4	12.40	1.455	117.34	0.37
IPHT 282b4	104	9.104	87.54	0.03

tunable laser in the 1460–1590 nm band, using the Jones matrix eigenalysis (JME) method. Two different lengths of each fiber cut were from the same delivery length. Results are listed in Table 6. Differential group delay (DGD) spectra are shown in Figs. 17 and 18. PCF length uncertainty was 2%.

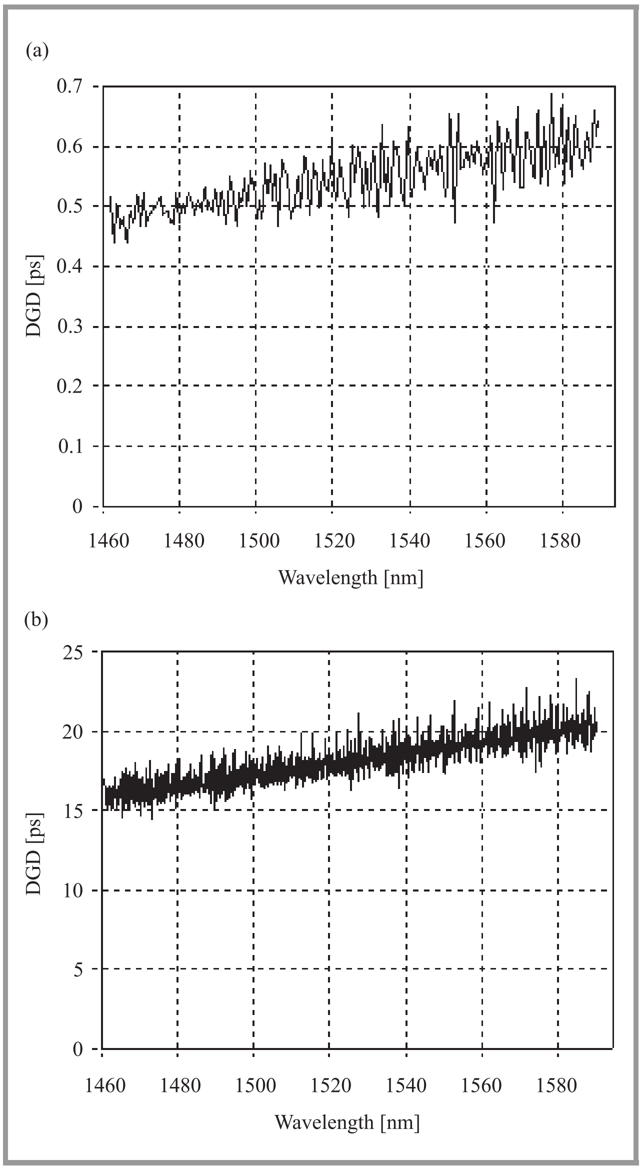

Fig. 17. DGD spectra of IPHT 252b5 fiber: (a) $L = 0.50$ m; (b) $L = 16.08$ m.

The IPHT 252b5 fiber exhibited very high PMD coefficient and linear increase of DGD with wavelength, identical for both lengths tested.

Differential group delay distribution of IPHT 282b4 was flat with some random deviations. A lower PMD coefficient in the longer sample suggests some mixing of polarization modes, confirmed by somewhat irregular movement of state of polarization on Poincare sphere with wavelength. For the shorter sample of IPHT 282b4 and both lengths of 252b5 a circular movement was observed.

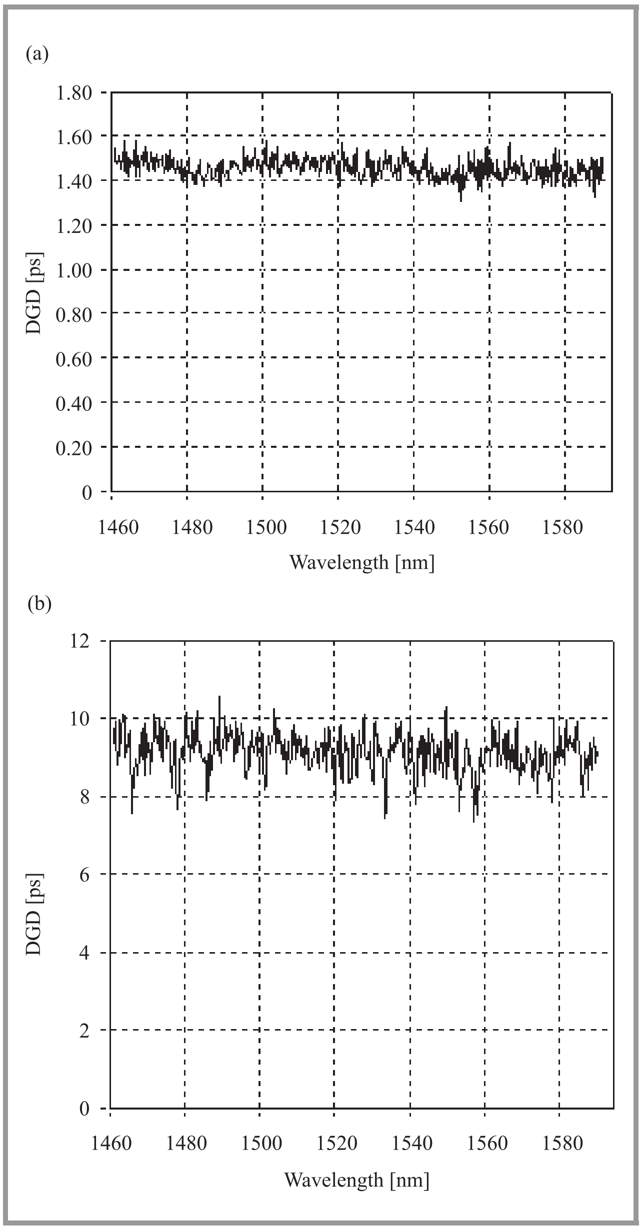

Fig. 18. DGD spectra of IPHT 282b4 fiber: (a) $L = 12.40$ m; (b) $L = 104$ m.

7. Temperature Cycling

Each fiber was subjected to a single temperature cycle with measurements of polarization parameters and loss, using Adaptif Photonics A2000 PMD analyzer and Agilent HP8168F tunable laser.

To minimize external forces acting on fiber under test, the short sample of IPHT 252b5 was loosely placed on a flat plate, while IPHT 282b4 was wound on a 160 mm diameter spool with soft foam bedding. Whole length of PCF and both PCF-SMF splices were placed inside the environmental chamber. Measurements at reference temperature (+20°C) were performed twice to detect any permanent change in fiber parameters, e.g., due to deterioration of protective coating.

Results are shown in Tables 7 and 8, and Figs. 19 and 20. PMD, PDL and insertion loss data are averages for the whole spectral range. Sample of IPHT 252b5 was spliced using old non-optimized method [1].

Table 7
IPHT 252b5 – temperature cycling test
(fiber length 1.02 m; $\lambda = 1480$–1550 nm)

Temperature [°C]	PMD [ps]	PMD coefficient [ps/km]	Relative PMD	PDL [dB]	Loss [dB]
+20	1.104	1082.4	1.0000	0.44	17.97
–20	1.100	1078.4	0.9964	0.46	17.92
0	1.102	1080.4	0.9982	0.42	17.93
+20	1.104	1082.4	1.0000	0.45	17.96
+40	1.106	1084.3	1.0018	0.45	17.96
+60	1.107	1085.3	1.0027	0.52	17.96

Table 8
IPHT 282b4 – temperature cycling test
(fiber length 12.40 m; $\lambda = 1490$–1590 nm)

Temperature [°C]	PMD [ps]	PMD coefficient [ps/km]	Relative PMD	PDL [dB]	Loss [dB]
+20	1.456	117.45	1.000	0.03	4.21
–30	1.538	124.03	1.056	0.03	4.21
–10	1.502	121.13	1.032	0.03	4.21
+10	1.474	118.87	1.012	0.03	4.21
+30	1.445	116.49	0.992	0.03	4.21
+50	1.419	114.44	0.975	0.03	4.21
+70	1.393	112.34	0.957	0.03	4.22
+20	1.466	118.23	1.007	0.03	4.21

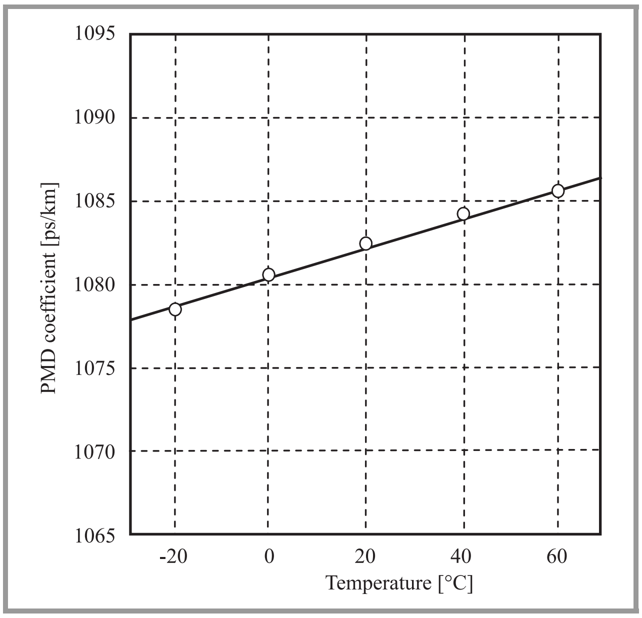

Fig. 19. Temperature characteristics of PMD – IPHT 252b5.

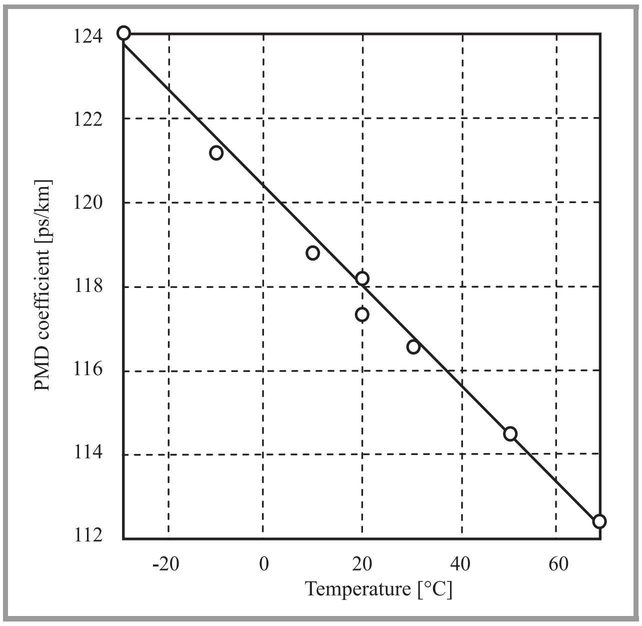

Fig. 20. Temperature characteristics of PMD – IPHT 282b4.

Temperature coefficients of PMD were $+7.9 \cdot 10^{-5}$/K for IPHT 252b5 and $-9.7 \cdot 10^{-4}$/K for IPHT 282b4.

Temperature dependence of PMD in IPHT 282b4 is similar to PANDA fibers, where birefringence is produced by strain generated by mismatch in thermal expansion of fiber parts. This effect is characterized by fictive zero-strain temperature of approximately +1100°C and negative temperature coefficient of about $-9 \cdot 10^{-4}$/K, matching the test data. Low and positive temperature coefficient of PMD in IPHT 252b5 indicates that its PMD is not resulting from mechanical strain, but non-symmetrical geometry of fiber core and surrounding holey structure.

Both samples exhibited excellent stability of loss with temperature. This applies also to fusion splices, exposed to variable temperatures during tests. Permanent changes of fiber attenuation and PMD due to temperature cycling are within measurement uncertainty.

8. PMD Versus Fiber Twist

8.1. Test Procedure and Results

Twisting of fiber reduces its PMD, as the circular strain causes periodic rotation of polarization states and prevents accumulation of differential group delay along the fiber. This applies both to PMD resulting from non-symmetry of fiber core [6], and PMD induced by external forces acting on the fiber [7]. However, circular strain also produces PMD proportional to twist rate, so progressive twisting causes PMD to drop first – when initial fiber birefringence is reduced, but increase later [6].

Experimental investigation of this effect in PCF is easier than in telecom single mode fibers, because many PCFs have high PMD coefficients and short sample is sufficient. Earlier twisting tests on PCF [8] gave PMD versus twist characteristics similar to conventional fibers.

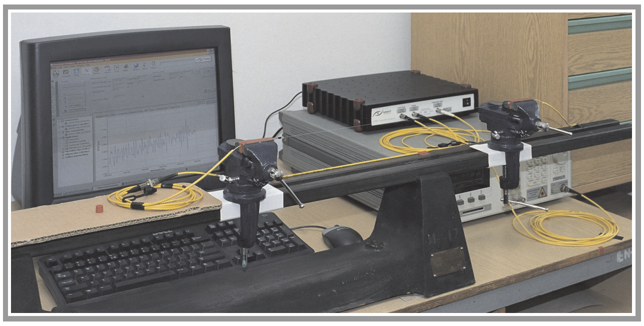

Fig. 21. Twist test of IPHT 252b5 (twisted length 0.50 m). PMD analyzer (Adaptif Photonics A2000), PC and tunable laser source (HP8168F) visible in the background.

A straight sample of each PCF was suspended between supports (Fig. 21) by gripping splice protection sleeves. One end of PCF was fixed, while the other was rotated as required. To avoid twisting of pigtails and interconnecting fibers, the sample was disconnected each time the movable end was to be rotated and re-connected before measurement.

Increase of PMD after initial reduction was not observed in both fibers till the maximum twist rate applied. Figures 22 and 23 are plots of relative PMD versus twist rate.

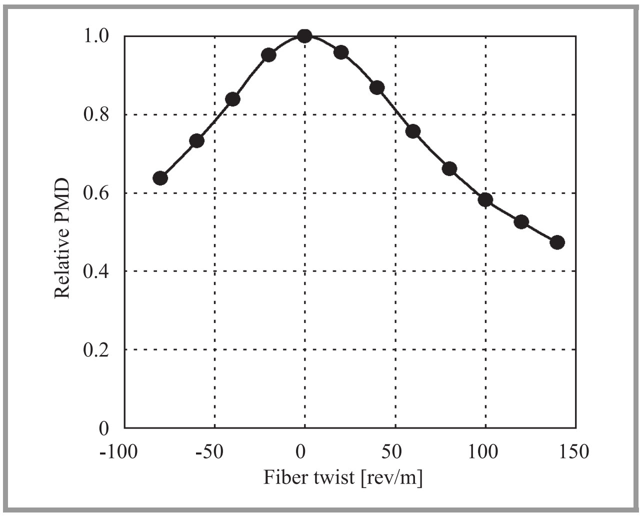

Fig. 22. PMD versus twist rate – IPHT 252b5. Twisting in two directions.

Lesiak and Woliński [9] reported only a small ($\leq 0.7\%$) decrease of PMD in two PCF samples twisted up to 40 rev/m. The fibers tested had PMD coefficients comparable to IPHT 252b5: 2300 ps/km and 730 ps/km, but lacked fully symmetric holey package, as one row of holes near the core

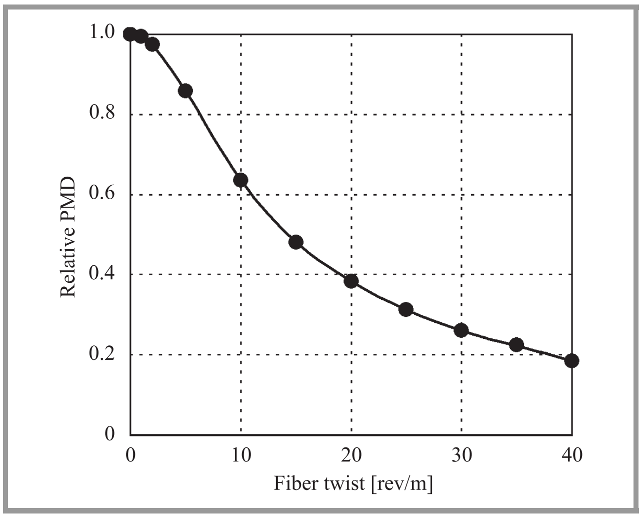

Fig. 23. PMD versus twist rate characteristics – IPHT 282b4.

was missing or modified. This difference deserves further investigation.

8.2. Comparisons

Fibers shared similar characteristics of PMD reduction with twist, but with a different sensitivity: twist rates required for a 50% PMD reduction were 133 rev/m for IPHT 252b5 and 14 rev/m for IPHT 282b4, respectively. Test on IPHT 252b5 demonstrated PMD reduction independent of twist direction, as expected for fibers drawn without spinning from a preform made of straight rods and tubes.

Plots in logarithmic scale (Figs. 24 and 25) indicate that DGD and PMD reduction follows the formula:

$$DGD = \frac{DGD_0}{1+\left(\frac{\gamma}{\gamma_{th}}\right)^x},$$

where DGD_0 is the DGD of untwisted fiber, γ is the twist rate, γ_{th} is a threshold twist rate corresponding to 50% re-

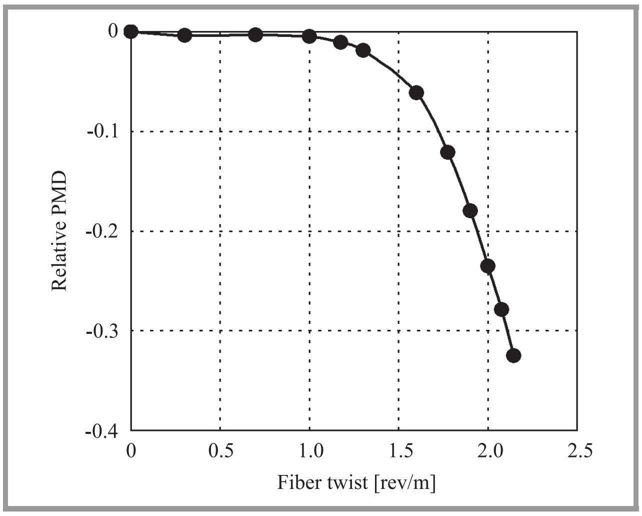

Fig. 24. PMD versus twist rate – IPHT 252b5 (logarithmic scale).

duction of DGD and x is a fixed exponent. While analysis presented in literature suggest either $x = 1$ [8] or $x = 2$ [7], our experimental data are best fitted by $x = 1.3$–1.7.

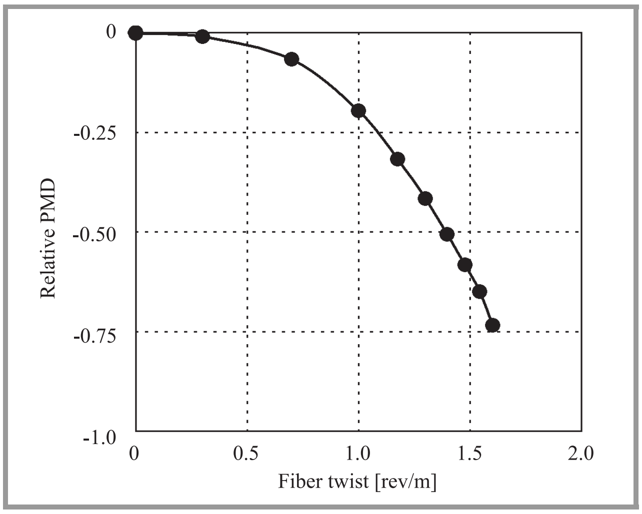

Fig. 25. PMD versus twist rate – IPHT 282b4 (logarithmic scale).

The DGD reduction with twist is wavelength-dependent: in IPHT 252b5 it was weaker with wavelength, in IPHT 282b4 stronger. In both samples, spectral distribution of DGD was flattest in untwisted state.

9. Elasto-Optic Coefficient

When optical fiber is elongated, decrease of effective refractive index partly compensates for increase of transmission delay due to extra length. This effect is important for design of fiber strain sensors.

Fiber under test was suspended vertically between fixed and movable clamp; delay was monitored by sending signal modulated at 69.632 MHz and measuring signal phase (Fig. 26). Tests were performed on sample of IPHT 252b5 being 10.50 m long, with applied strain up to 0.62%.

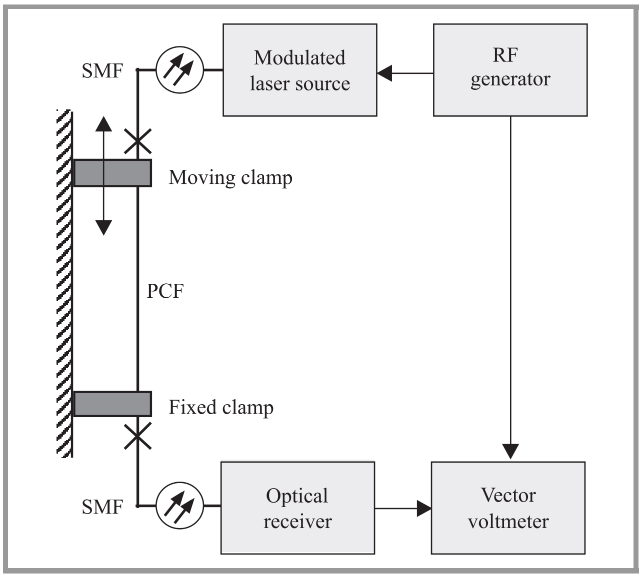

Fig. 26. Test setup for investigating elasto-optic coefficient of PCF.

Change in transmission delay in strained fiber was calculated from phase shift of signal received at the end of this fiber versus reference signal from generator:

$$\Delta t = \Delta\varphi / 360 f \,,$$

where: Δt – change in transmission delay [s], $\Delta\varphi$ – phase shift [deg], f – modulation frequency [Hz].

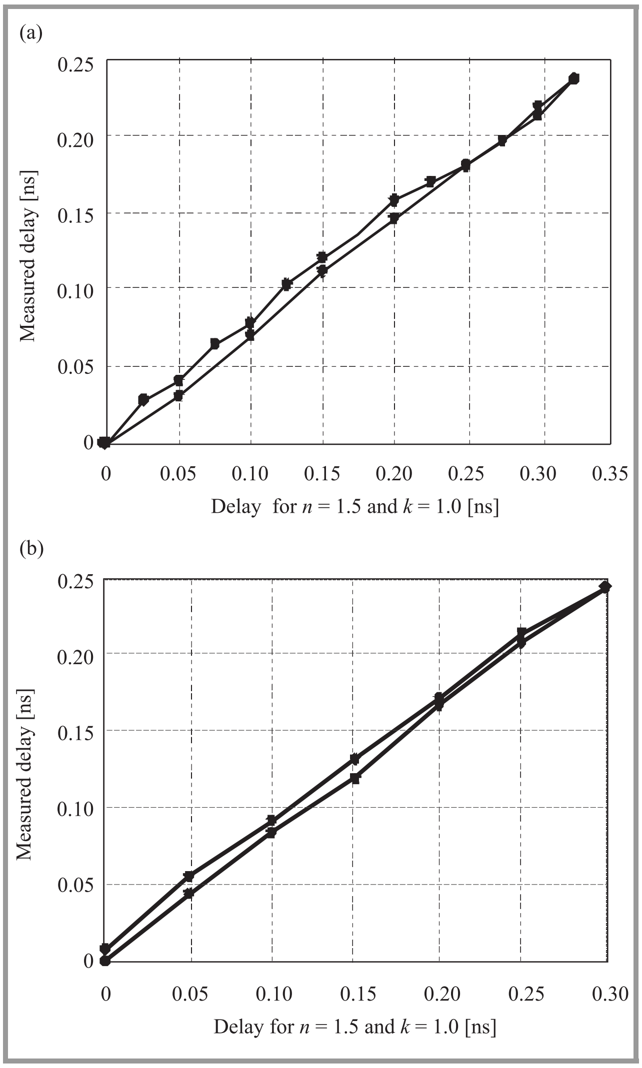

Fig. 27. Transmission delay introduced by fiber elongation versus effect of adding the same length of fiber, IPHT 252b5: (a) $\lambda = 1297$ nm, $k = 0.734$; (b) $\lambda = 1541$ nm, $k = 0.810$.

Measured change in transmission delay was compared to imaginary delay introduced by adding the same length of undisturbed fiber to transmission path. Their ratio is expressed as elasto-optic coefficient k:

$$k = c\Delta t / \Delta L n \,,$$

where: c – speed of light in vacuum ($3 \cdot 10^8$ m/s), ΔL – fiber elongation [m], n – fiber refractive index (~ 1.50).

Figure 27 presents test data for IPHT 252b5 and two wavelengths. Values of k are little lower than for conventional SMF having $k \sim 0.80$ at 1300 nm, and similar as for dispersion-shifted fibers (DSF) and nonzero dispersion shifted fibers (NZ-DSF). This is quite surprising, considering small size and very strong doping (36% GeO_2) of core in this PCF.

10. Conlusions

Experiments on a two photonic crystal fibers of different designs have revealed properties unusual for conventional solid silica fibers, like strong PMD with very different temperature and twist dependence in each PCF tested. This proves such properties can be tailored to particular requirements by modifying PCF design. Moreover, PMD twist dependence does not exactly follow existing models.

Several other results are mostly consistent with previous reports, including:

– high polarization mode dispersion;

– very strong backscattering signal;

– high attenuation with spectral characteristics different from conventional fibers.

Such properties facilitate tests on short samples (0.5–100 m). In particular, twist dependence of PMD is extremely difficult to characterize in conventional single mode fibers due to long lengths required. Strong backscattering helps in OTDR measurements of short PCF lengths despite necessity to use short pulses. However, it makes OTDR measurements of splicing and coupling loss difficult and may be a limitation in applications where high return loss is required.

On the other hand, elasto-optic coefficient describing variations of transmission delay in axial strain conditions is similar in PCFs and conventional single mode fibers, defying predictions.

Fusion splicing of photonic crystal fibers to SMF, essential for measurements and in several applications can often be done with fairly low loss, but procedure must be individually tailored to each PCF.

Acknowledgements

The author is very grateful to our COST-299 partners, Kay Schuster and Jens Kobelke of IPHT Jena, Germany, for supplying fiber samples. The assistance of fellow NIT researchers, Tomasz Kossek and Tomasz Osuch during spectral loss measurements is kindly appreciated. Research presented in this paper has been financially supported by Polish Ministry of Science and Higher Education as special research project COST/39/2007.

References

[1] K. Borzycki, "Testing of highly doped and photonic crystal optical fibers", *J. Telecommun. Inform. Technol.*, no. 3, pp. 65–73, 2008.

[2] Corning SMF-28e Optical Fiber Product Information, Corning Inc., PI1344, Jan. 2005.

[3] Matched Cladding Single-Mode Fiber, OFS Fitel, fiber-106-0103, Jan. 2003.

[4] B. Edvold and L. Gruner-Nielsen, "New technique for reducing the splice loss to dispersion compensating fiber", in *Proc. ECOC-1996 Conf.*, Oslo, Norway, 1996, vol. 2, pp. 245–248.

[5] Y. Wang, H. Bartelt, S. Brueckner, J. Kobelke, M. Rothhardt, K. Mörl, W. Ecke, and R. Willsch, "Splicing Ge-doped photonic crystal fibers using commercial fusion splicer with default discharge parameters", *Opt. Expr.*, vol. 16, no. 10, pp. 7258–7263, 2008.

[6] R. E. Schuh, X. Shan, and A. S. Siddiqui, "Polarization mode dispersion in spun fibers with different linear birefringence and spinning parameters", *J. Lightw. Technol.*, vol. 16, no. 9, pp. 1583–1588, 1998.

[7] K. Borzycki, "Temperature dependence of polarization mode dispersion in tight-buffered optical fibers", *J. Telecommun. Inform. Technol.*, no. 1, pp. 56–66, 2008.

[8] J. Zhou, K. Tajima, K. Nakajima, K. Kurokawa, T. Matsui, Ch. Fukai, and I. Sankawa, "PMD suppression method for photonic crystal fiber", in *Proc. OFC-2005 Conf.*, Anaheim, USA, 2005, paper OTuA6.

[9] P. Lesiak and T. Woliński, "Simultaneous twist and longitudinal strain effects on polarization mode dispersion in highly birefringent fibers", *Opto-Electr. Rev.*, vol. 13, no. 2, pp. 183–186, 2005.

Krzysztof Borzycki was born in Warsaw, Poland, in 1959. He received the M.Sc. degree in electrical engineering from Warsaw University of Technology in 1982 and a Ph.D. degree in communications engineering from National Institute of Telecommunications (NIT), Warsaw in 2006. He has been with NIT since 1982, working on fusion splicing, optical transmission systems, measurement methods and test equipment for optical networks, as well as standardization and testing of optical fiber cables and DWDM systems. Other activities included being a lecturer and instructor in fiber optics and technical advisor to Polish cable industry. He has also been with Ericsson AB research laboratories in Stockholm, Sweden, working on development and testing of DWDM systems between 2001 and 2002. He has been active in several European projects since 2003, including Network of Excellence in Micro-Optics (NEMO) and COST Actions 270, 291 and 299. This included research on PMD in cables operating in extreme environments, and testing of specialty fibers. Dr. Borzycki is an author or co-author of 1 book, 2 Polish patents and 45 scientific papers in the field of optical fiber communications, optical fibers and measurements in optical networks, as well as one of "Journal of Telecommunications and Information Technology" editors.

e-mail: k.borzycki@itl.waw.pl

National Institute of Telecommunications

Szachowa st 1

04-894 Warsaw, Poland